Oceanographic Surveys with Autonomous Underwater Vehicles: Performance Metrics and Survey Design

by

Jeffrey Scott Willcox

B.S. Electical Engineering, Massachusetts Institute of Technology, 1993

Submitted to the Department of Ocean Engineering
and
Department of Electrical Engineering and Computer Science
in partial fulfillment of the requirements for the degree of

Master of Science in Ocean Engineering
and
Master of Science in Electrical Engineering

at the

MASSACHUSETTS INSTITUTE OF TECHNOLOGY

February 1998

Author .....
Department of Ocean Engineering and
Department of Electrical Engineering and Computer Science
January 16, 1998

Certified by .....
James G. Bellingham
Lecturer, Department of Ocean Engineering
Thesis Supervisor

Certified by .....
Arthur B. Baggeroer
Professor of Electrical and Ocean Engineering
Thesis Supervisor

Accepted by .....
John Kim Vandiver
Chairman, OE Committee on Graduate Students

Accepted by .....
Arthur C. Smith
Chairman, EECS Committee on Graduate Students

Oceanographic Surveys with Autonomous Underwater Vehicles: Performance Metrics and Survey Design

by

Jeffrey Scott Willcox

Submitted to the Department of Ocean Engineering
and
Department of Electrical Engineering and Computer Science
on January 16, 1998, in partial fulfillment of the
requirements for the degree of
Master of Science in Ocean Engineering
and
Master of Science in Electrical Engineering

Abstract

To obtain synoptic data, a survey system must be capable of mapping an ocean structure faster than significant changes in the structure occur. For most, if not all, traditional methods of subsurface sampling, the requirement of synopticity must be relaxed due to physical and economic operational limitations of the sampling platforms [1, 2]. However, recent work with autonomous underwater vehicles [3, 4, 5, 6, 7, 8] has expanded the operational boundaries of these platforms to the point where it is possible to obtain synoptic or near-synoptic measurements of small scale, rapidly evolving processes using AUVs. This expansion of capability brings with it a correspondingly large number of options for constructing surveys, which in turn lead to a wide range of survey performances. This work addresses the question of how to best survey a dynamic phenomena within the constraints of vehicle operational characteristics and available energy.

A fundamental difficulty in doing oceanographic surveys with autonomous underwater vehicles (AUVs) is the coupling of space and time through the AUV survey trajectory. Also, the finite velocity and energy capacity of an AUV imposeses serious constraints on the extent of the survey domain and on the spatial and temporal survey resolutions. Given an oceanographic process of interest with its associated spatial and temporal scales, what are the AUV survey trajectories which will give the best survey performance in terms of some performance metric? What should this performance metric be? These are the fundamental questions which will be addressed in this thesis.

The focus of this thesis is the development of tools to determine how to effectively use AUVs to survey small-scale oceanographic processes. Contributions of this work include an examinations of the broad domain of scientific and engineering problems inherent in surveying oceanographic processes with AUVs. This extended examination provides context for the remainder of the thesis in which we develop a quantitative survey error metric which accounts for errors due to both spatial undersampling and temporal evolution of the sample field. The accuracy of the survey error metric is established with surveys through

a simulated oceanographic process. We also develop the AUV "survey envelope" using the physical constraints (minimum and maximum AUV speed, total energy capacity) of the survey platform. The survey envelope delineates a region of survey parameter space within which an AUV can sucessfully complete a mission. By combining the survey error metric with the survey envelope, we create a survey analysis tool which can be used to gain insight into the AUV survey trajectory design problem. We demonstrate the application of this survey analysis tool with a survey design for an open-ocean deep convection event.

Thesis Supervisor: James G. Bellingham
Title: Lecturer, Department of Ocean Engineering

Thesis Supervisor: Arthur B. Baggeroer
Title: Professor of Electrical and Ocean Engineering

Acknowledgments

I want to thank my office mates with whom I have shared many enjoyable discussions, both academic and otherwise, and who have helped make these years fruitful, exciting, and a bit more humane: Andrew Bennett, Nuno Cruz, Max Deffenbaugh, Stefan Deuker, Anna Galea, John Kim, Claudia Rodriguez, Chris Smith, and Yanwu Zhang. Special thanks to Yanwu for his help on open-ocean deep convection in Section 5.4.

I also want to thank the research and support staff at the MIT Sea Grant College Program for providing me with such a stimulating environment in which to work. Much appreciation to Dr. Bradley Moran and Mr. Robert Grieve and particular gratitude to Dr. James Bales for his careful and critical review of the manuscript.

My deepest appreciation goes to my advisors, Dr. James Bellingham and Prof. Arthur Baggeroer, who have engaged me in numerous insightful discussions and provided sound guidance throughout the course of this thesis. Special thanks to Dr. Bellingham for giving me the opportunities to work in one of the most exciting labs around and to see a bit of the world while doing it.

I want to thank my wife, Dianne Egnor, and my family: Mom, Dad, Rob, Chris, and Christie. Your love and support has brought me through the hard times as well as the good. Special thanks to Dianne for helping with several of the LaTeXfigures, for lots of editing, and for providing encouragement when the task seemed too great. This thesis is dedicated to you all.

Support for this work was provided by the Office of Naval Research under grant numbers N00014-95-1-0994 and N0001-95-1-1316, and by the MIT Sea Grant College Program, grant number NA46RG0434, through its Adaptive Sampling and AUV Scientific and Industrial Applications initiatives.

Contents

List of Figures

List of Tables

Chapter 1

Introduction

It is clear that capabilities for synoptic observation of dynamic random fields in the ocean are much needed. Unfortunately, the wide range of length scales of both temporal and spatial variability found in these processes makes the surveying of dynamic phenomena in the world's oceans problematic. To obtain synoptic data from ground-based observations, a survey system must be capable of mapping an ocean structure faster than significant changes in this structure occur. For most, if not all, traditional methods of subsurface oceanographic sampling, the requirement of synopticity must be relaxed due to physical and economic operational limitations of the sampling platforms [1],[2].

Consequently, a variety of new and traditional observational techniques are available to the ocean scientist. One of the newest of these techniques is the Autonomous Underwater Vehicle. AUVs combine many of the traditional sampling technologies with a highly mobile platform, allowing the collection of spatially correlated samples without the substantial cost associated with an array of sensing elements. When surveying with AUVs, we want to find ways of allocating our scarce observational resources to maximize the information content of the collected data. Because they are a relatively new technology, it is also not yet well understood how to best utilize AUVs in oceanographic experimentation. This work will explore the issues inherent in surveying oceanographic phenomena with AUVs and will develop quantitative metrics for measuring the effectiveness of these surveys.

1.1 Motivation

In this section we examine the characteristics of traditional observational systems as well as those of the autonomous underwater vehicle. A comparison of these characteristics will give insight into the suitability of the various sampling platforms for specific scientific programs or for studying a particular oceanographic process. We will also discuss the synergistic combination of these observational systems for oceanographic research through the implementation of autonomous ocean sampling networks (AOSNs). These discussions will demonstrate the importance of emerging technologies, such as AUVs and AOSNs, in the future of oceanographic research. We conclude this section with a brief statement of the problems which will be addressed in this work.

1.1.1 Traditional Observational Systems

Several different observational platforms are widely in use, measuring oceanographic phenomena over length and time scales spanning several orders of magnitude [1]. The observational platforms with the greatest spatial coverages are satellites. While satellites can provide images of wide expanses of the ocean surface (several hundred kilometer swaths) almost instantaneously, these observations cannot capture the complex subsurface dynamics of the process under study. Also, the spatial resolutions of satellite-based observational systems are typically too coarse to yield useful data for most small scale oceanographic phenomena. Lastly, these observations must be ground-truthed with in situ measurements. Such in situ observations are, in turn, most often made by dedicated oceanographic research vessels or by ships of opportunity, using a variety of dipping and/or towed instruments. In this scenario, the survey sampling resolutions are determined by factors such as the speed of the ship, the number of stations where the ship stops, the total at-sea time of the ship, and, in the case of towed instruments or remotely operated vehicles, the complex cable dynamics of the towed instrument or ROV. A typical "tow-yo" survey would have track separations of at least several kilometers. Another constraint on ship-borne observations, and often the most important one, is the economic cost of manning and maintaining the research vessel.

To address this last constraint, another class of observational platforms has been de-

signed which requires the support of an ocean-going vessel only during the installation and retrieval of instruments. Drifters, gliders, and moorings fall into this category. Drifters and gliders consist of small, self-contained instrument packages which either passively drift along with the current on the surface or at some fixed depth (drifters), or which utilize some mechanism to exercise limited control over their spatial location (gliders). One of the main attractions of drifters and gliders is that they can be deployed (either as single units or in groups) and left in place for long durations, allowing them to cover broad (basin-scale) geographic areas. Unfortunately, the scientist cannot specify the path that the drifters or gliders will take on their long journey. In some instances, drifters become confined to a limited region due to the action of currents associated with fronts or meso-scale rings or eddies [1]. Gliders are designed to alleviate this problem by exercising some modest degree of control over their heading and depth by taking advantage of temperature gradients or some other low power source of energy in the ocean to develop a small degree of control authority. Nevertheless, the main drawback of drifters and gliders remains the lack of control over the spatial position of the instrument. The inherently Lagrangian or mixed Lagrangian/Eulerian nature of their measurements can also make it quite difficult to extract salient information from drifter and glider measurements [9].

At the other end of this spectrum of unmanned observational systems are moorings. Like drifters and gliders, moorings are also self-contained instrument packages. However, instead of moving with the water mass they are fixed at a given location and depth via a cable attached to an anchor on the ocean floor. A surface expression (buoy) may also be present, allowing the mooring to transmit data back to the scientist via radio or satellite. While time-series data can be taken from individual moorings, a network of moorings is required to generate spatially-correlated measurements. For moorings, the expense of deploying a spatial array constrains the observational system.

Other issues which effect the use of drifters, gliders, and moorings in oceanographic experimentation are reliability, data storage, and data retrieval. Due to economic and operational pressures, the typical drifter, glider, or mooring deployment is limited to a maximum of two years. In some systems, it is possible to transmit data back to the scientist via satellite but the strict power limitations placed on the transmitters necessitate a very

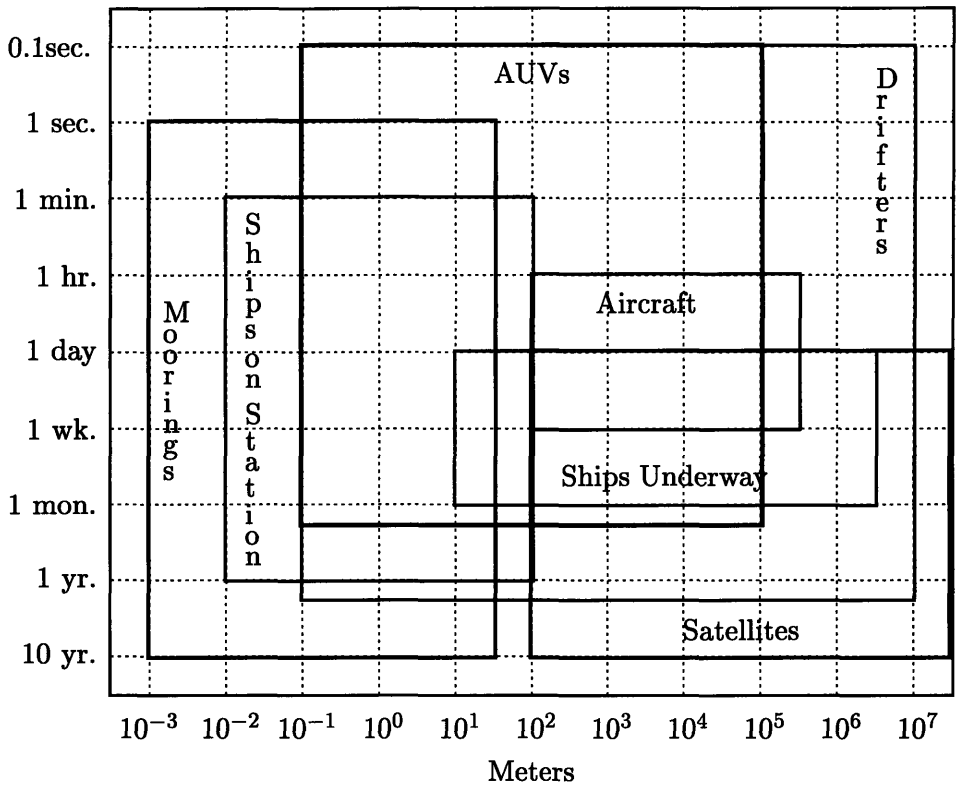

Figure 1.1: Sampling regimes for various sensor platforms. The labeled boxes give the maximum and minimum spatial and temporal sampling resolutions for the specified platforms. Drifters and AUVs are seen to be the most versatile platforms in terms of the range of measurements resolutions which they can achieve. The values on the spatial and temporal axes are not necessarily achievable simultaneously (a fast temporal sampling at a broad spatial resolution is not possible for most of these platforms). Figure after Dickey [1].

slow bit rate. Thus, usually only a small percentage of the data taken can be transmitted and the rest must be stored on-board the instruments. The scientist will typically have to wait until the end of the deployment to retrieve data from the instrument. Although great strides have been made in the last few years in producing denser storage media, the vast amount of data which can potentially be gathered by these instruments indicates that data storage will remain problematic in these systems for many years to come.

The length and time scales spanned by all of these observational systems cover several orders of magnitude in both dimensions. Figure 1.1 shows the regions of applicability for each of these platforms. The values on the spatial and temporal axes are indicative of the range over which each instrument can operate in each dimension. The boxes shown should not be construed as implying that all combinations of length and time scales contained

within these boxes are necessarily achievable by the observational systems. For instance, a fast survey with widely separated track lines is not possible for most of these systems even though such surveys are contained within the bounds shown.

1.1.2 Autonomous Underwater Vehicles

The autonomous underwater vehicle (AUV) combines the functionality of many of the observational systems described above with a highly mobile sensor platform [10],[4]. The scientific objectives of the mission and the size and power requirements of the various instrument packages are a few of the factors affecting the choice of observational systems to be carried by an AUV. As the name implies, an AUV does not require external supervision to complete an assigned mission. Furthermore, cost permitting, several AUVs can be employed to increase the coverage of the phenomenon of interest. Primarily due to their small size, AUVs are able to conduct sampling surveys with greatly improved spatial resolution in comparison to ship-borne towed instrument surveys, but the increases in spatial resolution come at the expense of a reduction in total deployment time (see Figure 1.1). Fortunately, recent work with AUVs [10],[4],[6],[7] has expanded the operational boundaries of these platforms to the point where it is possible to obtain synoptic or near-synoptic measurements of small scale, rapidly evolving oceanographic processes [11, 12]. For instance, the Odyssey IIb class of AUVs, built and operated by the MIT Sea Grant AUV Laboratory, have been or are scheduled to be employed in studies of hydrothermal plumes [13],[14], Arctic ice-fracture mechanics and under-ice topography surveys [4],[15],[16], tidal convergence fronts [17], and open-ocean deep convection [18],[19].

1.1.3 Autonomous Oceanographic Sampling Networks

Obviously, no single sensing platform can meet all oceanographic exploration needs. In fact, because of the grand scale of the typical oceanographic phenomenon, it is often prudent to use any and all of available resources. An autonomous ocean sampling network, shown in Figure 1.2, embodies such a combination of resources [20]. By combining traditional sampling methods with new technologies and existing expertise in the areas of AUV design, communications, and control, a new paradigm for scientific ocean presence has been created.

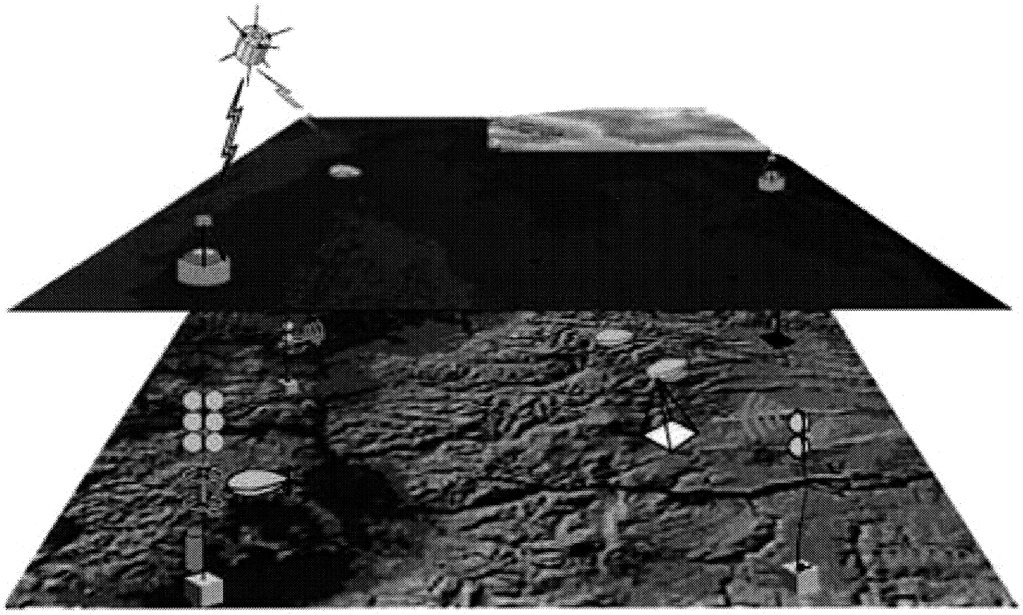

Figure 1.2: Autonomous Ocean Sampling Networks (AOSNs) are a new paradigm for oceanographic observation relying on the synergistic exploitation of both new and traditional sensing/sampling platforms, including moorings, drifters, satellites, and AUVs. The autonomous underwater vehicle plays a vital role in the AOSN since it is the mobility of the AUV which provides the network its major resource for reacting to rapidly evolving and spatially distributed oceanographic phenomena. The AUVs also greatly enhances the spatial coverage of the network. Figure by Bellingham.

The AOSN utilizes satellites, moored instruments, gliders, drifters, and multiple AUVs to gain synoptic coverage of episodic oceanographic phenomena. Like AUVs, AOSNs do not require that the scientist (or a support vessel) be present during the collection of data. The network is remotely monitored by the scientist and tasks are down-loaded to the various instruments for autonomous execution. AOSNs can be particularly beneficial when the phenomena of interest are associated with harsh oceanographic or meteorological conditions.

1.1.4 Oceanographic Context

The work of this thesis has been undertaken in anticipation of an experiment to take place in the Labrador Sea during the winter of 1997/98. In this experiment, an AOSN will be used to study open-ocean deep convection. This phenomenon is known to occur in only a few places in the high latitudes of the northern and southern hemispheres. The Labrador Sea has been one of the more active of these sites over the last several years. Since open-

ocean deep convection is responsible for setting in motion the transport of 1-2$\times 10^{12}$ watts of heat northward each year [18], this process has a critical role in the transfer of heat from the atmosphere into the oceans and is vital to global climate change [21]. The length scales of interest in open-ocean deep convection range from small-scale plumes (less than 1 km across) to meso-scale preconditioning (approximately 100 km) [22]. The event is episodic in nature. Characteristic time scales range from 6 to 12 hours for the violent overturning of the water column to several days or weeks for the sinking and spreading of the cold convection chimney.

Because of the episodic nature of this process, autonomous sensing platforms such as moorings and AUVs are ideally suited to the study of open-ocean deep convection. These instruments can be left on station unattended and can be either automatically or remotely triggered to collect data at the onset of a convection event. Because the exact spatial location of a convection event cannot be predicted in advance of the onset of this process, moorings are not expected to be very successful in capturing a convection event. On the other hand, the ability of an AUV to transit to the event greatly improves its chances of recording a convection event.

Open-ocean deep convection is not the only oceanographic process which we might wish to study using AUVs. For instance, we might wish to examine ocean current eddies which have an important role in the general circulation of the worlds oceans. Eddies in ocean currents have characteristic length scales in a range of 10-100's km and evolve on time scales of several weeks to months. Plumes from hydrothermal vents or pollution sources are another dynamic phenomenon which we might wish to examine. Diffusing plumes occur with characteristic length scales of 0.1-1 km and can last anywhere from hours to days for a pollution outflow event or up to several weeks for a large hydrothermal event. Lastly, we may wish to study the dynamics of an ocean frontal zone where two bodies of water collide and mix. Frontal dynamic zones can be extremely localized in space and time. For instance, recent investigations in the region of the Haro Strait with AUVs [17] have found that fronts can have characteristic lengths of as little as 100 meters and can form and disappear within the space of 15-30 minutes. This is probably more extreme than would be seen in open ocean fronts and can, therefore, be taken as a lower bound on the length and time scales of

ocean fronts.

1.1.5 Problem Statement

Given an oceanographic process of interest with its associated spatial and temporal scales, what are the AUV survey trajectories which give the best survey performance in terms of some performance metric? What should this performance metric be? These are the fundamental questions which will be addressed in this thesis. The focus of this thesis is placed on the development of tools to determine how to effectively use multiple AUVs for surveying small-scale oceanographic processes. A metric of the total survey error will be developed and its use as an adaptive experiment design tool will be demonstrated.

1.2 Thesis Tasks

A fundamental difficulty of sampling with AUVs is the coupling of space and time through the AUV survey trajectory. Unlike conventional sampling techniques where, for example, an array of sensors take samples at numerous locations in space at each sampling instant, an AUV samples only a single point in space at each sampling time. Because of the finite velocity and limited energy capacity of an AUV, this places serious constraints on the extent of the AUV's survey domain and on the spatial and temporal survey resolutions at which the survey is conducted. In the limiting case of a process which does not significantly evolve in time over the course of a survey mission (geomagnetic fields, for instance), the operational constraints of the AUV are no longer restrictive. However, if the AUVs are being employed to study phenomena which evolve on time scales comparable to or faster than the total survey time, then the spatial field sampled by the AUV will be seriously corrupted by temporal evolution of the dataset, a phenomenon which we call "blurring". For AUV studies of oceanographic processes, this problem dominates other sampling and survey design issues. Given such a process, how do we design the trajectory which an AUV must follow in order to obtain the greatest amount of information about the spatial and temporal structure of this process subject to the above constraints? This is the fundamental question which this thesis will address. In this work we will develop a quantitative framework for evaluating AUV

performance and use this framework to design AUV surveys of oceanographic processes. The tasks required in developing these capabilities are outline below.

1.2.1 Exploration of Issues

There are numerous difficulties or challenges involved in surveying oceanographic processes with AUVs. We will enumerate these issues in an attempt to put the current research effort into the context of broader issues or problems. Specifically, we will explore vehicle engineering and operational challenges, algorithmic and computational difficulties, issues in survey designs and adaptive sampling, and simulation and modeling problems, as well as sampling theoretic issues. We will not provide solutions for most of these problems, we will only point out their existence. This discussion serves to place the AUV survey problem in perspective. Problems which we will address are described below.

1.2.2 Survey Performance Metrics

To compare differing survey trajectories with each other, a performance metric for an AUV survey is required. In general, this performance metric may take the form of a cost functional which is based upon a combination of various user defined parameters such as the total AUV survey mission time, the size of the realized survey domain, and/or the degree to which some scientific objective has been met. Total survey performance increases as the cost functional decreases and is said to be "optimal" when the cost functional is minimized. The cost functional is also sometimes called the objective functional indicating that the user has chosen to give precedence (heavier weighting) to the scientific objective over the economic and logistical costs incurred.

In this thesis, the performance metric will be defined to give heaviest weighting to the scientific quality of the survey as given by a combination of a total survey error with a measure of the energy cost of a given survey. The total survey error will be based on estimation errors in a reconstruction of the process field from survey samples and will incorporate errors due to the (assumed) spatial undersampling of the process field as well as the temporal "blurring" inherent in reconstructing temporally evolving, spatial fields from survey samples. The energy economics of AUV surveys will also be calculated. These

two metrics, total survey error and survey energy consumed, will be combined to form the survey performance metric.

1.2.3 Process Simulations and Error Metric Verification

The theoretical total survey error metric will need to be verified. To this end, a simulation of a spatially homogeneous and isotropic, temporally stationary random field will be implemented. The simulation will use the technique of "sampling from the spectrum" [23, 24], allowing for a simulation which is not inherently discretized, has an arbitrary domain shape and size, and does not require the computation of off-trajectory field values. This last characteristic is an essential component in making the simulation technique computationally feasible. Simulated random fields will be employed to test the validity of the total survey error metric through a series of simulated AUV surveys through the random fields.

1.2.4 Simple Survey Designs and Vehicle Customization

The survey performance metric will be employed to quantitatively compare the results from differing strategies, facilitating research into optimal survey designs. Simple survey designs will be made and shown to be optimal for a restricted class of target random field processes. The performance metric will also be employed in an examination of various AUV survey strategies as applied to open-ocean deep convection. The problem of optimal location of observations from a control theoretic viewpoint will be left for future work.

In addition to guiding the design of survey strategies, it will also be shown that the survey performance metric can be utilized in the optimization of the design of the AUVs themselves. The survey performance metric allows the researcher to tailor the choice or design of an AUV to a specific oceanographic process. We will demonstrate the use of the survey performance metric to identify useful vehicle redesign parameters within the context of a specific oceanographic experimental scenario.

1.3 Thesis Organization

Before engaging the problem at hand, we begin with an exploration of relevant background material (with an emphasis on AUVs and the Odyssey IIb vehicle) and a discussion of some of the problems and challenges which, although worthy in their own right, will not be addressed in this thesis. This is done so that the reader can place the contributions of this thesis in context. These two discussions take place in Chapter 2. After these preliminaries, we turn to the development of performance metrics to characterize AUV surveys of oceanographic processes in Chapter 3. These performance metrics are concerned with both the energetics and the field reconstruction errors involved in surveying spatially distributed, temporally evolving fields using AUVs. The total survey error metric developed in this chapter will be subjected to verification through simulated surveys in Chapter 4. The combined use of the performance metrics for survey design as well as AUV choice/design will be explored in Chapter 5. We also demonstrate the application of the survey performance metrics to the design of an AUV survey of open-ocean deep convection in this chapter. Finally, an overview of contributions and a discussion of future directions for this research will be given in Chapter 6.

Chapter 2

Background and Problem Domains

2.1 Introduction

The intent of this chapter is two-fold: to present background material in areas related to the research undertaken in later chapters and to raise many of the difficult and challenging issues which are inherent in sampling oceanographic phenomena with AUVs. With regards to the former goal, Section 2.2 gives background information in the areas of sampling and reconstruction of process fields, error analysis and performance metrics, modeling and simulation of oceanographic processes, experiment design, and autonomous underwater vehicles. A brief introduction to the Odyssey IIb class of AUVs is given in Section 2.3. Next, we examine some of the difficulties associated with surveying oceanographic phenomena with AUVs in Section 2.4. The discussion is broken into several broad problem domains: engineering challenges, computational and algorithmic challenges, survey design issues, and difficulties inherent in sampling oceanographic processes with AUVs. Sampling issues are given more in-depth examination due to their vital role in the following chapters of this work. Concluding remarks are made in Section 2.5.

2.2 Background and Related Work

In order to reconstruct a particular realization of an oceanographic process, we will in general require observations in one temporal and three spatial dimensions of a given dynamic

field. Even if reconstruction of the process is not needed, we still require multidimensional observations of the process to be able to estimate its spatial and temporal spectra. In fact, many seemingly disparate disciplines are connected by their reliance upon multidimensional observations as a means to gain new knowledge of the various phenomena of interest. This provides a link between these disciplines at the most basic and theoretic levels. For this reason, we examine literature from oceanography, meteorology, hydrology, geophysics, electrical engineering, and statistics in developing the following list of related works. The specific applicability of these sources to the current work varies substantially from field to field. We separate the related works into several broad categories: sampling and reconstruction, error analysis and performance metrics, modeling and simulation, experiment design, wavelets and multiscale stochastic processes, and autonomous underwater vehicles. We touch briefly on the contributions from each of these areas below.

2.2.1 Sampling and Reconstruction

A large body of literature exists with regards to the sampling of deterministic functions and stochastic processes in the one-dimensional case. These results, primarily from electrical engineering and statistics, date back to the work of Fourier and beyond. Although significant contributions were made by both Cauchy and Nyquist, it was not until the middle of this century that sampling theoretic results were combined into a coherent framework through the works of Shannon [25],[26] and Wiener [27], with later generalizations by Papoulis [28]. All of these works address the unidimensional sampling problem, from either the deterministic function or stochastic process perspectives. An extensive summary of results in unidimensional sampling theory is given by Jerri [29]. The works of Petersen and Middleton [30] and Miyakawa [31] provide the necessary extensions to multiple dimensions in the deterministic and stochastic cases, respectively. Dudgeon and Mersereau [32] give an overview of multidimensional deterministic signal processing. All of these works make the basic assumption that samples are taken uniformly in space or time or both. This will not be the case for spatial samples along the trajectory of an AUV. The works of Bretherton [33] and Marvasti [34] on nonuniform sampling give important insights into this issue.

2.2.2 Error Analysis and Performance Metrics

All but the most trivial sampling scenarios involve aliasing and/or truncation errors. Shannon [25] provides the basic result for errors due to aliasing and Jerri [35] gives a comprehensive review of the literature on estimation errors. Applications of these results to reconstruction from nonuniform sensor arrays are found in numerous disciplines: Bras [36] examines reconstruction errors as applied to random fields in hydrology and Robinson [37] gives examples of error analysis in the area of oceanography. The work of Bretherton [38] on error maps for interpolation arrays has proven to be an invaluable resource. Finally, Bellingham [11] and Willcox [12] analyze the errors inherent in reconstruction of random processes from AUV-surveyed samples, incorporating both spatial aliasing and temporal evolutionary effects.

2.2.3 Modeling and Simulation

While modeling of oceanographic processes will not be the primary focus of this work, numerical simulations of multidimensional stochastic processes will be required to verify the techniques developed herein. These simulations are, in turn, based upon simple stochastic models of dynamic fields. The references below deal with modeling and simulation issues from a variety of disciplines: Mejia [39] in hydrology, Handcock [40] in meteorology, and Goff and Jordan [41],[42], Robinson [37], and Jones and Marshall [22] in oceanography. Additionally, an efficient method for simulating non-stationary and/or anisotropic random fields is developed in the hydrology literature by Mantoglou and Wilson [43],[44]. Gauss-Markov processes and Markov Random Fields (MRFs) are described in a book by Vanmarcke [45] and reviewed in the paper by Derin [46]. Multiscale representations of MRFs are developed by Luettgen [47], and Irving [48] discusses multiscale model identification. Although the focus of this thesis will not be on the accurate simulation of specific oceanographic processes, insights gained from the above works will be useful in the development of simulations which are representative of and qualitatively similar to real oceanographic processes.

2.2.4 Experiment Design

Due to limited resources, it is rarely possible to sample space-time processes at the multidimensional equivalent of the Nyquist rate. This will of course lead to reconstruction errors. These errors can be minimized by a judicious allocation of sampling resources. Rodriguez-Iturbe and Mejia [49] examine this problem as applied to the design of a rain gauge network for monitoring precipitation. Similarly, Bretherton [38] examines the efficiency of oceanographic sampling arrays by making trial and error adjustments to array configurations in an attempt to trade off spatial coverage and interpolation accuracy. Kumar [50] from electrical engineering and Hogg [51] from oceanography, examine optimal experiment designs for parameter estimation. Finally, Fedorov [52] addresses the problem of multidimensional experiment design from the viewpoint of the statistician. The common thread running through each of these works is an attempt to accurately estimate the multidimensional covariance function and to use this knowledge to appropriately allocate experimental resources.

2.2.5 Autonomous Underwater Vehicles

The development of autonomous underwater vehicles (AUVs) has a long and rich history. Although we will not try to do justice here to the numerous AUV platforms which have been built for various applications, the vehicles described by Yoerger [10], Bellingham [4], Von Alt [6], and Smith [7] give a representative sampling of some of the small oceanographic research AUVs which have been developed in the last few years. In has been only recently that AUV technology has reached the point were these platforms have become useful for real oceanographic experimentation. The number of references on the actual use of AUVs in oceanographic research is small. Bellingham [11] and Willcox [12] discuss the development of a performance metric for AUV survey design, while gradient search algorithms for AUV exploration of thermal or chemical plumes are compared in Burian [53]. Yoerger [8] reports on the use of an AUV for magnetic surveying of the sea floor, and Schmidt [17] describes the application of AUV technology to the exploration of coastal fronts. Even though they are beginning to be accepted in the oceanographic community as reliable sensor platforms, research and development work on AUVs is still quite active. As AUV technology matures, we will see increasing use of AUVs in oceanographic research settings.

Figure 2.1: The Odyssey IIb Autonomous Underwater Vehicle (AUV) is retrieved after a successful mission. The Odyssey IIb is a third generation AUV designed and built at the MIT Sea Grant AUV Laboratory. A fleet of five Odyssey IIb vehicles are currently operational. These vehicles are highly robust, having completed over 300 deployments world-wide with no vehicle losses.

2.3 Odyssey IIb

The Odyssey IIb vehicle, Figure 2.1, is a third generation AUV designed and built at the MIT Sea Grant AUV Laboratory. The vehicle's outer fairing has the streamlined shape of a wide torpedo and measures 2 m in length by 0.6 m in diameter (at its widest point). The outer fairing serves only to decrease drag and improve the controllability of the Odyssey while the inner fairing forms the rigid "backbone" of the vehicle. The volume of the vehicle is free-flooded save for two 17-inch glass spheres which serve as the main pressure vessels. These spheres house the main vehicle computer (MVC), attitude sensors, batteries and power management equipment, and miscellaneous payload electronics.

A fleet of five Odyssey IIb vehicles are currently operational. These five AUVs are shown in Figure 2.2 in various stages of preparation for a mission. The outer fairing has been removed from the first, third, and fourth vehicles, displaying the inner fairing on the first vehicle (in the foreground) and the wet cabling and spheres in the third and fourth vehicles. The two hemispheres in the inner fairing are the cradles for the pressure spheres.

(a)

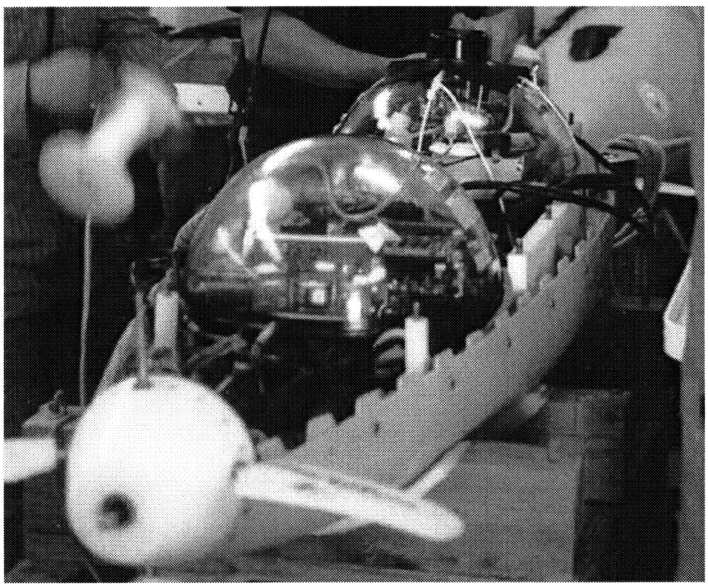

(b)

Figure 2.2: Inside the Odyssey IIb AUV. The fleet in various stages of assembly is shown in (a). The outer fairing has been removed on the first, third, and fourth vehicles. The first vehicle, in the foreground, shows the inner fairing which provides mechanical rigidity and cradles the spherical pressure housings. The third and fourth vehicle also have their inner fairings removed exposing the spheres, wet cabling, and various sensors. A detail of the inner vehicle is shown in (b). The pressure spheres house the main vehicle computer, batteries, and some sensor electronics.

Chemistry	Mass (kg)	Number of Cells	Energy (kW-hr)	Comment
Ag-Zn (LR30)	28.2	56	3.6	10 hr rate at 0° C
Li-ion (Yardney)	20.5 (est.)	128 (est.)	2.4 (est.)	7 hr rate at 25° C
Ni-Cd (DD)	37.8 (est.)	122	1.6 (est.)	5 hr rate at 25° C
Li-Thionyl Chloride (DD)	26.9	122	10.25	280 hr rate at 25° C

Table 2.1: Possible battery packs for the Odyssey IIb AUV assuming a single 17-inch glass sphere (pressure housing) carrying the maximum number of cells. The first three battery chemistries are secondary (rechargeable) cells and the last is a primary (single use) cell technology. The Li-ion cells are not yet commercially available. The comments for each chemistry give the discharge time and temperature assumed in calculating the energy capacity of each battery pack. Since the number of cycles possible on a rechargeable pack is dependent upon the rate and depth of discharge of prior cycles on the battery pack and can vary substantially from cell to cell, this quantity can typically only be roughly estimated (in the absence of extensive field experience with a particular battery chemistry). We have determined that the Ag-Zn pack has a lifetime of approximately 30 cycles when deployed on the Odyssey IIb AUV. Figure after Bales [54].

We can see an acoustic tomography source mounted on the nose of the first vehicle as well as a modem/homing transponder mounting on the aft sphere (protruding through the inner fairing). A detail of the inside of the Odyssey IIb with the inner fairing removed is shown in Figure 2.2(b) which also shows a closer view of the tail cone of the vehicle. The tail cone is a modular unit containing the thruster and the pitch and yaw actuators and control surfaces (the upper rudder fin and the propeller have been removed from the tail cone in this picture).

The Odyssey IIb vehicle is powered by batteries which reside in the aft sphere. Not surprisingly, the energy source available to the vehicle during any given mission is one of the most important constraining factors in mission planning. For this reason, we would like to have a battery which is as energy-dense as possible. Several different battery chemistries have been studied (see Bales [54]) for the Odyssey IIb's battery pack. Table 2.1 gives some

Dimensions	2 m (length) $\times$ 0.6 m (max. diameter)
Displacement	165 kg
Thruster	1 electric (brushless) 20 lbs max. thrust
Depth Rating	6000 m
Energy	Battery, up to 10 kW-hr
Endurance/Range	12 hours at 5 km/hr max.
Control	Fully autonomous or acoustically controlled
Payloads	CTD, ADCP, Cameras, Sidescan Sonar Acoustic Tomography, Turbidity
Navigation	Compass and rate gyros, Acoustic LBL system
Fleet Status	5 operational AUVs
Reliability	Highly robust: over 300 deployments

Table 2.2: Specifications and capabilities of the Odyssey IIb class of AUVs.

possible Odyssey IIb battery packs based on these battery chemistries. These possible battery packs assume a maximum volume of one 17-inch glass sphere (as pressure housing) carrying the maximum number of cells. The first three battery chemistries are secondary (rechargeable) cells and the last is a primary (single use) cell technology. The Li-ion cells are not yet commercially available. The comments for each chemistry gives the discharge time and temperature assumed in calculating the energy capacity of each battery pack. Since the number of cycles possible on a rechargeable pack is dependent upon the rate and depth of discharge of prior cycles on the battery pack and can vary substantially from cell to cell, this quantity can typically only be roughly estimated (in the absence of extensive field experience with a particular battery chemistry). The Odyssey IIb battery pack most commonly used is based on the Ag-Zn chemistry. Our experience with these battery packs indicates that a useful lifetime of approximately 30 recharge cycles is possible with careful monitoring and control of the discharge and recharge of the battery pack.

A summary of the specifications and the capabilities of the Odyssey IIb AUV are given in Table 2.2. These vehicles have proven to be highly robust, having been deployed in over 300 missions world-wide, in such diverse missions as under-ice mapping in the Arctic, exploration of plumes from thermal vents on the Juan de Fuca Ridge, studying ocean fronts in the Haro Strait, and searching for giant squid off the coast of New Zealand.

2.4 Problem Domains

As with any new scientific tool or methodology, there are many issues and uncertainties in doing oceanographic surveys with AUVs. Some of theses issues are straightforward in nature and can be easily understood (if not remedied) while others can be quite subtle. The following discussion is included in this work at this point so that the reader may better understand the context within which the developments of later chapters is undertaken. We also raise some issues here which will be neglected in subsequent chapters, either for the sake of clarity or to reduce the complexity of the task at hand. The following list of problems and challenges is also not meant to be exhaustive. Rather, it is intended to convince the reader that surveying with AUVs is a discipline which, while much progress has been made of late, is still in its infancy, containing many issues yet to be explored.

2.4.1 Engineering Challenges

The references mentioned in Section 2.2.5 are primarily concerned with the development of the autonomous underwater vehicle from an engineering or technological standpoint. Even though AUVs have begun to enjoy a certain amount of success in the oceanographic community, there is still much basic level engineering work to be done to improve the capabilities and the robustness of AUV survey systems. We discuss some salient engineering problems below.

Limited Energy Capacity

Battery power is one of the fundamental metrics by which any autonomous system is measured. As shown in Table 2.1, many competing battery chemistries are available for use on an AUV. However, none of these chemistries can give an AUV both high speed and long endurance capabilities. There is a fundamental trade-off between speed and mission duration, and this trade-off must be considered when designing or choosing an AUV for a particular experiment. The AUV's energy system should be matched to the spatial and temporal scales of the oceanographic process of interest. Until improved battery technologies are available, AUVs will be constrained to relatively low operational speeds (3-8 knots)

since propulsion loads dominate AUV energy consumption.

Limited Computational Power

Sophisticated electronics and control systems are required for an AUV to successfully meet mission objectives. However, the sophistication of the computers necessary to carry out such tasks pales in comparison to the computational requirements involved in running models of oceanographic phenomena in real time. To implement model-based adaptive sampling strategies on AUVs, we need to run models of the phenomena of interest on the vehicles concurrent with the collection of survey data. To place such computational capabilities on an AUV would incur too great an energy cost, and, in many cases, the equipment would be too large to fit the space available inside the AUV. For this reason, it is not currently possible to implement model-based sampling strategies with AUVs if the computation is to be done in real-time using the AUV's computational resources alone. This situation will surely change as smaller, faster, and more energy-efficient computational engines become available. We can also ameliorate this problem by off-loading the AUV's computational burden onto an external compute enginer via telemetering of the AUVs mission data. This presumes an adequate (fast) communication link between the AUV and the external computation platform. As we will see below, this presumption is not always valid.

Sensor Noise and Navigation Errors

Investigators rely on accurate descriptions of the sensor noise associated with the surveying process when analyzing sampled data. Even though the AUV is not itself a sensor but a mobile sensor platform, it can introduce noise into the various observations through many modalities. The most powerful of these is due to uncertainties in vehicle position. Errors in vehicle location make it difficult to infer the spatial structure of a phenomenon. Understanding the effects of these errors is essential when analyzing data from AUV surveys. Furthermore, improving the navigational accuracy of AUVs requires both internal (compass, rate gyros, INS) and external (acoustic, GPS) navigational aids, as well as computational resources, to take advantage of the data collected from these resources. This remains an active area of research in the AUV community.

Communications Systems

Communication in the ocean over even modest distances can be quite problematic when high data rates are necessary. Nevertheless, fast and reliable communications systems will be required to realize the full potential of the AUV for the coordinated multiple vehicle surveys implied by the AOSN paradigm (Section 1.1.3). Periodic communication from the AUV to a base station is also desirable during survey missions to facilitate adaptive and off-board model-based sampling strategies. These issues remain to be adequately addressed.

2.4.2 Algorithmic and Computational Challenges

Algorithmic and computational problems predominately arise from three areas: (i) the mismatch of properties of the sampling process or the physical phenomena of interest with the assumptions required by the common data processing/process modeling techniques, (ii) inadequacies or inefficiencies of the algorithms, or (iii) our imperfect understanding of the processes of interest. While these problems are usually independent of the data collection method or system, they are often exacerbated in AUV survey scenarios. The fact that AUVs are often used to study processes at length and time scales which have not previously been possible leads to a fundamental lack of understanding of the evolutionary dynamics of the phenomena of interest at the scales of the AUV survey.

Non-Causality of Spatial Variables

Several efficient estimators exist which operate on a single causal variable, time. It is the causality of the the temporal variable which allows these algorithms, such as the Kalman filter and the RTS smoothing algorithms, to proceed in a highly efficient, recursive manner. However, oceanographic processes typically evolve in three spatial and one temporal dimension. Since the spatial variables of the processes do not exhibit this time-like quality of causality which admits efficient, recursive algorithms, the optimal inversion of spatial data (even without an added temporal dimension) is computationally expensive. This fundamental difficulty is encountered in almost all inversion techniques for spatially distributed data. Multiscale processing, which will be discussed further in Chapter 6, addresses this difficulty, but, since it is a new methodology, it is not yet suitable for application to real-time

computation of process field estimates.

Non-stationarity/Non-homogeneity of Processes

Another challenge to surveying with AUVs is the fact that real oceanographic processes are often non-stationary in time and/or non-homogeneous in space. A survey of such fields would need to be able to locally react to non-stationarity/non-homogeneity to accurately reconstruct the process field. That is, the AUV must be able to react by sampling more densely in regions of high spatial or temporal variability. To do this, the vehicle must be able to identify these variations in the process in real-time. This is not practical in many cases due to the inadequacy of the available field inversion techniques both in computational complexity and in their inability to invert non-stationary/non-isotropic data.

Inadequate Field Inversion Techniques

Most space-time field inversion techniques create estimates which assume that the underlying fields are stationary and homogeneous. This assumption is incorporated into the inversion usually as an explicit statistical model of the correlation structure of the process of interest. Such techniques fail when the correlation models do not meet these criteria. Thus, we see that these techniques require prior knowledge about the process under investigation in order to specify realistic correlation structures. Another inadequacy of many inversion methods is that they do automatically produce estimation error statistics. This can make it difficult to assess the validity of interpolated fields. Because each inversion method is unique in its characteristics, we discuss the two most popular methods and a promising new technique below.

Kriging A variant of Gauss-Markov estimation where only the mean is computed. Also know as method of empirical orthogonal functions (EOFs) or universal kriging when estimating more than just the mean. This algorithm is statistically "optimal" but suffers from the fact that it is extremely computationally intensive. This method also requires an a priori statistical model of the correlation structure of the field. It would not be possible to compute kriged estimates of a field on the fly using an AUV's main

vehicle computer due to the large quantity of data collected during AUV surveys. See Isaaks and Srivastava [24] for further detail.

Objective Mapping Also known as objective interpolation or objective analysis, this is in essence a least-squares estimation technique and, consequently, is also computationally expensive. This method is further hampered by the fact that it provides no statistical estimate of the estimation error. While objective mapping has achieved sucess in the fields of oceanography, meteorology, and geophysics, the computational complexity of the algorithm precludes its use for real-time computation on an AUV computers. An extended discussion of objective mapping can be found in Wunsch [55].

Multiscale Processing This new processing technique gains efficiency by representing multiple spatial dimensions in terms of a single causal variable, scale. The algorithms admitted by this change of variables are analogous to numerous state-space algorithms, such as the Kalman filter. This method also requires an a priori scale-spaces covariance model for the process of interest. Given this model, multiscale techniques are remarkable fast. However, developing a scale-space model for a process can be quite difficult since no system identification or realization theory exists for the technique. This technique has the advantage of producing estimation error fields as part of the ongoing field inversion. For further detail, see the theses of Chou [56], Fieguth [57], and Irving [48].

2.4.3 Survey Design and Adaptive Sampling

There is a need to develop operational paradigms for AUVs which take advantage of the unique abilities of these vehicles. Survey sampling with AUVs is fundamentally different from the ways in which other oceanographic instruments have previously been used. Because AUVs have only recently become useful tools for oceanographers, we are only now learning how to effectively and efficiently use this new tool. The topics discussed below are areas which further work is required in order to achieve this goal.

Identifying the Proper Sampling Domain

In Figure 1.1 we saw that the ranges of space and time over which the oceanographer might wish to sample, using either AUVs or more traditional sampling systems, are quite broad. Deciding which processes are appropriately studied using an AUV is an important first step in learning how to use AUVs in an oceanographic research or exploration setting. This is not always as simple as defining whether or not a particular process falls within the AUV survey domain "box" of Figure 1.1, since this box represents only the spatial and temporal *boundaries* of AUV operation and should not be construed to imply that all combinations of survey spatial resolution and total survey time which fall within this box are necessarily achievable with an AUV. In general, careful consideration of the underlying sampling strategy is required when determining whether or not an AUV would make a useful contribution towards the study of a particular oceanographic phenomena.

Appropriately Sized Surveys

There are two broad classes of problems which oceanographers typically address. The first is the spectral estimation problem, which involves designing a series of AUV missions from which an estimate of the spatial spectrum of the phenomena is to be made. The second broad problem category is field estimation, where an estimate of the spatial field of the process of interest is reconstructed from survey observations. The simplest way that this later problem can be addressed is through a grid survey, where the resolution of the spatial grid and the total survey time must be traded-off against each other in order to achieve an "optimal" reconstructed field. This question will be addressed in detail in Chapter 3.

Reactive Surveys

The uniform grid survey mentioned above requires that some prior knowledge of the process of interest be used to help determine the appropriate trade-off between spatial resolution and mission duration. However, this scenario is not well suited for missions in which the objective is to determine fluxes of a variable (such as heat, for example) or to otherwise characterize highly localized and dynamic phenomena. One way to address such surveys is to allow the AUV to alter the mission trajectory based on incoming data. A simple version

of such a scenario is a search mission in which an AUV searches in a regular pattern until a distinctive feature is detected. The then AUV enters into a feature tracking mode, where it reactively surveys the phenomena. In this scenario, not only does the vehicle react to the presence of the detected feature, but it must also react to the evolution of the feature to continuously reposition itself within the feature or to move along the boundaries of the feature. Some work on reactive survey algorithms has been done (for example, [53]), with results that are promising but as yet unrealistic for oceanographic research. Continued work on this particular type of survey is much needed, particularly to guard against, detect, and correct poor surveys decisions due to noisy data .

Coupled Model/Observational Systems

In order to improve the reactivity of an AUV survey, we would like to be able to incorporate spatially diverse measurements into a physical process model and use the predictive power of the coupled observational/modeling system to dynamically alter the trajectory of the AUV to improve the quality of the collected data. Numerous difficulties arise in trying to implement such a system. These difficulties include the following:

Communication A communication infrastructure is required to take advantage of distributed observational assets. The complexity of such a system grows precipitously as the speed of the network (or the volume of data being transmitted) increases. Although such networks are in common use on land (i.e., the internet), the complexities of sound propagation in water hinders the application of prior experience to the development of underwater communication networks. Another challenge with such systems is that they typically are very power consumptive (although not nearly so consumptive as AUV propulsion systems), restricting their use with many battery powered observational assets.

Data Assimilation The data gathered from the various observational platforms will represent observations over a broad range of space and time scales, as well as many physically incompatible phenomenological variables (such as temperature and topography). These data must be assimilated to drive the evolution of the process model.

Data assimilation techniques remain an active area of research.

Model Computation Assuming that we have a model of an oceanographic process (we let the development of such models lie within the purview of the oceanographer), we must be able to run this model in (near) real-time to take advantage of its predictive ability to adaptively alter the AUV's survey trajectory or the configuration of other observational assets. As discussed previously, the computational burden of these oceanographic models is enormous, making the implementation of a coupled observational/modeling system quite difficult if the computation must be done on-board an AUV.

Control Finally, the scientist must be able to exercise high-level control of such a network through a low-bandwidth (typically satellite) channel. This requires that the network of sampling systems be essentially autonomous, with only supervisory control from the scientist. Operational algorithms must be developed to enable such a system.

Multiple Vehicle Operations and Coordinated Surveys

Surveying phenomena with multiple vehicles is one of the most direct ways to reduce the error in an uniform grid survey of a process, provided that the surveys conducted by the individual vehicles are coordinated to minimize errors in the reconstructed field. This requires that vehicles know the location of their companion AUVs as well as have a shared survey plan. This can accomplished with current technologies. New possibilities arise when we let one or more of the vehicles share the lead in an adaptive survey which reacts to the data collected by the loose network of vehicles. Research efforts in communication, modeling, and vehicle behaviors will be required to realize coordinated surveys with several AUVs.

2.4.4 Sampling Theoretic Issues

A fundamental difficulty is sampling with AUVs is the confounding of space and time through the AUV survey trajectory. Of course, when the processes of interest does not evolve significantly over the duration of the survey mission, this is not longer a difficulty

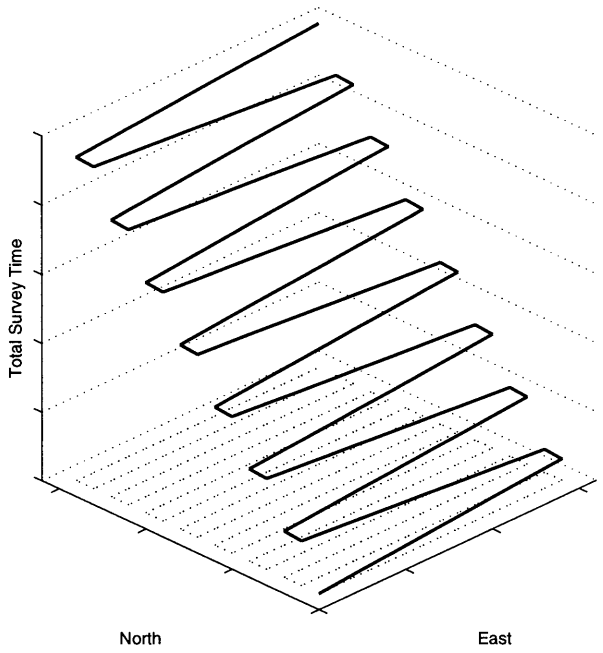

Figure 2.3: Surveying in both space and time. Due to the finite velocity of the AUV, any survey which ranges over spatial dimensions must also range over the temporal dimension as well. Here, the mission is a simple "lawn-mower" survey where the AUV surveys back and forth in a plane. In reality, the AUV is surveying in a three dimensional space consisting of two spatial dimensions and one temporal dimension, as shown. This phenomenon of mixed space-time sampling is fundamental to all surveys which employ AUVs or any moving sensor platform.

since the measurements essentially range only over space. However, many if not most of the processes which we wish to sample with AUVs are ones which evolve rapidly in both space and time, and spatial and temporal undersampling is inevitable.

Space-Time Confusion

As stated above, perhaps the most fundamental difficulty in sampling with AUVs is the intertwining of space and time samples through the AUV survey trajectory. Unlike conventional sampling techniques where, for example, an array of sensors takes samples at numerous locations in space at each sampling instant, an AUV samples only a single point in space at each sampling time (or a few points if multiple AUVs are employed). Due to the finite velocity of the AUV, any survey which ranges over spatial dimensions must also range over the temporal dimension as well. A simple "lawn-mower" survey mission is shown in Figure 2.3. The AUV surveys back and forth in a two dimensional plane. In

reality, though, the AUV is surveying in a three dimensional space consisting of two spatial dimensions and one temporal dimension, as shown. This phenomenon of mixed space-time sampling is fundamental to all surveys which employ AUVs or any moving sensor platform. In the limiting case of a process which does not significantly evolve in time over the course of a survey mission (geomagnetic fields, for instance), the velocity constraint on the AUV is no longer restrictive. However, if the AUVs are being employed to study a phenomenon which evolves on time scales comparable to or faster than the total survey time, then the spatial field sampled by the AUV will be seriously corrupted by temporal evolution of the dataset, a phenomenon which we call "blurring". For AUV studies of oceanographic processes, this problem dominates other sampling and survey design issues. Therefore, an understanding of the effects of temporal blurring is necessary in analyzing data from AUV surveys of oceanographic processes.

Currents and Doppler

Consider for the moment the following thought experiment. We wish to study, using an AUV, a time evolving, uni-dimensional spatial field which consists of a single plane propagating wave with propagation speed, c, propagating in the $+x$-direction. The AUV surveys at its own speed, v. Consider the problem of estimating the spatial frequency of this process. If the AUV is moving in the positive direction, then the estimate made from the survey measurements of the wavenumber of the plane wave will be lower than its actual value due to the familiar Doppler effect. Indeed, if the vehicle's speed and the propagation speed of the plane wave are equal ($v = c$), then the wavenumber estimated from the survey samples will be zero. If the AUV's speed is greater than the propagation speed of the process of interest, then the estimated wavenumber will be too high. A similar phenomenon occurs when the AUV moves in the $-x$-direction.

While this effect is a well-known perturbation in many estimation problems, the effect is greatly magnified in the case of oceanographic processes due to the low propagation speeds observed. Thus, instead of a perturbation of a small percent of the actual value, we see that the estimated wavenumber can differ by more than 100 percent of the actual value and can even have the wrong sign. Obviously, the Doppler effect can be quite disastrous to an

AUV oceanographic survey. In the case where the propagation speed and the vehicle speed are both known, the correct wavenumber can be calculated (to some experimental precision which is not affected by the Doppler effect). If one of these speeds is not known precisely, then it is not possible to estimate the wavenumber of the plane wave with any accuracy.

This problem is exacerbated by the presence of oceanic currents within the survey domain. This introduces a third speed (velocity in the more general case of multiple spatial dimensions) which must also be precisely known in order to make accurate estimates. To see this, consider the case of an AUV which has an earth relative measure of its own speed (such as would be given by an acoustic long-baseline (LBL) navigation system). We assume perfect knowledge of the propagation speed of the process of interest. If an unmeasured (unestimated) current were present in this survey domain, we would, again, not be able to accurately estimate the wavenumber of the single wavenumber component. Fortunately, it is often the case that accurate values for the maximum magnitude of the local currents are known, allowing errors bounds to be placed on the estimate of the single wavenumber.

So far, we have discussed a highly idealized deterministic process, a single plane wave. This is of course a gross oversimplification of processes that we would explore with an AUV. Two issues immediately spring to attention. The first is the fact that there will be a spectrum of waves composing any real oceanographic phenomenon. While we have seen that it is difficult to estimate a single wavenumber, the task is even more daunting when there is a continuum of wave numbers for which you want to estimate the spectral density. Second, an actual oceanographic process of interest most likely does not obey the linear (wave-equation) dispersion relation which we assumed above, with the implication that we cannot know the propagation speed of a measured wave unless we know its wavenumber exactly. This, of course, poses a serious limitation to surveys with AUVs.

Non-Uniform Sampling in Multiple Dimensions

Perhaps one of the most fundamental departures from the typical sampling theoretic domain is the fact the AUV measurements need not be taken on any uniform grid. Because of this, the number of available interpolation and estimation techniques decreases while the computational complexity increases. This is a significant disadvantage since the computational

complexity of these inversion techniques typically grow as the cube of the total number of sample points. Thus, for an AUV survey of one hour and a standard sampling rate of 5 Hz, we would generate eighteen thousand survey samples, necessitating the inversion of a matrix of size eighteen thousand by eighteen thousand for a standard Kriging inversion [24]. This is clearly not feasible. Given current technology, the question is not how long would it take, but could it be done at all, even for a relatively short survey. Of course, we can ameliorate this problem by binning the data before inverting. However, this can reduce the fidelity of the reconstructed field beyond useful limits for many oceanographic applications. Thus, we see that irregular sampling can place serious practical constraints on the problem of surveying oceanographic phenomena with AUVs.

2.5 Discussion

In this chapter we have given references on topics related, either directly or indirectly, to the problem of surveying oceanographic processes with AUVs. These references are not certainly not exhaustive, but give pointers into the literature for the benefit of the reader. We have also presented an overview of the specifications and capabilities of the Odyssey IIb class of AUVs. We utilized this presentation to raise some of significant vehicle design and engineering issues.

We have also examined several other issues and challenges inherent in surveying with AUVs in this chapter. These issues are necessary context for the development of later chapters. They also point to areas in which further exploration is required. In particular, the lack of computationally efficient inversion algorithms for spatially distributed data is a difficulty which goes to the heart of the whole sampling problem. We will see in Chapter 6 that new and promising spatial data processing techniques are on the horizon. The application of these techniques to the AUV survey sampling problem has the potential to revolutionize the way that oceanography is practiced, through the realization of fully functional coupled observational/modeling systems. However, for this to be possible, many of the engineering challenges identified in Section 2.4.1 must also be addressed. Power management and improved battery technologies will be vital to the implementation of autonomous ocean

sampling networks, as will the development of reliable and fast underwater communication and navigational networks. Finally, advances in the area of reactive and adaptive survey design will be necessary as an enabling technology of the AOSN paradigm.

Chapter 3

Performance Metrics

3.1 Introduction

The effectiveness of a survey can be addressed quantitatively only within the framework of a given oceanographic experiment. For one problem, it may be the best measurement of total heat flux through a surface, for another it may be characterization of horizontal variability across an ocean front. For the purposes of this thesis, the objective will be to obtain the best representation, in a least-squares sense, of a measured scalar field. There are two major sources of error, arising from the finite spatial resolution of the survey and the finite time required to sample. Temporal evolution of the ocean during a survey has the effect of "blurring" the true field, driving one to increase vehicle speed and minimize survey distance; however, vehicle speeds are strongly energy constrained, and decreasing the survey distance effectively reduces the sampling resolution (assuming a fixed survey area). Thus, the trade-off is fundamentally between errors introduced by temporal "blurring," and errors introduced by spatial undersampling.

Perhaps the most important constraint on an underwater survey system is its energy capacity [58]. Consequently, an important figure of merit is the energy required to accomplish a survey. In a practical sense, energy is minimized by reducing the distance a vehicle must travel and optimizing its speed for efficiency. It will be shown that for surveys which are not time-constrained, the energy reduction is linearly proportional to the reduction of distance traveled. For time constrained surveys, the energy savings achieved by the

distance-reducing strategies can approach the cube of this reduction of distance.

Compared to vehicles deployed and operated from surface vessels, energy saving takes on an additional dimension for long-deployment systems like the Autonomous Ocean Sampling Network (AOSN) [20]. For vehicles which are serviced between missions, perhaps on an oceanographic vessel, there is little incentive to use less than the vehicle's total useful energy capacity in any given mission. Instead the objective is to make best use of the energy available, since the logistical expenses (such as ship time) are likely to dwarf the cost of the energy onboard the vehicle. However, choices about the consumption of energy are more complex in long-deployment scenarios, such as in AOSNs, since the bulk of the system's energy is stored at network nodes rather than in the vehicles themselves. In this case, the trade-off is between many low-resolution surveys, and a few surveys at a higher resolution. Issues of the complexity and reliability of the docking and recharging mechanisms must also be addressed. Thus, for long-deployment systems, there may be an incentive to use less than the total energy capacity of the vehicle during each mission.

This chapter provides some tools for quantifying the trade-off between different survey strategies. In Section 3.2 we review the energy economics of surveying with AUVs and generate an energy consumption function which is dependent upon the survey sampling resolution, λ, and the total survey time, τ. Next, we analyze the errors inherent in these surveys as functions of λ and τ in Section 3.3 and combine these errors to form an overall survey performance metric. Finally, Section 3.4 reviews the analysis of the preceding sections, discussing the assumptions made and the overall utility of the performance metrics.

3.2 Energy Analysis

One of the most important constraints on an underwater survey system is its energy capacity [58]. Consequently, an important figure of merit is the energy required to accomplish a survey. An AUV's energy consumption for a given survey mission is determined by three parameters: the area over which the survey is made, the resolution of the survey, and the total time that it takes to complete the survey. Let us consider for the moment a simple grid survey at spatial resolution λ, over a fixed square area A. The total linear distance, L,

Symbol	Value	Description
H	40 W	Hotel Load
η	0.35	Propulsion Efficiency
C_d	0.006	Drag Coefficient
S	3 m	Wetted Surface Area
ρ	1000 kg/m	Density of Water

Table 3.1: Parameters for the Odyssey IIb vehicle and sea water.

traversed in the survey is given by

$$L \approx \frac{A}{2\lambda} - 2\lambda \approx \frac{A}{2\lambda}, \tag{3.1}$$

where 2λ is the distance between points or tracklines in a uniform grid survey. The relationship above is clearly only an approximation since the shape and size of the survey relative to the survey resolution must be taken into account. However, for a rectangular area with both sides significantly larger than λ, the approximation will be good. Assuming that this approximation holds, the vehicle speed required to complete a survey in a given time is

$$V = \frac{L}{\tau} \approx \frac{A}{2\lambda\tau}, \tag{3.2}$$

where τ is the total survey time. Finally, given V and τ, we compute the total energy consumption [20] for a survey,

$$E_{tot} = \left[\frac{\rho C_d S V^3}{2\eta} + H\right]\tau, \tag{3.3}$$

where ρ is the density of water, C_d is the drag coefficient for the vehicle, S is the vehicle's wetted surface area, η is the propulsion efficiency, and H is the vehicle hotel load. Values for these parameters for the standard Odyssey IIb AUV are given in Table 3.1. The first term in the right hand side of Equation (3.3) is associated with the propulsion of the vehicle through the water; the second term is due to the energy consumed by the vehicle's computer, sensors, electronics, etc. (the "hotel" load). We see from Equation (3.3) that E_{tot} decreases with decreasing V and/or τ. Unfortunately, Equation (3.2) indicates that V and τ cannot both decrease at the same time without changing the resolution of the survey. We must make

a trade-off between these two mission parameters to minimize the total energy consumed during the survey. If we divide the total energy consumed by the total survey distance we have an equation for the energy consumption per unit distance,

$$\frac{E_{tot}}{L} = \frac{\rho C_d S V^2}{2\eta} + \frac{H}{V}. \tag{3.4}$$

Taking the derivative of Equation (3.4) with respect to velocity, V, and setting this equal to zero gives us the optimal vehicle speed

$$V_{opt} = \left(\frac{H\eta}{\rho C_d S}\right)^{\frac{1}{3}}. \tag{3.5}$$

This velocity is optimal in the sense that it minimizes energy consumption per unit distance traveled. This relationship is shown in Figure 3.1, where we see that at its optimal speed of 0.92 m/s, the Odyssey IIb class of AUVs will achieve an energy performance of 65.27 J/m. This corresponds to a maximum survey path length (or range) of approximately 275 km based on a 5 kW-hr (1.8×10^7 J) battery pack. Note further that by increasing the operational speed of the AUV to twice the optimal speed the energy consumed per unit distance also approximately doubles. This is because we are in an approximately linear region of the energy consumption curve (Figure 3.1) due to our proximity to the global minimum. This fact is fortunate since typical operating speeds for the Odyssey IIb vehicles fall in the range of 1.5 to 2.0 m/s.

By substituting Equation (3.5) into Equation (3.3), we find that the minimum total energy consumption required to complete a survey at spatial resolution λ in time τ is

$$E_{min} = \frac{3LH}{2V_{opt}} = \frac{3}{2}\tau H. \tag{3.6}$$

This is a lower bound on the total energy consumed in a time constrained survey.

3.2.1 Application

To further illustrate our discussion of survey economics, we will employ an example. Let the survey domain be a fixed square area, $A = 9$ km^2, and compute the total survey

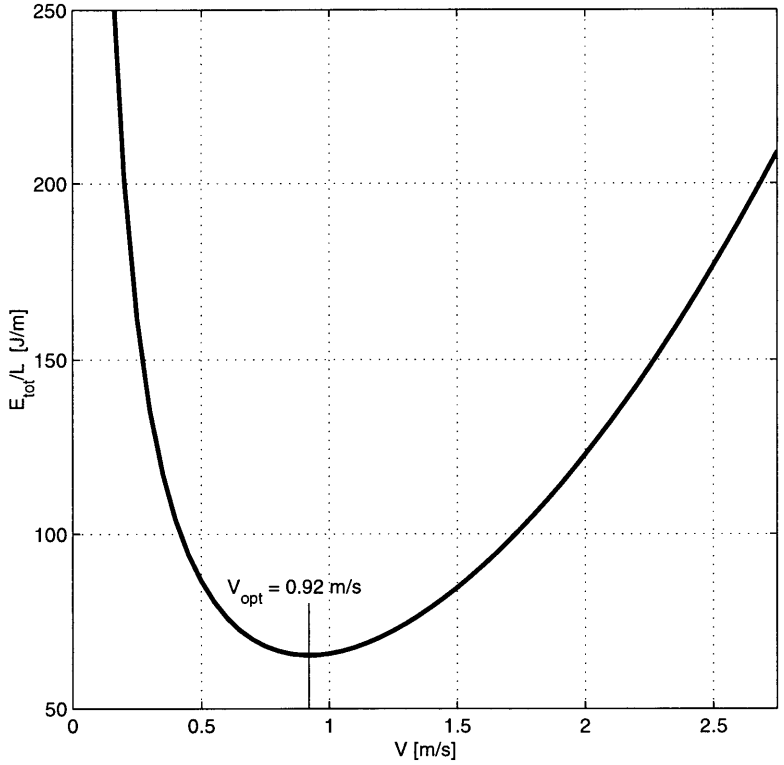

Figure 3.1: The energy consumed per unit distance as a function of vehicle speed for the Odyssey IIb AUV. The optimal velocity is 0.92 m/s with a corresponding optimal energy consumption per unit distance of 65.27 J/m. From Equation (3.4) we see that the energy consumed per unit distance increases asymptotically as $1/V$ for speeds less than V_{opt} and as V^2 for speeds greater than V_{opt}.

energy as a function of (λ, τ). The results of this computation are shown in Figure 3.2. The contours show the energy that would be consumed during a survey for any given pair of survey parameters (λ,τ). We have plotted energy consumption contours in equal step sizes beginning at a value which is one sixteenth of the total energy contained in an Odyssey IIb battery pack and ending at a contour corresponding to eight times the energy of the Odyssey IIb battery pack. This covers the range of current and near future battery technology. The behavior of the contours for higher total energy consumption (lower left portion of plot) should be evident from the contours shown. From this figure we see that the total survey energy is greatest for surveys which are densely sampled and/or completed quickly. However, we must also consider the effects of physical constraints imposed by the AUV on the surveying process. There are two such constraints.

For the sake of this example, let us assume that we have a 5 kW-hr battery available.

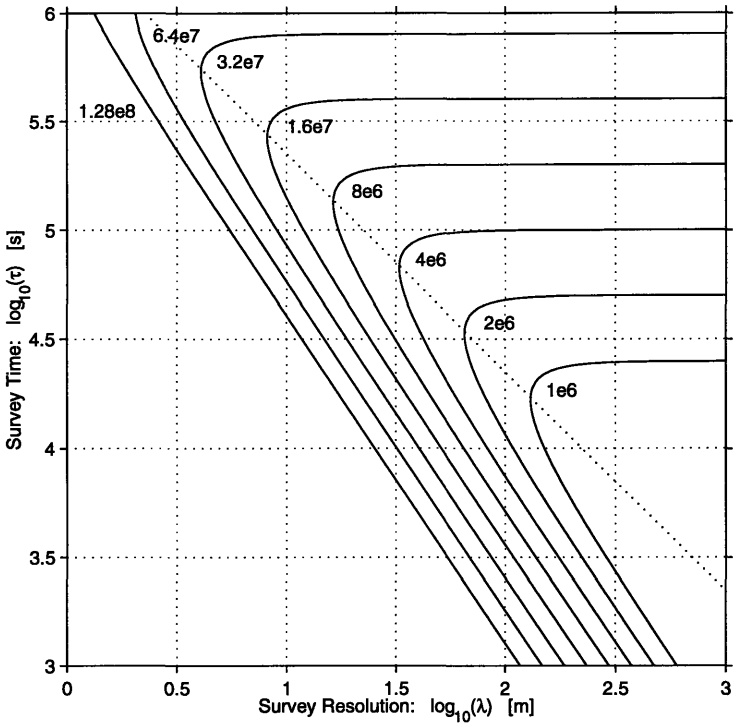

Figure 3.2: Total survey energy consumption as a function of survey spatial resolution, λ, and total survey time, τ, for a grid survey of a square survey domain with $A = 9\,\mathrm{km}^2$. Contours of energy consumption are plotted for values in the range $E_{Ody}/16 \leq E_{consumed} \leq 8E_{Ody}$, where $E_{Ody} = 1.6e7$ J is the energy contained in an Odyssey IIb battery pack. The dotted line divides two domains of the energy consumption curve. In the upper domain, the total energy consumed is independent of the spatial resolution at which the survey is conducted. These surveys are constrained by the vehicle hotel load. In the lower portion of the plot, spatial resolution and total survey time both influence the energy consumption of a given survey. As spatial resolution decreases (corresponding to finer grid spacing) the total survey energy increases while total energy consumption increases with decreasing survey time (faster vehicle speed). The typical AUV surveys will be designed to fall into the lower region of the total energy consumption plot.

This is realistic for a rechargable battery pack for Odyssey IIb given a focused research effort (primary cell technology is currently available for 10 kW-hr battery packs which would still fit in an Odyssey IIb pressure housing, but these packs would not be rechargable). The 5 kW-hr batteries constrain the total survey energy to be no more than 1.8×10^7 J. Also, hydrodynamic constraints on the vehicle require that it operate at velocities equal to or greater than 0.25 m/s to maintain control authority. When taken together, these energy and velocity constraints define a finite region of (λ, τ) space within which it is reasonable for the vehicle to operate. This region, referred to as the "survey envelope", is shown in Figure 3.3. The straight edges of the survey envelope correspond to the AUV speed

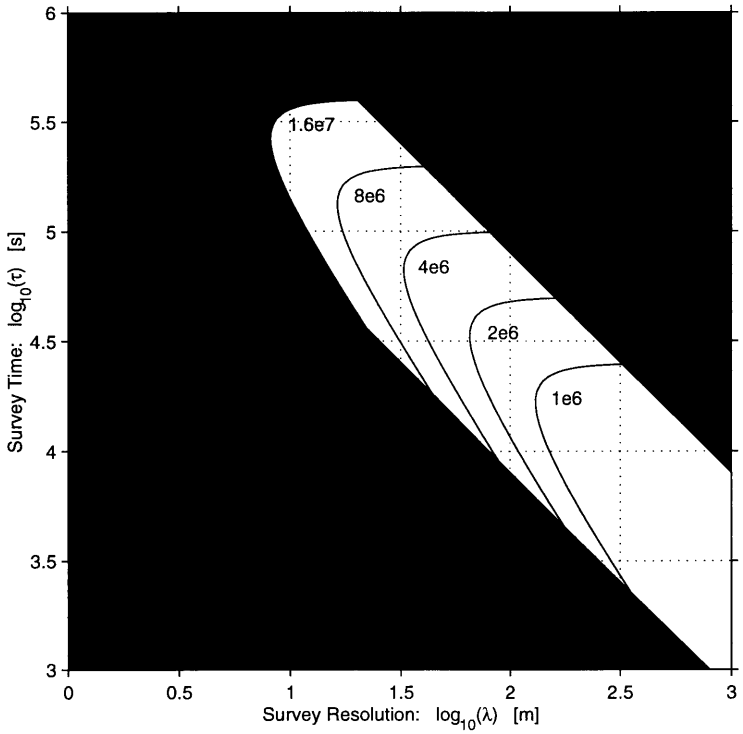

Figure 3.3: The Odyssey IIb survey envelope defines the operational region of the AUV in terms of the survey resolution λ and total survey time τ. This survey envelope is derived from the finite energy supply (batteries) of the vehicle and the vehicle's operational velocity range. The envelope shown is for a fixed square area grid survey with $A = 9\,[km^2]$.

constraints and the curved edge near the top of the envelope is due to the finite energy stored in the AUV's batteries.

3.2.2 Survey Trajectories for 3-D Sampling

The calculation of total survey energy as a function of (λ, τ), as shown in Figure 3.3, assumes a two-dimensional survey domain with a uniformly spaced grid survey trajectory (so that Equation (3.1) is a reasonable approximation). However, many (if not most) oceanographic survey missions with AUVs will require operation in all three spatial dimensions. This does not preclude use of the type of analysis that we have performed above. As demonstrated by Figure 3.4, two-dimensional grid survey patterns can be easily extracted from some types of three-dimensional survey trajectories. For the grid survey with superimposed "Yo-Yo" shown, the total survey energy will increase by a factor associated with the pitch angle of

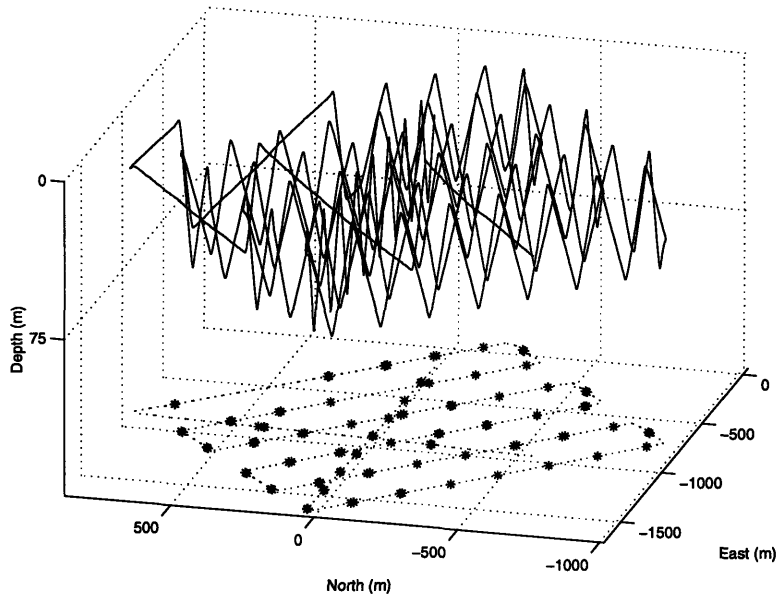

Figure 3.4: A three dimensional survey trajectory performed by the Odyssey II AUV on the Juan de Fuca Ridge, June 25, 1995. The trajectory is comprised of a grid survey in the horizontal dimensions with a "Yo-Yo" superimposed in the vertical. Horizontal samples locations (asterisks) for a plane of constant depth are shown below. Total mission time was 188 minutes.

the AUV. For instance, the pitch angle for the mission shown was 30 degrees, resulting in an increase of total mission path length by a factor of approximately 1.15. This, in turn, requires that the survey velocity increase by a factor of 1.15 if the AUV is to complete the mission in the same time that would have been required for the two dimensional array. Since the energy consumption for most AUV survey missions is dominated by propulsion costs, we can say that the increase in total survey energy consumption is proportional to this factor. In general, the propulsion portion of the total energy consumption (Equation (3.3)) will increase by a factor

$$f = \cos(\alpha)^{-3}, \tag{3.7}$$

where α is the pitch angle associated with the vehicle's "Yo-Yo". As the pitch angle increases, the propulsion energy required will increase more rapidly. There will be some maximum pitch angle above which the AUV cannot function efficiently due to stability and/or velocity limitations. Note also that a survey trajectory such as this inextricably couples the horizontal and vertical spatial resolutions of the survey. If we wish to sam-

ple very densely in a horizontal plane, we will be limited by the maximum pitch angle to very small vertical excursions. This represents a rather severe survey design constraint and motivates a future examination of multiple vehicle operations.

3.3 Error Analysis

In order to assess the degree of synopticity with which an AUV can measure a generic oceanographic process, an understanding of the survey errors inherent in the sampling strategy must be acquired. We have identified two major contributions to the survey error which are dependent upon the spatial resolution and duration of the survey. In terms of spatial resolution, the survey error is dominated by the loss of detail in the reconstruction of the field due the inevitable undersampling of the phenomenon. The dependence of the survey error upon total survey time can be derived from the autocorrelation function of the process of interest. If we have a reasonable understanding of the physics of the process under study (either from a model or experimental data), we will be able to generate analytic error surfaces in terms of λ and τ for any given survey strategy.

Prior to any discussion of survey errors, we must be explicit about the scientific goals of an AUV survey of a given oceanographic process. These scientific goals are embodied in the survey objective function, which is itself dependent upon the specific experiment and process under study. The objective function serves as a metric for the effectiveness of a given experiment in extracting the desired scientific information. For instance, for some processes we may wish to obtain an estimate of the energy density spectrum, $\mathcal{P}(\omega, \mathbf{k})$, of the process. For other processes, it may be that we wish to recover an accurate "snap-shot" of the spatial field. These two scenarios will lead to differing survey objective functions [59, 60], and, in turn, to differing survey strategies. Therefore, we will need to specify our objective function in order to measure the degree of success that we can achieve with a given survey strategy. For the following discussion, and throughout the remainder of this thesis, our goal will be to accurately reconstruct a "snap-shot" of a spatially distributed, time-evolving, scalar parameter process. That is, we want to reconstruct a spatial field which represents, as accurately as possible, the true field at some instance during the survey. This

estimated field will exhibit errors due to spatial undersampling and temporal "blurring" of the underlying phenomenon. For the sake of clarity of analysis, we will assume that any AUV navigational errors are negligible.

3.3.1 Spatial Survey Error

Let us begin by considering a spatially distributed process field, $y(\mathbf{x})$, that does not evolve in time. Assume that we have surveyed this field, producing the samples,

$$\hat{y}(\mathbf{x}_i) = y(\mathbf{x}_i) + w(\mathbf{x}_i), \tag{3.8}$$

where $\mathbf{x}_i$ is the location of the i^{th} sample and $w(\mathbf{x}_i)$ is a measurement noise which is zero mean, white noise with variance σ_w^2 and which is uncorrelated with $y(\mathbf{x}_i)$. From the noisy samples $\hat{y}(\mathbf{x}_i)$ we reconstruct a continuous field which, for simplicity of notation, we also refer to as $\hat{y}(\mathbf{x})$. This reconstructed field will be bandlimited by the multidimensional equivalent of the Nyquist frequency associated with the survey spatial resolution. We define the error field in terms of the real field and the survey reconstructed field as

$$\varepsilon(\mathbf{x}) = y(\mathbf{x}) - \hat{y}(\mathbf{x}), \qquad \mathbf{x} \in \mathcal{D}, \tag{3.9}$$

where $\mathcal{D}$ is the spatial domain of the survey.

We can define any number of error metrics in terms of this error field. Many popular metrics measure some function of the energy contained in the error field. We have chosen to define the error metric as the total energy contained in the error field normalized by the total energy contained in the two constituent fields. Thus, we define the spatial survey error metric to be

$$\varepsilon_\lambda = \frac{\int_{\mathcal{D}} |\hat{y}(\mathbf{x}) - y(\mathbf{x})|^2 d\mathbf{x}}{\int_{\mathcal{D}} \left[|\hat{y}(\mathbf{x})|^2 + |y(\mathbf{x})|^2 \right] d\mathbf{x}}. \tag{3.10}$$

The denominator serves to normalize the energy in the error field. It contains terms for both the estimated and true fields so that the spatial survey error will satisfy $0 \leq \varepsilon_\lambda \leq 1$.

The error metric is given the subscript λ to emphasize that it is a function of the survey sampling resolutions.

For any given experiment, the value of this metric will be a function of survey parameters such as the survey spatial resolution and the measurement noise variance and of the particular realization of the process field, $y(\mathbf{x})$. The dependence upon the process field will cause fluctuations in the value of the spatial survey error metric from experiment to experiment. We would like to be able to remove or average out these fluctuations. We do this by taking the expectation of Equation (3.10). When we take the expectation of the top and the bottom seperately, it becomes clear that the error metric will only take on values between zero and one, with $\varepsilon_\lambda = 1$ indicating that the true and reconstructed fields are totally spatially uncorrelated.

To understand the contribution of the survey process to the spatial sampling error, we begin with the multidimensional version of *Parseval's Theorem* [32], which states that the total energy contained in a signal is proportional to the integral of the squared magnitude of its Fourier transform, i.e.,

$$\int_{-\infty}^{\infty} |g(\mathbf{x})|^2 d\mathbf{x} = (2\pi)^{-n} \int_{-\infty}^{\infty} |G(\mathbf{k})|^2 d\mathbf{k}, \tag{3.11}$$

where $g(\mathbf{x}) \in \mathcal{R}^n$ is a spatially distributed (static) process, $G(\mathbf{k}) \in \mathcal{C}^n$ is its Fourier transform, and $\mathcal{G}(\mathbf{k}) \equiv |G(\mathbf{k})|^2$ is the spatial energy density spectrum of the process. For simplicity of notation, we use a single intregral sign to imply the n-dimensional intregral. In sampling the process field, we will create an estimate of the wavenumber distribution of the process of interest, $\hat{G}(\mathbf{k})$, which is band-limited by the multidimensional equivalent of the Nyquist frequency associated with the sampling resolution λ_s. Therefore, our estimate of the energy density spectrum, $\hat{\mathcal{G}}(\mathbf{k})$, will also be band-limited to this spatial frequencies range. This phenomenon is illustrated in Figure 3.5(c). By employing this multi-dimensional version of *Parseval's Theorem*, we can transform Equation (3.10) to wavenumber space. We define the error associated with spatial aliasing to be

$$\varepsilon_\lambda = \frac{E\left\{\int_{-\infty}^{\infty} \left|\hat{Y}(\mathbf{k}) - Y(\mathbf{k})\right|^2 d\mathbf{k}\right\}}{E\left\{\int_{-\infty}^{\infty} \left|\hat{Y}(\mathbf{k})\right|^2 d\mathbf{k} + \int_{-\infty}^{\infty} |Y(\mathbf{k})|^2 d\mathbf{k}\right\}}, \tag{3.12}$$

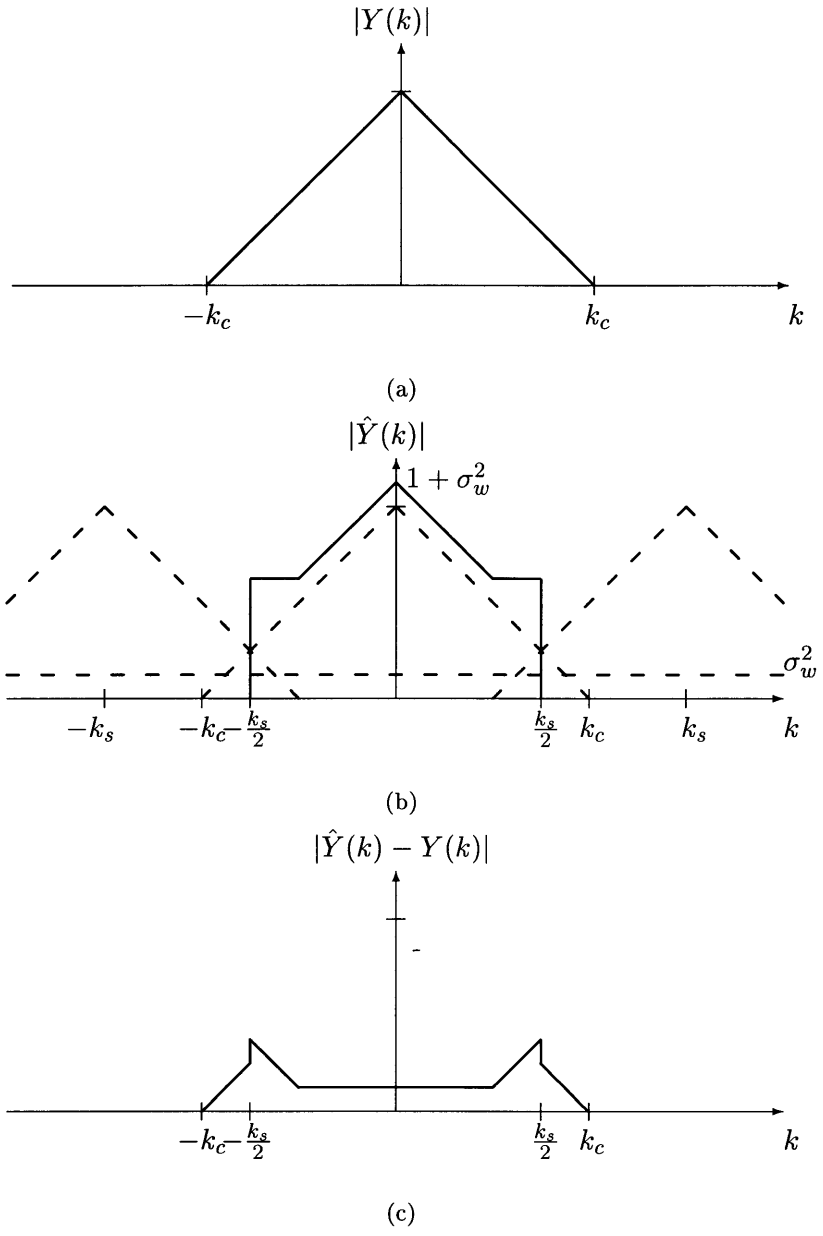

Figure 3.5: Examples of Fourier transforms of the process field, survey reconstructed field, and the associated error field. The Fourier transform of an unidimensional and bandlimited process field is shown in (a). The Fourier transform of the reconstructed field is given in (b). This transform includes the effects of spatial aliasing and a white measurement noise. The Fourier transform of the difference of these two fields is given by the difference of the two transforms, as shown in (c). Although it is shown as a bandlimited signal, the error field will in general contain energy at all wavenumbers due to the fact that the process field will in general be a non-bandlimited signal.

where we have also taken the expectation as described above. In order to interpret this error we must determine the value of $\left|\hat{Y}(\mathbf{k}) - Y(\mathbf{k})\right|$, the Fourier transform of the error field. This is simply the transform of an aliased version of the process field plus some measurement noise and is easy to compute provided that we know the Fourier transform of the process field. The necessary calculations are shown pictorially in Figure 3.5.

Figure 3.5(a) is an idealized version of the Fourier transform of some arbitrary process field. The transform shown as being bandlimited and unidimensional to enhance the clarity of the figure. In general, this transform will be neither bandlimited nor unidimensional. The Fourier transform of the reconstructed field is given in Figure 3.5(b). Note that the effect of aliasing is to "fold over" energy from wavenumbers higher than the sampling wavenumber, increasing the energy in the high wavenumber regions of the transform. The effect of the measurement noise is to increase the energy in the reconstructed field transform uniformly across the spectrum (recall that $w(\mathbf{x}_i)$ was assumed to be a white noise). The combined effects of spatial aliasing and measurement noise produce a reconstructed field transform (shown as a solid line in Figure 3.5(b)) which deviates significantly from that of the process field. Finally, in Figure 3.5(c) we see that the transform of the error field is simply the difference between the process and reconstructed field transforms. Although this transform is bandlimited in the example shown, the error field will generally have energy *at all* wavenumbers. Now, from Figure 3.5(c), we see that the numerator of Equation (3.12) is given by

$$E\left\{\int_{-\infty}^{\infty}\left|\hat{Y}(\mathbf{k}) - Y(\mathbf{k})\right|^2 d\mathbf{k}\right\} = 2\int_{\Omega}|Y(\mathbf{k})|^2\, d\mathbf{k} + \int_{\Upsilon}|W(\mathbf{k})|^2\, d\mathbf{k}, \tag{3.13}$$

where $W(\mathbf{k})$ is the Fourier transform of $w(\mathbf{x})$ and we have used the fact that $y(\mathbf{x})$ and $w(\mathbf{x})$ are uncorrelated to separate their Fourier transforms. The regions of intergration are

$$\Upsilon = \left\{\mathbf{k} \mid \mathbf{k} \in \left[-\frac{|\mathbf{k}_s|}{2}, \frac{|\mathbf{k}_s|}{2}\right]\right\}, \tag{3.14}$$

which is the support of the sampling process, and

$$\Omega = \left\{\mathbf{k} \mid \mathbf{k} \in \left[-\infty, -\frac{|\mathbf{k}_s|}{2}\right) \cup \left(\frac{|\mathbf{k}_s|}{2}, \infty\right]\right\}, \tag{3.15}$$

which is the region of wavenumber space which lies outside the support of the sampling function. Note that the Ω and Υ are exclusive sets and that they partition the whole n-dimensional k-space, i.e., $\Omega \cap \Upsilon = \emptyset$ and $\Omega \cup \Upsilon = \mathcal{R}^n$.

We can now further extend the definition of the spatial survey error as

$$\begin{aligned} \varepsilon_\lambda &= \frac{2\int_\Omega |Y(\mathbf{k})|^2 \, d\mathbf{k} + \int_\Upsilon |W(\mathbf{k})|^2 \, d\mathbf{k}}{2\int_{\Omega+\Upsilon} |Y(\mathbf{k})|^2 \, d\mathbf{k} + \int_\Upsilon |W(\mathbf{k})|^2 \, d\mathbf{k}} \\ &= \frac{2\int_\Omega \mathcal{P}(\mathbf{k}) d\mathbf{k} + \int_\Upsilon \mathcal{W}(\mathbf{k}) d\mathbf{k}}{2\int_{\Omega+\Upsilon} \mathcal{P}(\mathbf{k}) d\mathbf{k} + \int_\Upsilon \mathcal{W}(\mathbf{k}) d\mathbf{k}}, \end{aligned} \tag{3.16}$$

where $\mathcal{P}(\mathbf{k})$ is the energy density spectrum of the process $y(\mathbf{x})$, $\mathcal{W}(\mathbf{k}) = \sigma_w^2$ is the energy density spectrum for the noise process, and where Ω and Υ are the volumes of wavenumber space which respectively lie outside and inside the support of the sampling function [11, 12]. We see from this definition that there are two factors which contribute to the spatial survey error. The first of these arises from the familiar concept of signal-to-noise ratios (SNRs). As the SNR of the sampling process decreases, the noise terms in the numerator and denominator of Equation (3.16) dominate, causing $\varepsilon_\lambda \to 1$ as SNR $\to -\infty$, regardless of the spatial resolution at which the field is sampled. The other factors contribution to the spatial survey error arises because the reconstructed field is aliased with respect to the real field. This effect is governed by the first terms in the equation above. In the absence of measurement noise, the undersampling of the true field will cause $\varepsilon_\lambda \to 1$ as the bandwidth of the underlying process increases well beyond the range of the survey spatial resolution, i.e., $|\mathbf{k}_s| \ll |\mathbf{k}_c|$.

Now, since measurement noise cannot be controlled by the experiment designer, we will neglect these terms for the remainder of this thesis. Thus, we redefine the spatial survey error metric to be

$$\mathcal{E}_\lambda = \frac{\int_\Omega \mathcal{P}(\mathbf{k}) d\mathbf{k}}{\int_{-\infty}^{\infty} \mathcal{P}(\mathbf{k}) d\mathbf{k}}. \tag{3.17}$$

This metric is a number which ranges between zero and one, as desired. It specifies the fraction of the total energy present in the field that we have lost in the survey process. For instance, for $\mathcal{E}_\lambda = 0$, we have captured all of the energy with the survey and, hence, can perfectly reconstruct of the (static) process field.

3.3.2 Temporal Survey Error

In the previous section we assumed that the process of interest was static. We now let this process evolve with time. To accurately reconstruct the process, we would have to make our survey instantaneous. This is analogous to taking a snap-shot of the process and is, of course, impossible to achieve in practice with an AUV. The time evolution of the field will degrade the information which we obtain with our survey. Therefore, we must attempt to determine the degree to which our temporally "blurred" sample field can accurately represent the true field.

For the moment, consider the value of the process field at location $\mathbf{x}_i$ at time t, which we will denote with the symbol $y_i(t)$. If the survey begins at time $t = t_o$, then this location would be sampled at some later time, $t = t_o{+}t'$, due to the finite speed of the AUV (assuming that $\mathbf{x}_i$ is not the starting location of the survey). Note that $y_i(t)$ is not a continuous field as was $y(\mathbf{x})$ in Section 3.3.1 above. It is rather a collection of random variables at the finite number of spatial sample locations in the survey domain. There is no need to try (nor would it be possible) to reconstruct a time-series at each of the survey sample locations and, hence, a temporal aliasing error analogous to the spatial aliasing error of the previous section would not be appropriate here.

To construct a temporal survey error metric, we begin by taking the expectation of the squared error between the true field and survey sample value at the spatial location $\mathbf{x}_i$. This is given by

$$\begin{aligned} \varepsilon_{t,\mathbf{x}_i} &= E\left\{ \left[y_i(t_o) - \hat{y}_i(t_o{+}t') \right]^2 \right\} \\ &= E\left\{ y_i^2(t_o) + \hat{y}_i^2(t_o{+}t') - 2y_i(t_o)\hat{y}_i(t_o{+}t') \right\} \\ &= \sigma_y^2 + (\sigma_y^2 + \sigma_w^2) - 2\mathrm{cov}\left(y_i(t_o), y_i(t_o{+}t') \right), \end{aligned} \tag{3.18}$$

where σ_y^2 is the temporal variance of the process field, σ_w^2 is the variance of a zero-mean, white noise temporal measurement error which is uncorrelated with the process field. We use the uncorrelatedness of the field and the noise to reduce the last term in the above equation to a covariance function involving only the process field.

From Equation (3.18) we see that in the absence of measurement noise, $\varepsilon_{t,\mathbf{x}_i} \to 0$ as $t' \to 0$, since the process has no time to evolve before the sample is taken. However, as $t' \to \infty$, Equation (3.18) goes to $2\sigma_y^2$. Although this may seem peculiar at first, we can readily convince ourselves that this is correct. As $t' \to \infty$, the covariance will go to zero. We will then essentially have two completely uncorrelated random variables, each of which contributes its variance, σ^2, to the expected error. Therefore, in order to properly normalize $\varepsilon_{t,\mathbf{x}_i}$, we should divide by twice the variance of the process. We define our normalized point-wise expected error, ε_t', as

$$\begin{aligned} \varepsilon_t' &= \frac{2\sigma^2 - 2\mathrm{cov}(\, y_i(t_o), y_i(t_o+t')\,) + \sigma_w^2}{2\sigma^2} \\ &= 1 - R(t') + \frac{\sigma_w^2}{2\sigma_y^2}, \end{aligned} \tag{3.19}$$

where we have used the fact that the covariance divided by the variance is defined to be the autocorrelation function, $R(t)$. (Note that $R(t)$ is also the Fourier transform of the energy density spectrum, $\mathcal{P}(\omega)$.) The last term is a constant which depends on the variance of the measurement noise only. Since the ultimate goal of constructing these error metrics is to aid the experimenter in designing survey mission, we will ignore this last term since this parameter is not readily controlled. Also, the assumption that $\sigma_y^2 \gg \sigma_w^2$ is typically justifiable, again leading us to ignore this term in the remainder of this thesis.

Equation (3.19) computes an expected error for each individual sample in the survey. However, we require an error metric which captures the effect of temporal blurring for all of the samples in the field. We create this error metric by summing the point-wise expectred errors over the entire survey domain. In the limit, this can be done by integrating Equation (3.19) over the total survey time, τ_s, and taking the time average. Thus, we use

the point-wise error to define the temporal survey error as

$$\mathcal{E}_\tau = \frac{1}{\tau_s}\int_{-\tau_s/2}^{\tau_s/2} \varepsilon_{t'}(t)\, dt = \frac{1}{\tau_s}\int_{-\tau_s/2}^{\tau_s/2} [1 - R(t)]\, dt = 1 - \frac{1}{\tau_s}\int_{-\tau_s/2}^{\tau_s/2} R(t)\, dt, \tag{3.20}$$

where we have moved the time origin, t_o, from the beginning of the survey to the mid-point of the survey to minimize the overall error. $\mathcal{E}_\tau$ is given the subscript τ to emphasize that this error metric is a product of the temporal blurring of the process over the duration of the survey.

The temporal survey error metric measures the average correlation of the sample field with the true field. As $\tau_s \to 0$, the autocorrelation function will go to one and, hence, $\mathcal{E}_\tau \to 0$. This is what we would expect since we are essentially measuring the difference between two "snap-shots" of the process which have been taken at the same instance. On the other hand, as $\tau_s \to \infty$, $\mathcal{E}_\tau \to 1$ since the autocorrelation function goes to zero; this indicates that the sampled field and the field at $t = t_o$ are completely uncorrelated.

3.3.3 Total Survey Error

In the previous two sections we developed spatial and temporal survey error metrics. The spatial survey error metric gives the expected error in reconstructing a spatial field from an undersampled survey of that field. This error is derived from spectral energy which is aliased into the reconstructed field and can be thought of as the variance of the error field. The temporal survey error metric is an average of pointwise errors derived the temporal autocorrelation function. Unlike the spatial survey error, the temporal survey error metric is not cannot be related to a temporal error variance. This is a fundamental difference between the two error metrics.

We now combine these errors into a single survey error metric,

$$\begin{aligned} \mathcal{E}_{tot} &= 1 - (1 - \mathcal{E}_\lambda)(1 - \mathcal{E}_\tau) \\ &= \mathcal{E}_\lambda + \mathcal{E}_\tau - \mathcal{E}_\lambda \mathcal{E}_\tau. \end{aligned} \tag{3.21}$$

In Section 3.3.1, $\mathcal{E}_\lambda$ was interpreted as the fraction of spatial information about the process

which has been lost. Therefore, the factor $(1 - \mathcal{E}_\lambda)$ is the fraction of spatial information about the process which has been accurately recovered by the survey. Alternatively, one can think of these qualities as the fraction of detail which has been lost and retained by the sampling process, respectively. The reduction of this information by temporal blurring is given by the second term. Therefore, $\mathcal{E}_{tot}$ measures the uncertainty in our estimate of the process field at time t_o. For $\mathcal{E}_{tot} = 0$, we have a perfect estimate, while $\mathcal{E}_{tot} = 1$ indicates that we have gained no new understanding of the process. Actual surveys will fall between these two extremes.

Recall that both $\mathcal{E}_\lambda$ and $\mathcal{E}_\tau$ are computed from expectations. Therefore, the product of the two errors as written in Equation (3.21) makes the assumption that these two quantities are uncorrelated. This assumptions will not be valid for many of the oceanographic processes which we might envision studying with an AUV. Nevertheless, this total survey error metric should capture much of the gross structure performance of an AUV survey of these processes and will continue to be useful in designing surveying strategies for these experiments.

3.4 Discussion

The energy and error metrics developed in the sections above can be combined to create a survey design tool which will allow the experimenter to trade-off various vehicle design parameters to tailor an AUV to a particular scientific mission. This tool can also aid in the design of survey trajectories by providing an objective overall survey performance measure with which differing survey strategies can be directly compared. These issues will be addressed in Chapter 5.

Before moving on to these issues, we must first examine the validity of the error metrics discussed above. In developing these metrics, we made several simplifying assumptions in order to make the problem tractable. These assumptions are:

1. The process of interest is temporally stationary and spatially homogeneous. Although spatial isotropy is not a requirement, *per se*, imposed by Equation (3.17), it will nevertheless be assumed throughout the following Chapters in order to simplify the computations. Note, however, that spatial anisotropy is common in many oceanographic

processes, particularly those involving wave-like motions or currents.

2. The frequency and wavenumber spectra (or, equivalently, the spatial and temporal autocorrelation functions) of the process of interest are known. It is further assumed that these spectra (autocorrelation functions) are separable functions of frequency and wavenumber (time and space). This is a consequence of the assumption that the temporal and spatial error metrics are uncorrelated (see Section 3.3.3).This is a particularly poor assumption for most oceanographic processes and will place serious restrictions upon the class of processes for which this metric will be absolutely accurate.

3. Errors due to AUV positional uncertainties are negligible. This is equivalent to claiming that the uncertainties in the position of the AUV are much smaller that the spatial resolution scale of a given survey. This seems reasonable given some external navigational aid such as an acoustical long-baseling system [61], which can give positional uncertainties as low as 1-10 m.

4. The process of interest is the only oceanographic phenomenon at play within the survey domain. This excludes, for example, ocean currents and tides. As discussed previously, the presence of currents can severely impact the quality of AUV sampled data. This is also often a poor assumption for a real oceanographic experiment.

5. Errors due to the finite length of the AUV surveys (i.e., truncation errors) are negligible. While this may be a reasonable assumption for densely grided surveys, it will be an increasingly poor assumption for low-resolution surveys as the number of tracklines across a survey domain decreases.

6. All survey trajectories are "mow-the-lawn" (grid) patterms. No irregular trajectories are allowed. While this constraint can certainly be accommodated by the researcher, there are also situations in which grid surveys may be less efficient in terms of the amount and quality of data which they generate.

Problems that meet these assumptions can be addressed with the framework of error metrics developed above. In Chapter 4, we will explore the validity of the error metrics by

conducting simulated AUV surveys through synthetic, spatially-distributed, time-evolving oceanographic processes which conform to these restrictions.

Chapter 4

Random Field Simulations and Performance Metric Verification

4.1 Introduction

Synthetic data from random field simulations are often used by oceanographers and other scientists to assess the predictive ability of models, to generate input data for them, and to test the statistical validity of their results. The efficient generation of these multidimensional, random-field simulations remains an active field of research, primarily due to the inherent computational complexity and various inadequacies of the available simulation techniques. While numerous multidimensional simulation techniques exist, none is the optimum choice for all applications. Each of these techniques place certain restrictions (spatial isotropy, for instance) on the resulting simulated random field. Thus, choosing the simulation techniques which are most appropriate for the requirements of the experimenter requires careful consideration of the desired characteristics of the resulting random fields.

For this work, we would like to be able to simulate random fields which evolve in at least two spatial dimensions as well as in time. We will allow these fields to be spatially isotropic and temporally stationary. Indeed, these assumptions are necessary requirements for many of the simulation techniques which currently exist. A brief description of several of these methods is given below.

Cholesky Decomposition This technique decomposes the covariance matrix of a random spatial field into upper and lower triangular components, and then creates the random field by multiplying the lower triangular matrix by a vector of independent random variables [62]. Since the size of the covariance matrix to be decomposed grows as the square of the total number of points in the random field simulation, this method is suitable only for small simulations.

FFT Spectral Method This method uses an assumed spectral density (for either ω or $\mathbf{k}$), a dispersion relation relating ω to $\mathbf{k}$, and a field of random phases to generate spatially anisotropic, temporally stationary random fields using a Fast Fourier Transform as the underlying computational engine. Fields with high aspect ratios (that is, with elongated, rectilinear domains) can be simulated. The computational efficiency of the FFT algorithm makes this method attractive when uniformly spaced samples (in both space and time) are sufficient.

Turning Bands Method This technique for generating spatial fields reduces the amount of computation involved in a simulation by using several realizations of a random process on a line to generate a multidimensional random field. An interpolation scheme is use to produce the multidimensional field from the randomly oriented line processes [44]. While this method is not as computationally efficient as the Fast Fourier Transform method for large problems, it does have the benefit that the simulated field does not have to conform a regular grid. This is required for simulating surveys for highly irregular AUV trajectories. However, adding a temporally evolving component to this method is not straightforward. For this reason this method will not be employed.

Sampling from the Spectrum This technique generates isotropic spatial random fields by taking a normalized sum of several harmonic components at each point in the simulation [39]. The wavenumbers which define these harmonic components are themselves random variables which are distributed in accordance with the radial spectral distribution of the desired random field. While this method is not as fast as the FFT method when numerous harmonic components are used, it is more flexible in that it

allows the generation of multidimensional random fields with fully separable spectral densities in each dimension. This is in contrast with the FFT method which requires that a dispersion relation be employed for computational reasons. As with the Turning Bands method, the technique of sampling from the spectrum does not necessitate the discretization of the simulation domain. Furthermore, only those samples needed to simulate the AUV's trajectory through the field are computed. This is a significant computational advantage.

Multiscale Stochastic Processing This technique is motivated by the recognition that scale serves the same function for multidimensional spatial processes as does time for unidimensional processes [63, 64]. This realization allows efficient, inherently parallelizable, scale-recursive algorithms to be developed for the generation of synthetic random fields. Scale-recursive algorithms make this method far more computationally efficient than the other simulation techniques described above for large problems, allowing for the generation of simulation fields on denser grids than previously possible. However, this method is as yet still in its infancy and basic questions in system realization and indentification remain unanswered for general systems. For this reason, we will not employ this method.

In this chapter we present simulations of space-time random fields based on the technique of sampling from the spectrum. Although less computationally efficient than some of the other techniques, this method was chosen because it allows the generation of samples at arbitrary locations within the simulation domain, and it also has a straightforward extension to temporally evolving fields. It also does not require any unnecessary computation of field values which are not needed for the AUV's survey trajectory through the random field (unlike the Fast Fourier Transform technique). This method is described in detail in Section 4.2 and results from simulated AUV surveys are presented in Section 4.3. In Section 4.4 we compare the theoretical and simulated spatial and temporal survey errors. Finally, we discuss the implications for the application of the performance metrics developed in Chapter 3 to AUV survey experiment design in Section 4.5.

4.2 Process Simulation

Our simulation method is based on the method of *sampling from the spectrum.* Our description of this technique follows those of Bras and Rodriguez-Iturbe [23] and Mejia [39].

For clarity of exposition and for computational simplicity, we have chosen to simulate a time varying, two dimensional, random field, $y(\mathbf{x}, t)$, which is spatially homogeneous and isotropic and temporally stationary. Furthermore, the simulated fields will have zero mean and unit variance, i.e.,

$$\mathbf{m}_y = 0, \tag{4.1}$$

and

$$\sigma_y^2 = 1. \tag{4.2}$$

For the sake of simplicity, we have have chosen to use a separable exponential autocovariance function,

$$R(\ell, t) = R(\ell)R(t) = e^{-|\ell|/\lambda_o} e^{-|t|/\tau_o}, \tag{4.3}$$

where ℓ is the (scalar) distance between two points in the field, i.e., $\ell = |\mathbf{x}|$. Given Equations (4.1) and (4.2), we see that the autocovariance function is also equivalent to the autocorrelation function of the random field. The spatial correlation length is denoted by λ_0, and τ_o is the temporal correlation "length", or time constant. Since the autocovariance function above is a separable function of space and time, we know that the wavenumber-frequency spectrum of the process will also be a separable function of k and ω,

$$\mathcal{P}_r(k, \omega) = \mathcal{P}_r(k)\mathcal{P}_r(\omega), \tag{4.4}$$

where $\mathcal{P}_r(\cdot)$ denotes the radial energy density spectrum of the given variable(s) and we have relied upon the fact that the desired random field is spatially isotropic in order to write the wavenumber spectrum as a function of a scalar wavenumber, k. Thus, Equation (4.4)

represents the radial wavenumber-frequency spectrum of the desired random field. In the following sections, the technique of sampling from the spectrum will be derived for spatial random fields and then a simple modification will allow the extension of this simulation to time-varying processes.

4.2.1 Spatial Random Field

Since we have assumed that simulated process is both spatially homogeneous and isotropic, we can intregrate out the directional dependence in the spectral density, yielding the radial spectral density. The radial spectral density [23] of the random field described above is found by taking the Fourier-Bessel (Hankel) transform of the autocorrelation function,

$$\begin{aligned}
\mathcal{P}_r(k) = \mathcal{P}_r(|\mathbf{k}|) &\equiv (2\pi k)\mathcal{P}(k) \qquad (4.5)\\
&= 2\pi k\left(\frac{1}{2\pi}\int_0^\infty R(\ell)J_o(k\ell)\ell d\ell\right)\\
&= k\int_0^\infty e^{-\ell/\lambda_o}J_o(k\ell)\ell d\ell\\
&= \left(\frac{\lambda_0}{2\pi}\right)^2 k\left[1+\left(\frac{k\lambda_o}{2\pi}\right)^2\right]^{-\frac{3}{2}} \qquad 0\le k\le\infty, \qquad (4.6)
\end{aligned}$$

where k is the radial wavenumber, $J_0(\cdot)$ is the Bessel function of the first kind of order zero, and $\mathcal{P}(k)$ is the associated (non-radial) wavenumber spectral density of the isotropic random field. Anticipating its later use, we also compute the radial spectral *distribution* function for the random field,

$$\begin{aligned}
\mathcal{P}_D(k) &= \int \mathcal{P}_r(\kappa)d\kappa\\
&= \left(\frac{\lambda_0}{2\pi}\right)^2\int \kappa\left[1+\left(\frac{\kappa\lambda_o}{2\pi}\right)^2\right]^{-\frac{3}{2}}d\kappa\\
&= 1-\left[\frac{\left(\frac{2\pi}{\lambda_o}\right)^2}{k^2+\left(\frac{2\pi}{\lambda_o}\right)^2}\right]^{\frac{1}{2}} \qquad 0\le k\le\infty. \qquad (4.7)
\end{aligned}$$

Taking the above development into account as well as the assumptions Equations (4.1) and (4.2), we see that the statistics of the spatial random field are completely determined

by the length scale parameter, λ_o. Thus, simulation of a spatial random field begins by choosing this value and then selecting a vector of random wavenumbers from which the spatial random field will be formed. The way in which these random wavenumbers are selected is known as sampling from the spectrum and it is this process which gives the simulation technique its name. This method is as follows.

Let $\mathbf{u} \in \mathcal{R}^M$ be a random vector with elements u_i uniformly distributed on $[0, 1]$. Furthermore, let each element satisfy the equation

$$u_i = \mathcal{P}_D(k_i), \tag{4.8}$$

where the (scalar) radial wavenumbers, k_i, are the random wavenumbers which we seek. We solve for these wavenumbers by taking the inverse of Equation (4.8),

$$\begin{aligned} k_i &= \mathcal{P}_D^{-1}(u_i) \\ &= \frac{2\pi}{\lambda_o}\left[\frac{1}{(1-u_i)^2} - 1\right]^{1/2}. \end{aligned} \tag{4.9}$$

Figure 4.1 shows an histogram of a realization of the process of sampling from the spectrum. This figure was produced using a total of 300 samples from the radial wavenumber spectral distribution given, Equation (4.7). We see that the approximation to the desired radial wavenumber spectral density is excellent given a modest number of wavenumber samples. Note that the spectrum goes to zero as $k \to 0$. This is a consequence of the fact that the desired process has zero mean.

Finally, the vector of random wavenumbers generated above is used to simulate a zero mean, unit variance spatial random field via

$$y(x_1, x_2) = \sqrt{\tfrac{2}{M}} \sum_{i=1}^{M} \cos[k_i(x_1 \cos\alpha_i + x_2 \cos\alpha_i) + \theta_i], \tag{4.10}$$

where the α_i's are random directions uniformly distributed on $[0, 2\pi]$ and the θ_i's are random phases also uniformly distributed on $[0, 2\pi]$. Thus, the two-dimensional spatial random field consists of a collection of M waves of random wavenumber and phase each oriented in a random direction. The random wavenumbers are uncorrelated and the radial spectral

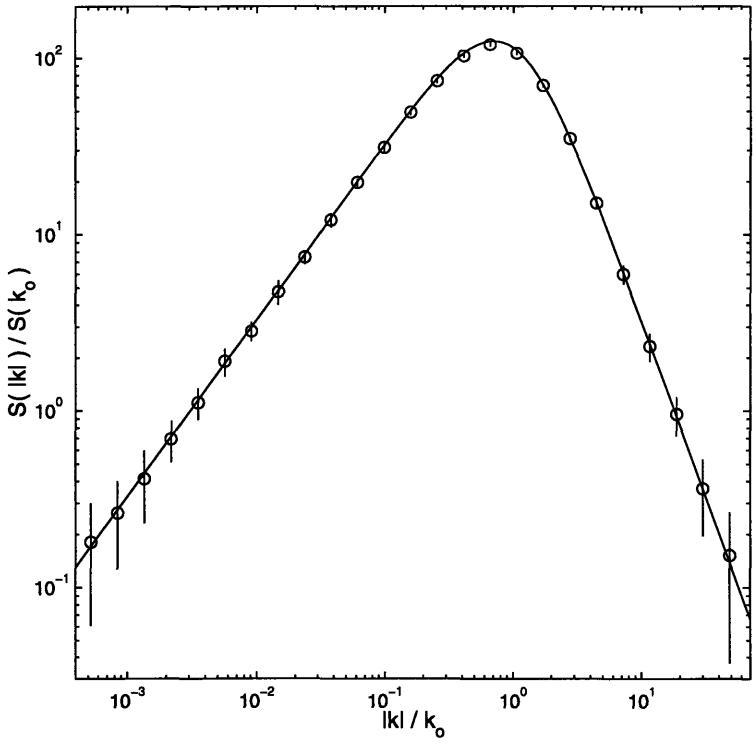

Figure 4.1: Distribution of wavenumbers generated via the inverse method. A histogram of the random wavenumbers generated via the inverse method to be used in a random field simulation are shown. The mean of 32 distributions is denoted by ∘ and ±1 standard deviation error bars shown as vertical lines. The theoretical wavenumber spectral density (solid line) given by Equation (4.6). The histogram was calculated using a total of 300 random wavenumbers samples.

density of the resulting field approximates that of Equation (4.6). An example of a typical spatial random field generated with this method is shown in Figure 4.2. The correlation length is set at one-quarter of the side length of the square simulation domain. While the lower wavenumbers obviously dominate the process, significant detail is also evident in the realization of the spatial random field.

4.2.2 Time Evolution

We want to modify the formulation of Equation (4.10) to add a time-varying component to the random field simulation. The method to do this is simple and straight-forward. We begin by generating a sequence of random frequencies using the method of sampling from the spectrum, as we did above for the spatial random field. In order to do this we must

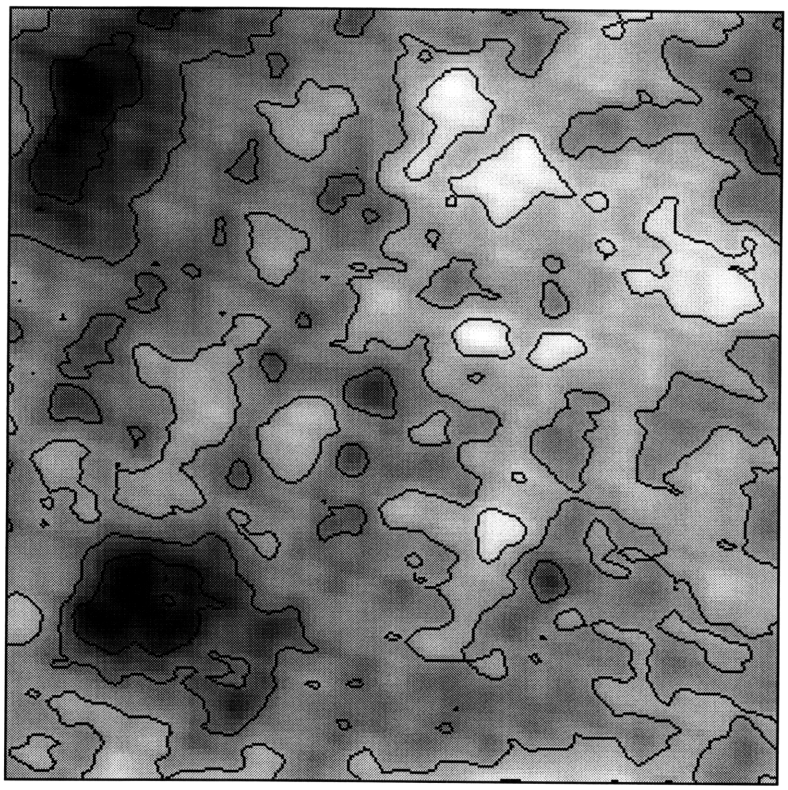

Figure 4.2: A realization of a simulated spatial random field. The simulation domain was a square area with side length of 2 km which was grided into 128 cells in each direction. The correlation length is $\lambda_o = 512$ m. Note that significant detail is visible even though most of the process energy is concentrated in the long wavelength portion of the spectrum. Contours are plotted to help bring out the gross structure of the process.

first specify the frequency spectral density and distribution functions which correspond to the temporal component of Equation (4.3). The frequency spectral density is given by

$$\begin{aligned} \mathcal{P}_r(\omega) &= \frac{1}{2\pi}\int_{-\infty}^{\infty} R(t)e^{-j\omega t}dt \\ &= \frac{1}{2\pi}\int_{-\infty}^{\infty} e^{-|t|/\tau_o}e^{-j\omega t}dt \\ &= \frac{1}{\tau_o}\left[\frac{1}{\left(\frac{2\pi}{\tau_o}\right)^2+\omega^2}\right], \qquad -\infty \leq \omega \leq \infty. \end{aligned} \tag{4.11}$$

The frequency spectral distribution corresponding to the prescribed temporal autocorrelation function is simply the normalized integral of the frequency spectral density and is given

by

$$\begin{aligned}\mathcal{P}_D(\omega) &= \int_{-\infty}^{\omega_s} \mathcal{P}_r(\Omega)d\Omega / \int_{-\infty}^{\infty} \mathcal{P}_r(\Omega)d\Omega \\ &= 1 + \frac{2}{\pi}\tan^{-1}\left(\frac{\omega_s}{\omega_o}\right) \\ &= 1 + \frac{2}{\pi}\tan^{-1}\left(\frac{\tau_o}{\tau_s}\right), \qquad -\infty \leq \tau_s \leq \infty, \end{aligned} \tag{4.12}$$

where τ_s is the total survey time and τ_o is the decorrelation time of the random field. Recall that any distribution of defined to be a monotonic function which ranges from zero at $\omega = 0$ to one at $\omega = 1$. Given this frequency spectral distribution, we can generate a sequence of random frequencies by inverting Equation (4.12), yielding,

$$\omega_i = \frac{1}{\tau_o}\tan(\pi u_i - \frac{\pi}{2}), \tag{4.13}$$

where, as before, the u_i are random variables uniformly distributed on $[0, 1]$. We use the resulting random frequencies to generate a time-series and then multiply Equation (4.10) by this series to simulate time evolution of the random field. Thus, we have

$$y(x_1, x_2, t) = \sqrt{\tfrac{4}{MN}} \sum_{i=1}^{M} \cos[k_i(x_1 \cos\alpha_i + x_2 \cos\alpha_i) + \theta_{1,i}] \times \sum_{j=1}^{N} \cos[\omega_j t + \theta_{2,j}], \tag{4.14}$$

where $\theta_{2,j}$ is a random phase uniformly distributed on $[0, 2\pi]$. With Equation (4.14), we can generate simulate surveys with arbitrary AUV trajectories and arbitrarily sized and shaped survey domains. This simulation technique is also quite efficient in that field values are produced only at the sample locations and instances required by the simulated AUV's trajectory.

From the construction of Equation (4.14), we see the separability of the space-time autocorrelation function (Equation (4.3)) reflected in the separability of the simulation formulation. While this may not be a desirable property for a simulated random field since it ignores the existence of possible connections between the spatial and temporal evolution of the simulated field which would naturally arise in the many real oceanographic process, the goal here is not to construct an accurate simulation of a specific oceanographic process

but to generate a simple simulation which will allow us to examine the validity of the performance metrics developed in Chapter 3. Before doing this, however, we must first examine the statistical accuracy of the simulation given by Equation (4.14).

4.2.3 Simulation Statistics

We will now explore the statistical accuracy of these simulated processes. Recall that we desire the random field to have zero-mean and unit variance. The expectation of the synthetic field is

$$\begin{aligned} E\{y(x_1,x_2,t)\} &= \sqrt{\tfrac{4}{MN}}\sum_{i=1}^{M} E\{\cos[k_i(x_1\cos\alpha_i + x_2\cos\alpha_i) + \theta_{1,i}]\} \\ &\quad \times \sum_{j=1}^{N} E\{\cos[\omega_j t + \theta_{2,j}]\}, \\ &= 0, \end{aligned} \tag{4.15}$$

where we have used the identity $E\{\cos(\omega\nu)\} = 0, \quad \forall\, \omega$. Similarly, the sample variance is given by

$$\begin{aligned} E\{y^2(x_1,x_2,t)\} &= \left(\sqrt{\tfrac{4}{MN}}\right)^2 \sum_{i=1}^{M} E\{\cos^2[k_i(x_1\cos\alpha_i + x_2\cos\alpha_i) + \theta_{1,i}]\} \\ &\quad \times \sum_{j=1}^{N} E\{\cos^2[\omega_j t + \theta_{2,j}]\}, \\ &= \left(\frac{4}{MN}\right)\left(\frac{M}{2}\right)\left(\frac{N}{2}\right) \\ &= 1, \end{aligned} \tag{4.16}$$

where we have used the fact that $E\{\cos(\omega_1\nu)\cos(\omega_2\nu)\} = \delta(\omega_1,\omega_2)$ and the identity $E\{\cos^2(\omega\nu)\} = 1/2, \ \forall\, \omega$, to simplify the sums.

It can be also shown [39, 23] that the resulting simulated random field is spatially homogeneous and isotropic and temporally stationary, as desired, and has a sample autocovariance function, $\hat{R}(\ell,t)$, the expectation of which equals the desired autocovariance

function, i.e., $E\{\hat{R}(\ell,t)\} = R(\ell,t)$, and which satisfies

$$\lim_{M\to\infty} \text{var}\{\hat{R}(\ell,t)\} = 0. \tag{4.17}$$

Thus, we see that simulated random field generated via Equation (4.14) will indeed exhibit the desired spatial and temporal statistics. The degree to which the sample autocovariance function agrees with the theoretical autocovariance function is dependent upon the number, M, of harmonic components included in the random field. Equation (4.17) indicates that this agreement will be asymptotically perfect as $M \to \infty$.

4.2.4 Summary

Before examining the simulated random fields generated via this method in the next section, we want to summarize the qualities and characteristics of the spatial random fields generated. The simulated fields have zero mean and unit variance, are spatially homogeneous and isotropic and temporally stationary, and the process is separable. The simulations can be modified so that the resulting random fields are anisotropic by allowing the radial wavenumber spectral density/distribution to be parameterized by the random directions, α_i, in addition to the parameter, u_i. Perhaps the most important feature of this simulation technique is the ability to calculate simulated values at any location within the field at any instance in time. This is required for surveys which follow irregular survey trajectories. In the next section we simulate simple "lawn-mower" surveys.

4.3 AUV Survey Simulations

Using the simulation technique described in the previous section, we have generated simulated AUV surveys of spatially varying, temporally evolving processes. These surveys implement a simple "mow-the-lawn" pattern over a square domain of varying spatial dimensions. Regardless of simulation domain size, the *true* field is always calculated on a 128x128 cell grid which spans the simulation domain. This true field is the instantaneous spatial field at the time $t = t_o$. The survey begins at time $t_o - \tau_s/2$ and ends at time $t_o + \tau_s/2$, where τ_s is the total time required to complete the survey (t_o may be set to zero without

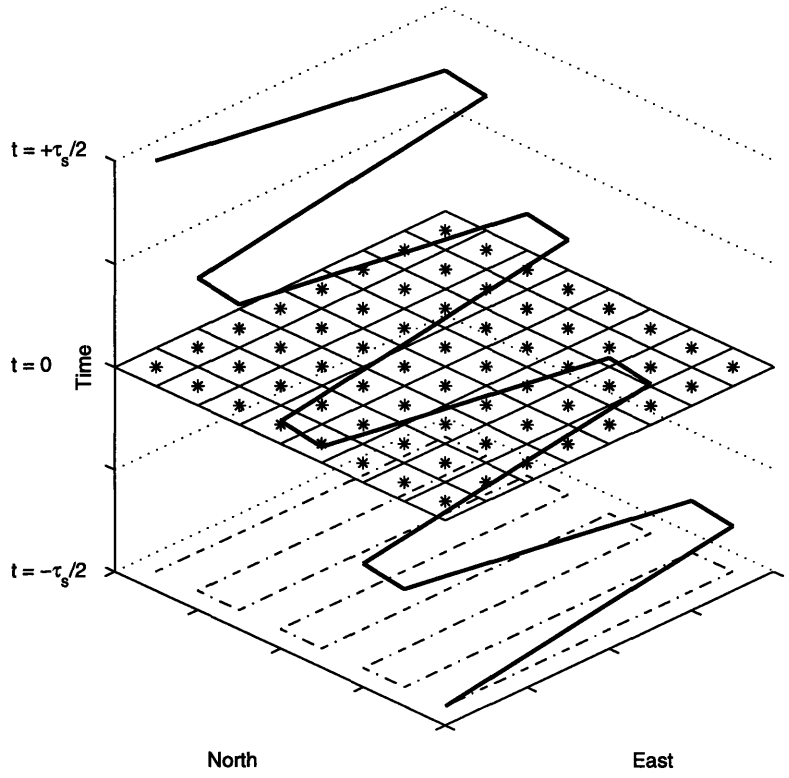

Figure 4.3: The sampling geometry of a simulated "lawn-mower" survey. The space-time trajectory of the AUV through the survey domain is shown as a dark line. The AUV survey begins at time $t = -\tau_s/2$ and ends at time $t = +\tau_s/2$ (total survey time is τ_s). The projection of this trajectory onto the spatial axes is shown as a broken line. Survey samples (denoted by *) are placed in a square spatial grid (whose resolution is now greater than that of the simulated field) as depicted by the grid in the plane $t = 0$. These samples are then interpolated up to the full resolution of the simulated field and compared to the instantaneous simulated field at the (temporal) midpoint of the survey, i.e., at $t = 0$.

loss of generality). Thus, the true field is a simulated random field taken instantaneously at the midpoint (in time) of the survey. The total survey time is such that the simulated trajectory will be consistent with the vehicles maximum velocity constraint. This true field will serve as the benchmark against which the fields reconstructed from the survey samples will be measured.

The AUV survey fields are generated in the following way. A spatial trajectory for a "lawn-mower" survey is computed and discretized on a square, uniform grid, as is shown in Figure 4.3. Beginning at the southwest corner of the simulation domain at time $t = t_o - \tau_s/2$, the field is sampled in the first cell. At each subsequent sampling instant, $t = t_o - \tau_s/2 + n\Delta t$, a value is taken at the corresponding location in the simulation domain. These spatially and

temporally distributed sample values build up a random field at a spatial resolution equal to or coarser than the true random field. The time between sample points, Δt, is dependent upon the speed of the AUV, the length of the survey trajectory, and the granularity of the spatial grid. Thus, the effects of temporal blurring and spatial aliasing will be present in the sampled field. If the field was taken at a coarser spatial resolution, then spatial interpolation is performed to place the reconstructed field on the same spatial grid as the true field. The spatial interpolation is performed with a bi-cubic spline interpolation method, which has the visual effect of smoothing the field.

In Figures 4.4 (b)-(f), simulated surveys are plotted for five successive spatial resolutions while τ_s is held constant. The "true" field, shown in Figure 4.4(a), is the instantaneous simulated field taken at the midpoint of the survey. The effect of surveying with coarser resolution is obvious, since less detail in the reconstructed fields for each successive reduction in the survey resolution, λ_s. Nevertheless, some of the gross characteristics of the true field (Figure 4.4(a)) are still discernable even at the coarsest spatial resolution survey.

Note also the evolution of the process in time. This is most easily seen by comparing Figure 4.4(b) with Figure 4.4(a), were we see that the field reconstructed from the survey has evolved over the duration of the survey in relation to the true field. The degree of evolution is controlled by the correlation time, τ_o, and the duration of the simulated survey, τ_s. We will see that if the survey time is decreased, less temporal evolution of the process will occur during the course of the survey. This agrees with our intuitive insight that faster AUV's will perform better in terms of capturing spatially distributed, time-varying phenomena.

Looking again at Figures 4.4(a) and 4.4(b) (or at Figure 4.2, which is shown in a larger format), we notice a curious banding. This banding is an artifact of the technique of sampling from the spectrum. In accordance with the spectral distribution given by Equation (4.7), the technique of sampling from the spectrum typically only generates a very few high wavenumbers, k_i, to be used in the generation of the random field. These few high wavenumbers are visible in the resulting realization because there are so few "nearby" high wavenumber harmonics to disrupt or blend the banding effect caused by the highest wavenumber components. This effect is also present in the temporal domain but does

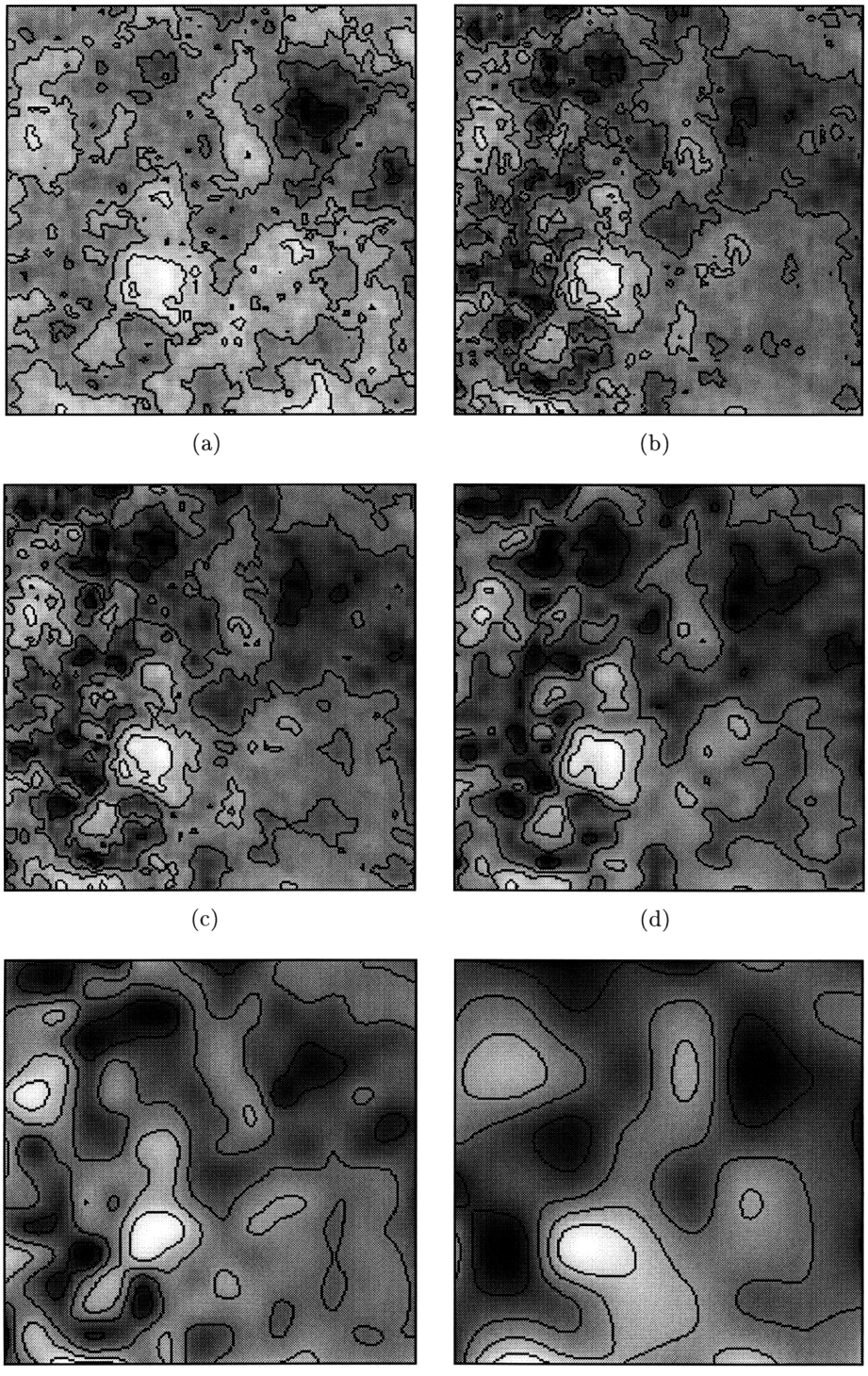

Figure 4.4: Fields reconstructed from simulated surveys of a random field with correlation time τ_o and correlation length λ_o. The surveys are made at differing survey resolutions: (b) $\lambda_s = \lambda_o$, (c) $\lambda_s = 2\lambda_o$, (d) $\lambda_s = 4\lambda_o$, (e) $\lambda_s = 8\lambda_o$, and (f) $\lambda_s = 16\lambda_o$. The field at $t = t_o$ is shown in (a). The total survey time for Figures (b)-(f) was $\tau_s = 1/2\,\tau_o$.

not visually manifest itself in the spatial survey plots. While the spatial "banding" effect may be visually unappealing, it does not represent a problem in terms of the statistics of the resulting random field. This effect is diminished for lower survey sampling resolutions since these resolutions correspond to wavelengths which are longer than those of the high wavenumber harmonic components of the simulated field. Such artifacts can adversely affect the calculation of AUV survey error in certain situations. In the next section, we will discuss the calculation of these errors.

Figure 4.5 compares the sample autocorrelation function in both the spatial and temporal domains with their respective theoretical autocorrelation functions, given by Equation (4.3). The spatial sample autocorrelation function (Figure 4.5(a)) is produced by averaging the individual sample autocorrelation functions from 16 realizations of a spatial simulation (no time evolution). Similarly, the temporal sample autocorrelation function is the average of the sample autocorrelation functions from 16 time-series simulations (no variation in space). The overall excellent agreement between the sample autocorrelation functions and their respective theoretical values indicated that the choice $M = N = 300$ provides sufficient harmonic components for the purposes of these experiments. The disagreement in the tails of the sample autocorrelation functions is due to the sparsity of high wavenumber/frequency harmonic components in the vectors of random wavenumbers/frequencies obtained through the process of sampling from the spectrum.

4.4 Survey Simulation Errors

One of the prime motivations for implementing the simulation process is to facilitate the verification of the performance metrics developed in Chapter 3. We begin by examining the spatial errors incurred in simulated AUV surveys of a static (not time varying) spatial random field and compare these errors to the proposed spatial survey error metric developed in Section 3.3. We will then look at the temporal survey errors from simulated surveys which vary in total survey time but have a fixed spatial resolution. Finally, we will explore the correspondence between the theoretical combined space-time error metric and the errors from time-varying and spatially aliases simulated AUV surveys. In each experiment the

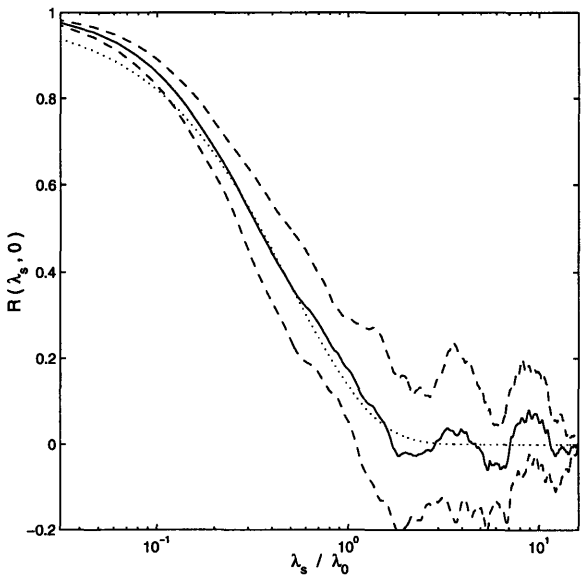

(a)

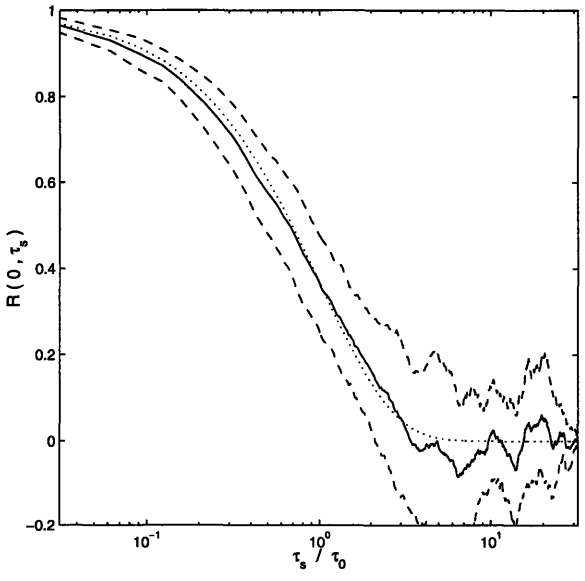

(b)

Figure 4.5: Sample autocorrelation functions compared to theoretical values. In (a), the spatial sample autocorrelation function is calculated from the average sample autocorrelation function from 16 spatial (no temporal evolution) simulated surveys. In (b), the temporal sample autocorrelation is calculated as the average from 16 time-series (no spatial variation) simulated surveys. The sample autocorrelation functions are represented by the solid lines and the dashed lines give the ± 1 standard deviation error bounds. The dotted line is each figure is the theoretical value of the spatial or temporal autocorrelation functions taken from Equation (4.3).

simulated survey errors are defined to be the normalized mean square of the difference between the field reconstructed from the simulated survey samples and the *true* field. This mean square error is normalized by the energy contained in the reconstructed and true fields. Thus, we have

$$\mathcal{E}_{sim} = \frac{\sum_i [y(\mathbf{x}_i, t_o) - \hat{y}(\mathbf{x}_i, t_i)]^2}{\sum_i [y^2(\mathbf{x}_i, t_o) + \hat{y}^2(\mathbf{x}_i, t_i)]}, \tag{4.18}$$

where $y(\mathbf{x}_i, t_o)$ is the "true" field, $\hat{y}(\mathbf{x}_i, t_i)$ is the reconstructed field, $\mathbf{x_i}$ ranges over all sample locations in the true field, t_o is the sampling instance in the middle of the simulated AUV survey (t_o may be set to zero without loss of generality). The sample times are given by

$$t_i = -\frac{\tau_s}{2} + \frac{i\tau_s}{N}, \qquad i = [0, 1, \cdots, N], \tag{4.19}$$

where $N+1$ is the total number of sample points in the true field. Recall from previous discussion that the true field is a random field simulation which is a "snap-shot" of the random field taken at time $t = t_o$ and with the greatest possible spatial simulation resolution.

4.4.1 Spatial Sampling Errors

To compute survey errors due to under-sampling of the simulated fields, several surveys were conducted with varying spatial resolutions. The total survey duration was $\tau_s = 10^{-5} \times \tau_o$. This, of course, does not correspond to any realistic AUV survey of an oceanographic process, but it gives surveys which are essentially instantaneous and ensures that no temporal survey errors will be present in the survey errors to be calculated from theses simulation experiments.

The spatial survey errors from these simulated AUV surveys were calculated via Equation (4.18) and compared to the theoretical spatial survey error of Equation (3.17). The results from these numerical experiments are presented in Figure 4.6. A total of sixteen simulated surveys were conducted for each survey spatial resolution. The means of the errors at each resolution are plotted as open circles and the ± 2 standard deviation error bounds are shown as vertical lines. In Figure 4.6 we see that the mean of the simulation spatial survey error closely follows that of the theoretical error (shown as a solid line). How-

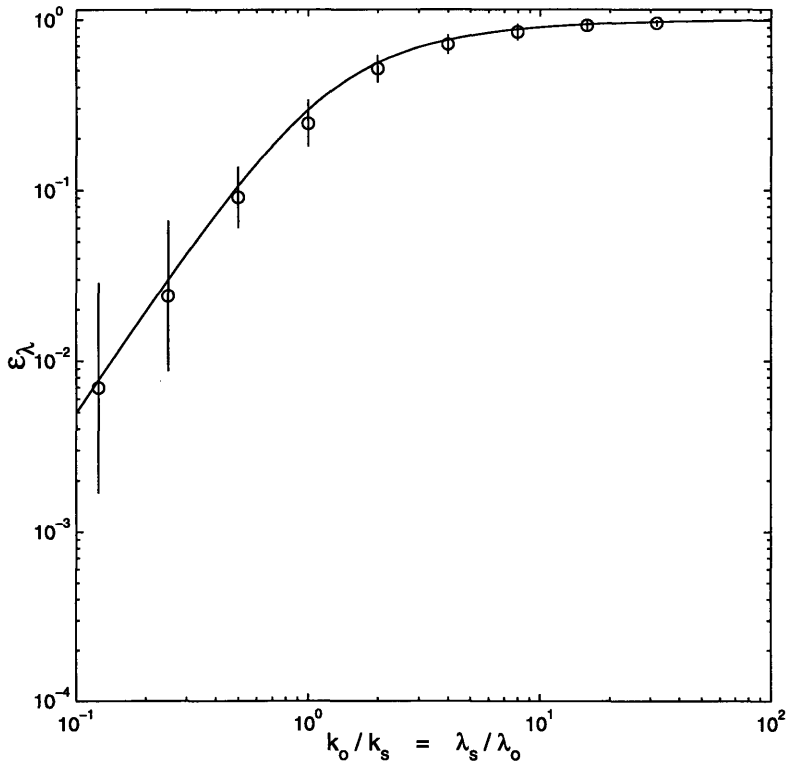

Figure 4.6: Spatial survey errors from simulated surveys. Simulated "lawn-mower" surveys where conducted for zero-mean, unit-variance random field processes with characteristic length and time scales of λ_o and τ_o, respectively, with a total survey time of $\tau_s = 1$ s. The spatial survey error was calculated via Equation (4.18) for sixteen simulated at each spatial resolution. For each resolution, the mean of the errors is denoted with an open circle and the ± 2 standard deviation error bounds are shown as vertical lines. The theoretical spatial survey error (Equation (3.17)) is shown as a solid line.

ever, it is also clear that the variance of the simulation spatial errors increases as $\frac{\lambda_s}{\lambda_o} \to 0$, because the simulation domain has to shrink in order to achieve high spatial resolutions without generating prohibitively large simulation grids. As the simulation domain shrinks, the effect of banding (Section 4.3) becomes more pronounced, causing increased variance in the simulation spatial errors. Since the vector of random wavenumbers used to generate the simulated random field changes for each simulation, a natural variation in the process of sampling from the spectrum causes an increased variation in the resulting simulation spatial errors. This effect diminishes as the size of the simulation domain increases (that is, with increasing λ_s/λ_o) since the highest wavenumber components have wavenumbers which are shorter than the simulation grid spacing. Therefore, even though these high frequencies are

present, the simulation aliases them into the lower-wavenumber end of the spectrum. This is, of course, an undesirable effect but is also unavoidable due to computational limitations. Overall, we see that the theoretical spatial survey errors of Equation (3.17) is an acceptable and valid formulation. The discrepancies between the simulated and theoretical error at high spatial resolutions is due to inadequacies in the simulation technique which arise from computational constraints.

4.4.2 Temporal Sampling Errors

To calculate the temporal survey errors, we simulate several AUV surveys at a constant, high spatial resolution but with varying total survey times, τ_s. The total survey time, τ_s, is varied over a range which encompasses total survey times which would be reasonable for an AUV to achieve. All surveys are conducted at the same spatial resolution as the true field to insure that spatial survey errors are not present in the calculation of the temporal simulated survey error. The size of the simulation domain and the spatial resolution of the surveys are held constant for all runs.

The temporal error from the simulated surveys is calculated via Equation (4.18) and compared to the theoretical temporal survey error given by Equation (3.20). The results of these numerical experiments are presented in Figure 4.7. A total of sixteen surveys are conducted for each value of the total survey time, τ_s. We see excellent agreement between the simulation and theoretical errors. The deviations of simulation errors from the temporal errors is again due to an artifact of the simulation process and is not indicative of difficulties with the formulation of the temporal survey error metric. We conclude that the temporal survey error metric of Equation (3.20) is valid.

4.4.3 Total Survey Errors

In order to validate the total survey error metric of Equation (3.21), we need to simulate surveys while varying both survey resolution and total survey time. We will now vary the spatial resolution, λ_s, and the total survey time, τ_s, of the simulated AUV surveys in such a way so as to cut a diagonal across the (λ, τ) error space which we have explored in the previous two experiments. The results of these simulations are shown in Figure 4.8. A total

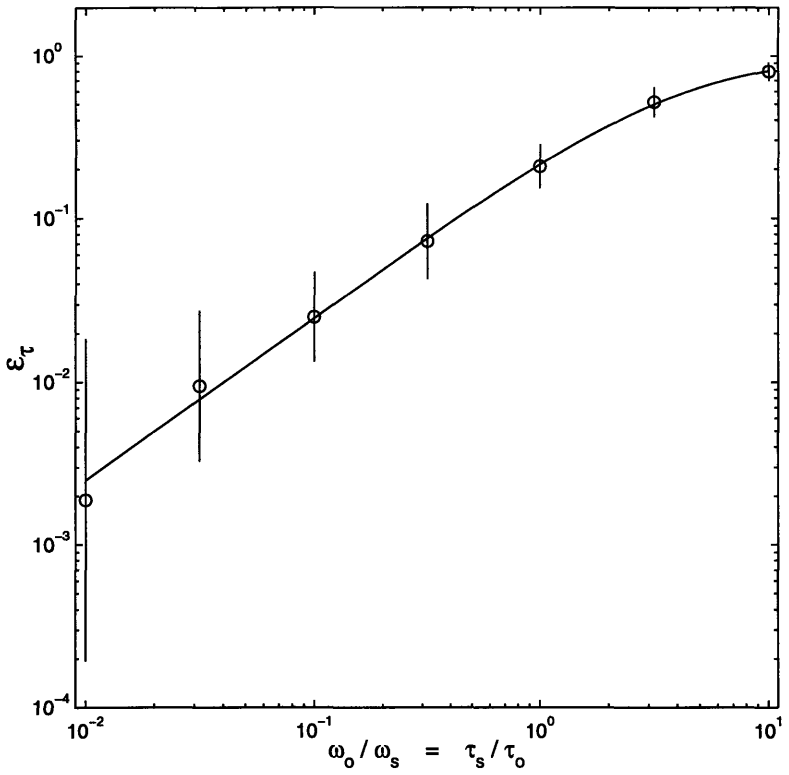

Figure 4.7: Temporal survey errors from simulated surveys. Simulated "lawn-mower" surveys where conducted for zero-mean, unit-variance random field processes with characteristic length and time scales of λ_o and τ_o, respectively. The total survey time, τ_s, is varied while the spatial resolution is held constant. The temporal survey error was calculated via Equation (4.18) and a total of sixteen simulated surveys were conducted at each temporal resolution. For each resolution, the mean of the errors is shown as an open circle and the ± 2 standard deviation errors bars are denoted by vertical lines. The theoretical temporal survey error (Equation (3.20)) is shown as a solid line.

of sixteen simulations are conducted for each pair of survey spatial resolutions and total survey times, (λ_i, τ_i). We see that the errors from the simulation are consistently slightly lower that their theoretical values over much of the range shown. Nevertheless, the shape of the two curves are highly consistent. This most likely indicates that a small constant multiplication offset is present in the simulated errors values. The good agreement between the simulation and theoretical errors validates the combined survey error metric of Section 3.3. The increased variation in the simulated surveys errors for high wavenumbers/frequencies is by now familiar.

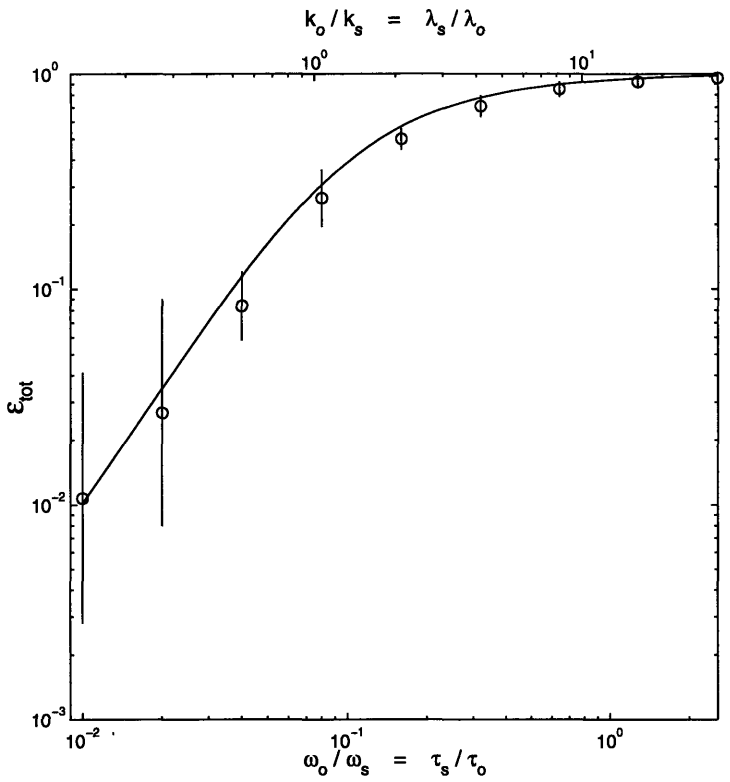

Figure 4.8: Total survey errors from simulated surveys. Simulated "lawn-mower" surveys where conducted for zero-mean, unit-variance random field processes with characteristic length and time scales of λ_o and τ_o, respectively. The total survey time, τ_s, and the survey spatial resolutions, λ_s, are both varied between each group of surveys. The total simulated survey error is calculated via Equation (4.18) and a total of sixteen simulated surveys were conducted at each resolution. The error means are denoted with an open circle and the ± 2 standard deviation error bounds are shown as vertical bars. The theoretical total survey error (Equation (3.21)) is shown as a solid line.

4.5 Discussion

In this chapter we have developed a simple space-time random field simulation based on the method of sampling from the spectrum. This technique is powerful in that it does not require unnecessary computation and is flexible in terms of the size and shape of the survey domain as well as its ability to compute field values along arbitrary space-time survey trajectories. Even though it was not necessary for the experimentation undertaken here, a slight modification of the simulation equation, Equation (4.14), would allow us to incorporate dynamics to couple the spatial and temporal evolution of the resulting random fields.

Having developed the random field simulation, we employed this capability in the gen-

eration of simulated AUV surveys of the random fields. We then used these simulated surveys in the to verification of the survey error metric of Equation (3.21) of Chapter 3. We found good agreement between the errors from the simulated surveys and the theoretical errors. This agreement is not surprising since the assumptions made in formulating the total survey error metric are met by the formulation of the simulated random fields. The most profound of these assumptions is that the wavenumber-frequency spectral density function is a separable function of wavenumber and frequency (or, equivalently, that the space-time autocorrelation function is a separable function of space and time lags). These assumptions were made in the formulation of the simulation so that the errors derived from the simulated AUV surveys of the random field could serve to validate the total survey error metric. However, this particular stipulation has the effect of precluding any coupling of the spatial and temporal evolution of the random field. Thus, the dynamics of the simulated fields are not representative of realistic oceanographic phenomena. If we were to simulate a random field which incorporated a dynamical constraint (such as a dispersion relation) on the space-time evolution of the field, we would find that the total survey error metric was no longer accurate, although it would still be useful for providing insight into the design of AUV surveys of real oceanographic phenomena. Problems such as this will be consider in the next chapter.

Chapter 5

Survey Analyses

5.1 Introduction

There are a number of critical trade-offs which can be made in the design of a grid survey, or in the design of an AUV for a specific oceanographic mission. To aid in making these decisions, certain questions must be answered: What is the best compromise between survey time and resolution? How large an area can be mapped with confidence? How does the survey improve if multiple vehicles are employed? How can current AUVs be improved to enhance their survey performance? These questions are the focus of this chapter.

Having developed an understanding of the energy economics of AUV surveys of oceanographic processes as well as the errors incurred in these surveys in Chapter 3 and having validated these error metrics in Chapter 4, we now employ these ideas in the creation of a tool which can be used to objectively compare various survey strategies. Because we require the context of a specific problem to derive concrete answers, Section 5.2 develops a numerical example based on a simple model of an ocean process. During the course of this example, our survey analysis tool will be developed. In Section 5.3, we employ the analysis tool to develop insights into issues of AUV selection and design and of experiment design in the context of the example oceanographic process of the previous section. We then demonstrate the application of the survey analysis tool to experiment design issues for AUV surveys of open-ocean deep convection in Section 5.4. This analysis is motivated by a field experiment to take place in the Labrador Sea in January, February, and March of

1998 in which three Odyssey IIb AUVs will be deployed in an AOSN configuration to study these episodic convection events.

5.2 Survey Analysis Tool

Let us assume, for the sake of example, that we wish to grid survey a process over a fixed square area, $A \approx 4km^2$, using an Odyssey IIb AUV. We also specify that the process of interest is described by a wavenumber spectral density given by

$$\mathcal{P}(\mathbf{k}) = \frac{2\mathbf{k}_o}{\mathbf{k}_o^2 + \mathbf{k}^2}, \tag{5.1}$$

where $\mathbf{k}_o = \frac{2\pi}{\lambda_o}$ is the "cutoff" wavenumber of this Lorentzian density. This density indicates that the process of interest is dominated by long-wavelength motions and has a spatial autocorrelation function given by

$$R(\ell) = e^{-|\ell|/\lambda_o}, \tag{5.2}$$

where λ_o is the correlation length scale. From our discussion of Section 4.2.1, we know that an equivalent description of this process is the radial wavenumber spectral density,

$$\mathcal{P}_r(k) = \left(\frac{\lambda_0}{2\pi}\right)^2 k \left[1 + \left(\frac{k\lambda_o}{2\pi}\right)^2\right]^{-\frac{3}{2}}, \qquad 0 \leq k \leq \infty, \tag{5.3}$$

which relies on the fact that the process is spatially isotropic to express the radial spectral density in terms of a strictly non-negative scalar wavenumber, k.

In keeping with the simulation process of Chapter 4, we further specify that the temporal autocorrelation function be given by

$$R(t) = e^{-|t|/\tau_o}, \tag{5.4}$$

where τ_o is the time constant of the example random field. Thus, we know from Section 4.2.2

that the frequency spectral density for this process is

$$\begin{aligned}\mathcal{P}(\omega) &= \frac{1}{\tau_o}\left[\frac{1}{\left(\frac{2\pi}{\tau_o}\right)^2+\omega^2}\right] \\ &= \frac{1}{2\pi}\left[\frac{\omega_o}{\omega_o^2+\omega^2}\right], \qquad -\infty \leq \omega \leq \infty, \end{aligned} \tag{5.5}$$

where ω_o is the cut-off frequency associated with the correlation time constant, τ_o.

We complete the description of the example random field by specifying that it have zero mean ($\mathbf{m}_y = 0$) and unit variance ($\sigma_y^2 = 1$) and that the spatial and temporal correlation scales are $\lambda_o = 2048$ m and $\tau_o = 10^5$ s, respectively. With these specifications, we can now calculate the spatial and temporal survey errors in addition to the total energy required to complete a survey of this process as functions of the survey parameters (λ_s, τ_s).

5.2.1 Spatial Survey Error

Recall from Equation (3.17) that the spatial survey error is given by

$$\begin{aligned}\mathcal{E}_\lambda &= \int_\Omega \mathcal{P}(\mathbf{k})d\mathbf{k} \Big/ \int_{-\infty}^{\infty} \mathcal{P}(\mathbf{k})d\mathbf{k} \\ &= \int_{k_s}^{\infty} \mathcal{P}_r(\mathbf{k})d\mathbf{k} \Big/ \int_{-\infty}^{\infty} \mathcal{P}_r(\mathbf{k})d\mathbf{k} \\ &= \mathcal{P}_D\,|_{k_s}^{\infty} \\ &= 1 - \mathcal{P}_D(k_s), \end{aligned} \tag{5.6}$$

where $\mathcal{P}_D(k)$ is the wavenumber radial spectral distribution function. We have changed from the multidimensional wavenumber spectral density to the radial wavenumber spectral density in moving from the first to the second line of the equation. This allows us to modify the limits of integration as shown.

We have used this equation to elucidate the connection between the spatial survey error and the wavenumber radial distribution function. The distribution function measures the fractional amount of the total spectral energy which is contained in wavenumbers up to the sampling wavenumber, k_s, and is a monotonic function of that sampling wavenumber. Using this fact, we now see that $\mathcal{E}_\lambda$ is also a monotonically increasing function of k_s. Therefore,

$\mathcal{E}_\lambda$ measures the fractional amount of the total spectral energy which lies outside of the support of the sampling process. Substituting the wavenumber radial spectral density, Equation (5.3), into this Equation (5.6) gives the spatial survey error for this example process,

$$\mathcal{E}_\lambda = \left[\frac{\left(\frac{2\pi}{\lambda_o}\right)^2}{k^2 + \left(\frac{2\pi}{\lambda_o}\right)^2}\right]^{\frac{1}{2}}\Bigg|_{k_s} = \left[\frac{\lambda_s^2}{\lambda_o^2 + \lambda_s^2}\right]^{\frac{1}{2}} \qquad 0 \leq \lambda_s \leq \infty. \tag{5.7}$$

5.2.2 Temporal Survey Error

We now turn our attention to the temporal survey error. For the process that we have specified, the autocorrelation function is given by

$$R(t) = e^{-|t|/\tau_o}. \tag{5.8}$$

Inserting Equation (5.8) in to Equation (3.20), we compute the temporal survey error to be

$$\begin{aligned} \mathcal{E}_\tau &= \frac{1}{\tau_s}\int_{-\tau_s/2}^{\tau_s/2}\left[1 - e^{-|t|/\tau_o}\right]dt \\ &= 1 + \frac{2\tau_o}{\tau_s}\left(e^{-\tau_s/2\tau_o} - 1\right). \end{aligned} \tag{5.9}$$

5.2.3 Total Survey Error

Finally, we combine the spatial and temporal survey errors via Equation (3.21) to form the total survey error, $\mathcal{E}_{tot}$. Inserting Equations (5.7) and (5.9) into Equation (3.21), we obtain

$$\begin{aligned} \mathcal{E}_{tot}(\lambda_s, \tau_s) &= \left[\frac{\lambda_s^2}{\lambda_o^2 + \lambda_s^2}\right]^{\frac{1}{2}} + \left[1 + \frac{2\tau_o}{\tau_s}\left(e^{-\tau_s/2\tau_o} - 1\right)\right] \\ &- \left[\frac{\lambda_s^2}{\lambda_o^2 + \lambda_s^2}\right]^{\frac{1}{2}} \times \left[1 + \frac{2\tau_o}{\tau_s}\left(e^{-\tau_s/2\tau_o} - 1\right)\right], \end{aligned} \tag{5.10}$$

where $0 \leq (\lambda_s, \tau_s) \leq \infty$. This function is plotted for our example problem in Figure 5.1(a). Note that the error contour lines are more closely spaced on the spatial resolution axis than on the total survey time axis. This is a consequence of the fact the the spatial error accounts

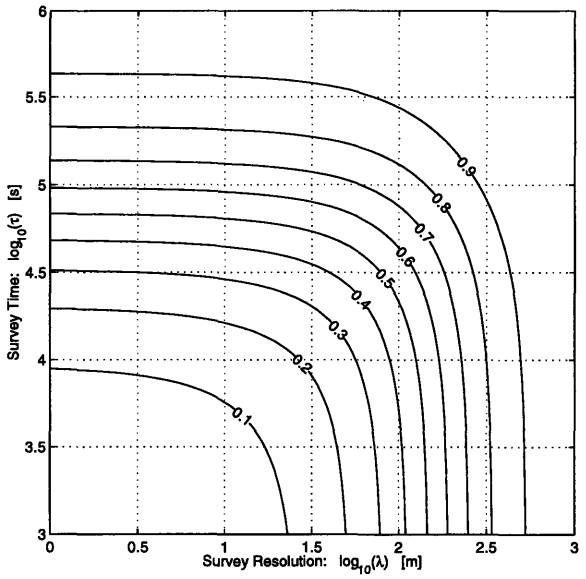

(a)

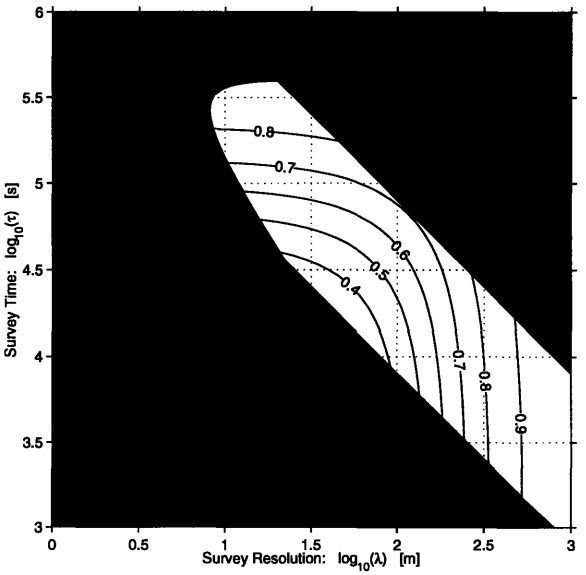

(b)

Figure 5.1: Total survey error and survey analysis plot as a function of (λ, τ). (a) The total survey error is calculated for a grid survey of the example process in a survey domain of area, $A = (2\text{km})^2$. Note that minimal error is achieved for surveys which are sampled densely and quickly. These surveys correspond to "snap-shots" of the process since they have finely grided samples which have been taken "instantaneously" in time. Conversely, $\mathcal{E}_{tot} \to 1$ for coarse and slow surveys, indicating that very little information about the process field has been recovered. (b) The combination of the survey envelope and total survey error forms a tool which can be used to optimize surveys in terms of various survey parameters. For instance, we can use these plots to choose survey resolutions and total survey times to minimize the total survey error subject to the physical constraints imposed by the sampling platform. Each point within the survey envelope gives the total survey error realized for a particular (λ, τ) pair. The minimum error possible for the present example is $\mathcal{E}_{min} = 0.33$.

for errors in two spatial dimensions whereas the temporal survey error accrues errors only in a single dimension.

5.2.4 Survey Analysis Tool

We have used the total survey error metric for our example oceanographic process, Equation (5.10), to generate of plot of the the this error as a function of survey spatial resolution and total survey time. Figure 5.1(a) indicates that surveys which have minimal survey error correspond to surveys which are quickly and densely sampled. However, as we saw in Section 3.2, fast and dense surveys also correspond to high energy consumption. A trade-off between energy consumption and the total survey error must be made to obtain optimal survey parameters. The focus of this section will be the development of an analysis tool which can be used to guide these trade-off decisions.

Recall that in Section 3.2 we generated a contour plot of the total energy consumed by an Odyssey IIb AUV for a uniform grid survey of a square survey domain of area, $A = 4\,\mathrm{km}^2$. Figure 3.2 gave the energy consumed as a function of the survey spatial resolution and total survey time, (λ_s, τ_s). We argued that some regions of this plot were not reachable by the AUV due to limitations on the vehicle speed and total stored energy. These limitations were embodied by the survey envelope, Figure 3.3, which partitioned the (λ_s, τ_s) space into accessible and inaccessible regions for an Odyssey IIb AUV.

If we combine the survey envelope with the total survey error by directly superimposing Figure 3.3 and Figure 5.1(a), we generate a plot which indicates the survey errors achievable for all combinations of the survey parameter pair, (λ_s, τ_s) by an Odyssey IIb AUV surveying the example process of the previous section. This is shown in Figure 5.1(b). Plots such as these are what we have termed the "survey analysis tool". They allow us to make objective judgements about the various issues involving AUV survey design and vehicle selection and/or design. For instance, using Figure 5.1(b), we can can readily determine the minimum error, $\mathcal{E}_{min} = 0.33$, which can be achieved with the Odyssey IIb AUV for this particular survey example. Surveying at any combination of (λ_s, τ_s) other than those specified by this minimum value will result in decreased survey efficiency. In the most general case, these plots would require three separate spatial dimensions and one temporal

dimension as well as three distinct correlation distances for the three cardinal directions. We have used that fact that the example process is spatially isotropic to reduce the spatial dimensionality. The use of this tool for survey analysis and vehicle design is the topic of the next section.

5.3 Applications

There are numerous internal and external parameters which effect the performance of an AUV survey of an oceanographic process. The complex interconnections of these parameters compound the difficulties of designing field experiments which makes extensive use of AUVs. The survey analysis tool of Section 5.2 was developed as an aid in sorting out these interconnections. In this section we will demonstrate the application of the survey analysis tool to this task. The external parameters mentioned above, such as the size of the survey domain and the choice of survey spatial resolution and duration, are examined in Section 5.3.1. The effects of the internal parameters, such as vehicle speed constraints, are discussed in Section 5.3.2. The example random process of Section 5.2 provides necessary context for the analyses below.

5.3.1 Survey Design

Although there are numerous external parameters which influence the performance of an AUV survey, the three parameters which have the greatest impact upon the overall survey performance are (i) the ratio of the survey spatial resolution to the characteristic length scale (correlation distance) of the process of interest, (λ_s/λ_o); (ii) the ratio of the total survey time to the time constant (correlation time) of the process, (τ_s/τ_o); and (iii) the non-dimensionalized size of the survey domain, (A/λ_o^2). In this section we will explore the effect of these three parameters on the overall survey performance through the application of the survey analysis tool and discuss the ramifications for AUV survey designs.

In Section 5.2.4 we showed that the survey analysis tool can be used to select the (λ_s, τ_s) pair which gives the minimum survey error for our example process. We now revisit this idea. In Figures 5.2(a)-(c), we show analysis tool plots for varying survey domain areas.

Area	$\varepsilon_{\mathbf{tot}}$	$\lambda_{\mathbf{opt}}$ (m)	$\tau_{\mathbf{opt}}$ (s)	Comment
$A = (1\text{km})^2$	0.18	24.5	8.71×10^3	Figure 5.2(a)
$A = (2\text{km})^2$	0.33	43.7	1.86×10^4	Figure 5.2(b)
$A = (3\text{km})^2$	0.44	64.6	2.88×10^4	Figure 5.2(c)
$A = (2\text{km})^2$	0.29	55.0	9.77×10^3	Figure 5.2(d), $V_{max} \rightarrow 2V_{max}$

Table 5.1: Total survey errors for surveys of the example process of Section 5.2 with one standard Odyssey IIb AUV. The example process has correlation length and time scales of $\lambda_o = 256$ meters and $\tau_o = 6$ hours, respectively. We see that smaller survey domains correspond to lower overall survey errors.

The minimum survey errors in each of these plots (Table 5.1) are located along the lower left corner region of the survey envelope. This is a consequence of the fact that we must sample densely and quickly to achieve small errors. Minimum survey errors lie along the boundaries of the survey envelope, indicating either that all of the vehicle's energy has been consumed (curvilinear portions of the boundary) or that the vehicle has reached its maximum speed constraint in attaining this minimum error (linear portions of the boundary). Note also that the minimum error is strongly tied to the area of the survey domain. This agrees with our intuition that smaller errors will be achieved in smaller survey domains. The size of the survey domain is the first parameter which the experimenter should choose when designing an AUV field program since this choice has the greatest impact on the overall survey performance.

Having made the choice of survey domain size, the researcher should then decide how many surveys should be made. If the generation of a high-resolution "snap-shot" of the process of interest is the overriding objective of the experiment, then a single survey which achieves a small error is desired. However, if greater errors can be tolerated, then multiple surveys are perhaps in order. Consider a survey of the example process in a domain of area $A = 1\text{ km}^2$. We see from Figures 5.2 and 3.3 that either one survey could be conducted at high spatial and temporal resolutions (with an error of, say, $\mathcal{E}_{tot} \approx 0.20$) or two or more surveys could be made (all with errors of, say, $\mathcal{E}_{tot} \approx 0.35$) before exhausting the vehicle' batteries. The ability to conduct multiple surveys with an AUV before it requires servicing is very attractive from an operational standpoint. It also adds a new dimension to the

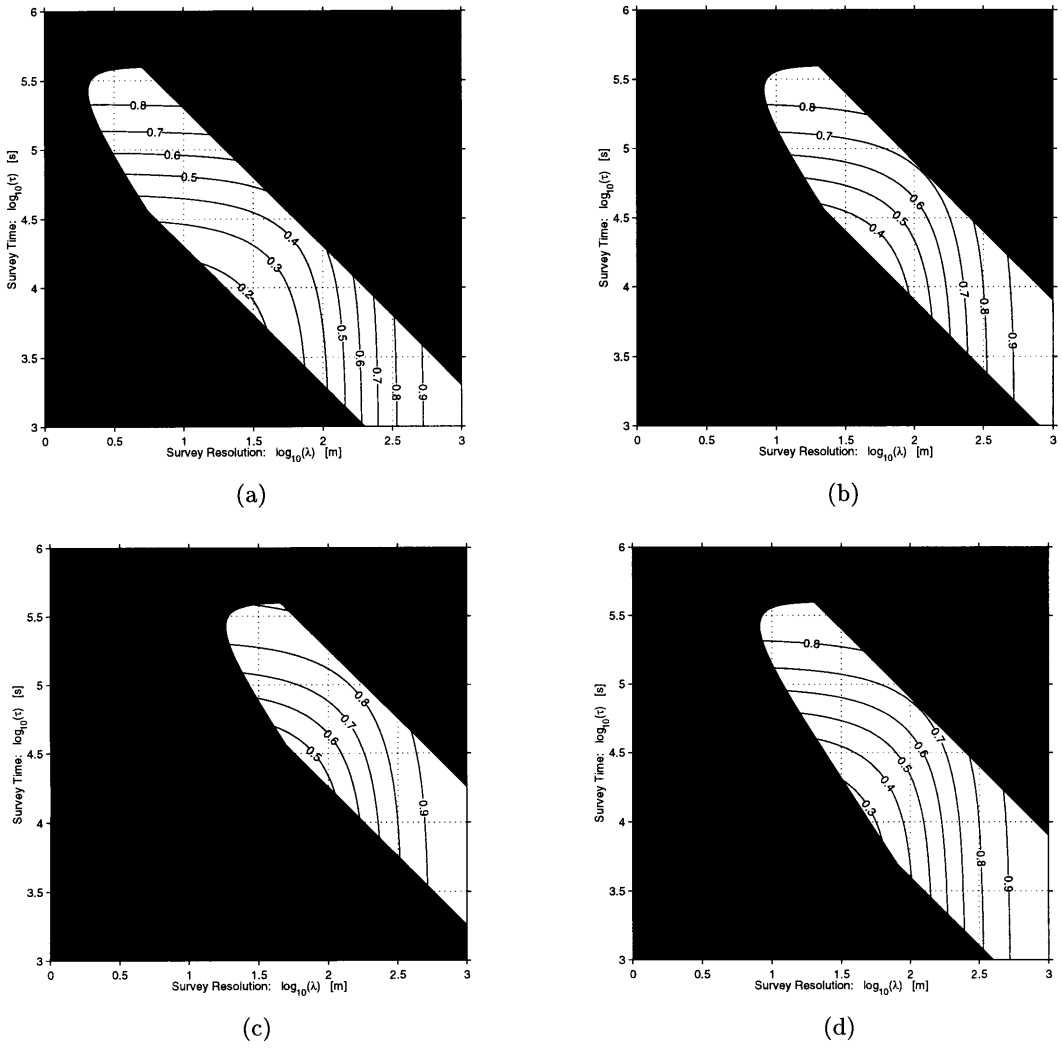

Figure 5.2: Total survey error with survey envelopes. The total survey error is calculated via Equation (5.10) for an example process random field which has correlation length and time scales of $\lambda_o = 256$ meters and $\tau_o = 6$ hours, respectively. Odyssey IIb vehicle parameters are used to generate the survey envelope. The size of the survey domain is $A = (1\text{km})^2$ in (a), $A = (2\text{km})^2$ in (b) and (d), and $A = (3\text{km})^2$ in (c). Figures (a)-(c) show the effect of changing the overall size of the survey domain on the total survey error. We see that surveys in smaller domains achieve lower total survey errors since these surveys can be conducted on denser grids and completed more quickly than surveys over larger domains. Figure (d) is calculated for a vehicle which has a maximum speed which is twice that of the standard Odyssey IIb AUV. For this survey we see that the total survey error is determined by the energy constrained portion of the survey envelope. This serves to elucidate the way in which different components of the survey envelope (energy or velocity constraints) determine the total survey error. The size of the survey domain is $A = (2\text{km})^2$. Minimum survey errors for each plot are given in Table 5.1.

survey/experiment design process. Although it has not been addressed in this work, we can see that an extension of the survey performance metric that takes into account the correlated observations from several AUV missions is desired to facilitate the design field experiments which incorporate multiple surveys with AUVs.

Yet another dimension of the survey design problem illuminated by the survey analysis tool is the fact that a continuum of surveys are possible at any given value of $\mathcal{E}_{tot}$ (except in the case $\mathcal{E}_{tot} = \varepsilon_{min}$). Looking again at Figure 5.2, we see that if we stipulate a desired total survey error performance criterion, say, $\mathcal{E}_{tot} = 0.5$, for example, then all of the (λ_s, τ_s) pairs lying along the curve defined by this criterion correspond to valid surveys which achieve the desired performance. The surveys along this curve trade-off spatial resolution against total survey time to maintain a constant value for the total survey error. Again, the survey designer must determine which of these surveys would be most well suited for a particular scientific program. This decision is illustrated with an example.

Consider only the two surveys lying on the curve $\mathcal{E}_{tot} = 0.5$ which touch the boundaries of the survey envelope. From Figure 5.2, we see that one of these surveys will be as fast as possible but will have poor spatial resolution. The other survey will have fine spatial resolution but will take a long time to complete. These surveys also differ in that the slow but densely sampled survey is constrained by the size of the vehicle's battery while it is the AUV's maximum speed which limits the fast but coarsely sampled survey. In fact, after reviewing Figure 3.3, we see that the fast but coarse survey consumes only about half of the available energy, leaving open the possibility of a second survey. Again, the researcher must make a choice regarding the utility of differing survey strategies using the insight gained from the application of the survey analysis plots.

We have demonstrated above how the survey analysis tool can be used as an aid in the design of AUV survey experiments. In the next section we will discuss the use of this tool in selecting and/or designing AUVs which are tailored to specific scientific missions or which meet certain broad operational objectives.

Area	Parameter	ε_{tot}	λ_{opt} (m)	τ_{opt} (s)	Figure
$(2\text{km})^2$	H, η, Battery	0.33	43.7	1.86×10^4	5.3(a)-(c)
$(2\text{km})^2$	Four AUVs	0.22	35.5	8.91×10^3	5.3(d)
$(3\text{km})^2$	Four AUVs	0.34	57.5	1.41×10^4	Not Shown

Table 5.2: Total survey errors for surveys of the example process of Section 5.2 with modified vehicle parameters. The example process has correlation length and time scales of $\lambda_o = 256$ meters and $\tau_o = 6$ hours, respectively. We compare these survey analysis plots with that for a survey of the same example process with a single Odyssey IIb AUV.

5.3.2 Vehicle Design

Internal variables which influence AUV survey performance are factors such as the capacity of the vehicle's battery, the efficiency of its propulsion system, the vehicle's hotel load, and its maximum speed. In the discussion to follow, we will employ the survey analysis tool to gain insight into the effects of these variables on the overall performance of an AUV survey. Because it is difficult to increase the maximum speed of an AUV while maintaining a small form factor (an assumed design constraint), we entertain the possibility of multiple vehicle surveys. A small fleet of AUVs can perform a coordinated grid survey of a given domain more quickly than a single vehicle could complete this survey. Employing multiple vehicles in a survey is roughly equivalent to surveying with a single modified AUV which has a greater maximum speed (assuming uniform grid surveys). For this reason, we classify the decision to use multiple vehicles as a vehicle design parameter. Survey analysis plots with modified vehicle parameters are shown in Figures 5.3 and 5.4 for surveys of the example process of Section 5.2. We compare these survey analysis plots to those of surveys of the same process and and over the survey domain but with an unmodified Odyssey IIb AUV.

In Figure 5.3, survey analysis plots are shown for surveys of the example process by modified standard Odyssey IIb vehicles. These surveys were conducted over a domain of area $A = (2\,\text{km})^2$. These plots illuminate the effect of modifying various vehicle parameters on overall survey performance. The minimum survey errors and corresponding $(\lambda_{s,opt}, \tau_{s,opt})$ for these surveys are given in Table 5.2. We discuss the effects of modifying the vehicle parameters below:

Reduced Hotel Load In Figure 5.3(a), the vehicle's hotel load, H, is reduced to 1/4 of

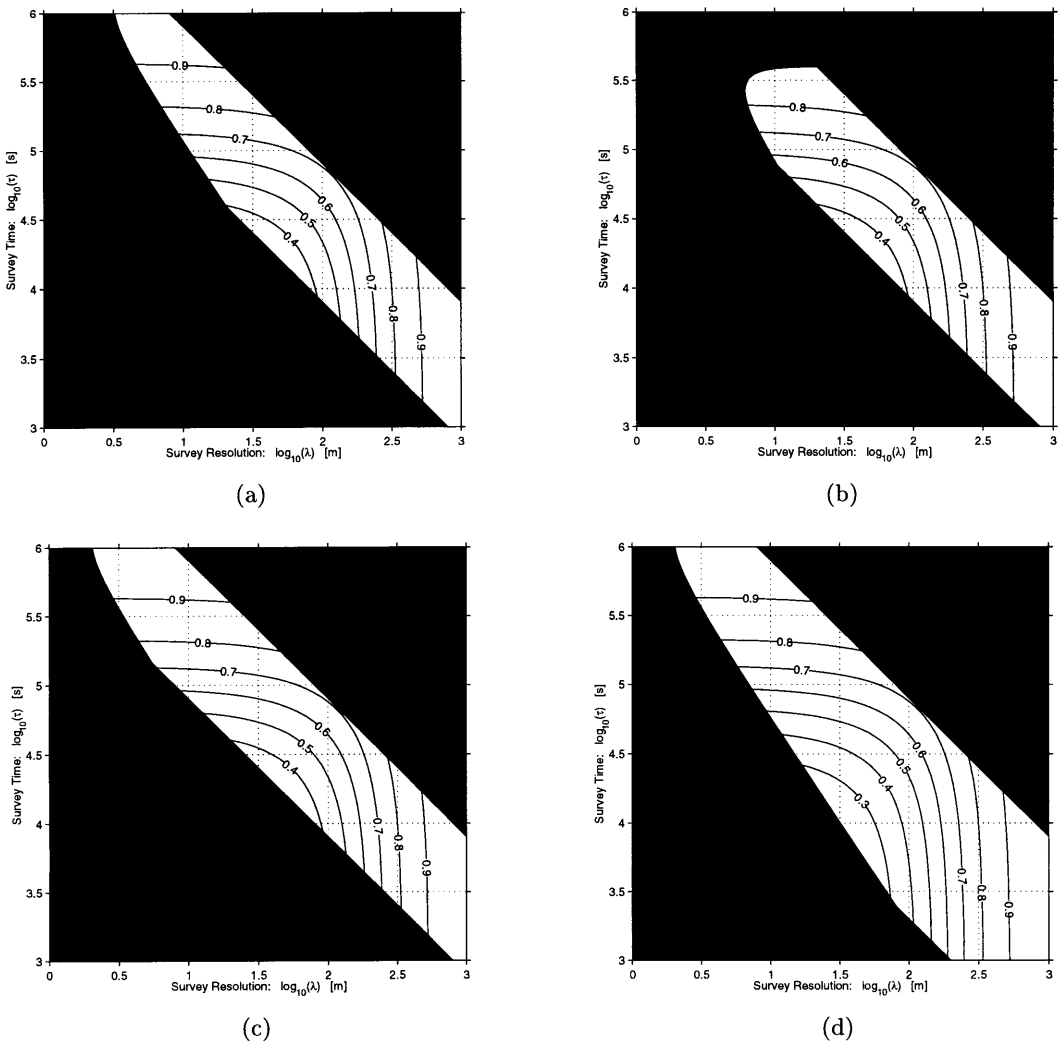

Figure 5.3: Survey analysis plots for modified parameters. The survey envelope is calculated with modified vehicle parameters. The underlying total survey error plot is for a survey domain of area $A = (2\text{km})^2$. (a) The vehicle's hotel load, H, is reduced to 1/4 of the standard Odyssey IIb value. Comparing the shape of the survey envelope to that of the standard Odyssey IIb vehicle (Figure 5.2(b)), we see that decreasing the hotel load has increased the survey envelope, but only to allow longer total survey times. The minimum survey error is the same as for the standard Odyssey IIb configuration: $\varepsilon_{min} = 0.33$. (b) The vehicle's inefficiency, $(1 - \eta)$, is reduced to 1/4 of its previous value. This pushes the energy boundary (upper left) of the survey envelope toward the left side, allowing some more densely sampled surveys. However, since the minimum survey error lies towards the lower left of the plot, the minimum survey error remains the same. (c) The vehicle's battery is made 4 times larger. The survey envelope increases towards the upper left corner. Again, the minimum survey error does not change. (d) Four standard Odyssey IIb vehicles are employed in this survey. This dramatically effects the survey envelope by moving the maximum velocity constraint towards the lower left. We see that the energy boundary of the survey envelope is now the limiting factor. The minimum survey is significantly reduced: $\varepsilon_{min} = 0.22$.

the standard Odyssey IIb value. Comparing the shape of the survey envelope to that of the standard Odyssey IIb vehicle (Figure 5.2(b)), we see that decreasing the hotel load has also changed the shape of the survey envelope, pushing the energy boundary of the envelope towards the upper left corner of the plot. However, this does not result in a reduction in the minimum survey error over that of the standard Odyssey survey since the minimum error is determined by the vehicle speed constraint for this example. The minimum survey error is $\varepsilon_{min} = 0.33$.

Increased Propulsion Efficiency In Figure 5.3(b), the vehicle's propulsion inefficiency, $(1 - \eta)$, is reduced to 1/4 of its previous value, resulting in an overall increase in propulsion efficiency. This pushes the energy boundary (upper left) of the survey envelope toward the left side, allowing some more densely sampled surveys. However, since the minimal survey errors lie towards the lower left of the plot, the minimum survey error does not change. These surveys do require less energy to conduct since the propulsion inefficiency has decreased. This can be beneficial if the field program calls for more than one AUV survey mission to be completed by the vehicle.

Increased Battery Capacity Next, the vehicle's battery is made four times larger, Figure 5.3(c). The survey envelope increases towards the upper left corner. Again, the minimum survey error does not change. The fact that the minimum error does not change even when a larger battery is used indicates the severity of the maximum velocity constraint.

Multiple Vehicle Surveys Because it is quite difficult in general to increase an AUVs maximum velocity without increasing its size or moving to a different energy source (such as chemical/combustion engines), we examine the use of multiple vehicles in Figure 5.3(d). Four Odyssey IIb vehicles are employed in these surveys. These vehicles have reduced battery capacity so that the total energy available for the survey is the same as if a single Odyssey IIb AUV were being used in the survey. The use of multiple vehicles dramatically affects the survey envelope by moving the maximum velocity constraint towards the lower left. We see that the energy boundary of the survey envelope is now the limiting factor. The minimum survey error is significantly

Area	Parameter	$\varepsilon_{\mathbf{tot}}$	$\lambda_{\mathbf{opt}}$ (m)	$\tau_{\mathbf{opt}}$ (s)	Figure
$(2\text{km})^2$	Hotel	0.29	55.0	9.77×10^3	5.4(a),(b)
$(2\text{km})^2$	η, Battery	0.25	33.1	1.22×10^4	5.4(c)
$(2\text{km})^2$	Four AUVs	0.22	37.2	8.51×10^3	5.4(d)

Table 5.3: Total survey errors for surveys of the example process of Section 5.2 with modified vehicle parameters for a fast vehicle, i.e., $V_{max} \rightarrow 2V_{max}$. The example process has correlation length and time scales of $\lambda_o = 256$ meters and $\tau_o = 6$ hours, respectively. We compare these survey analysis plots with that of a survey of the same example process using a single Odyssey IIb AUV.

reduced: $\varepsilon_{min} = 0.23$.

Table 5.2 also gives the minimum survey error for a survey scenario in which four vehicles are used to survey the example process over a domain of size $A = (3\text{km})^2$. The total survey error for this survey is just slightly more than the errors for the single modified AUV surveys in the smaller domain. Thus, four vehicles are required to achieve equivalent survey performance when the survey domain is increased by a factor of 2.25. This demonstrates again that the choice of the size of the survey domain dominates the overall survey performance for grid surveys.

We see from the analyses of Figure 5.3 that any technique which can be used to increase an AUV's maximum speed will result in lower minimum survey errors. In light of this fact, we have repeated the analysis of Figure 5.3 using a hypothetical vehicle which is twice as fast as the standard Odyssey IIb vehicle (i.e., $V_{max} = 5$ meters/second). These survey analysis plots are shown in Figure 5.4 and the minimum survey errors and corresponding $(\lambda_{s,opt}, \tau_{s,opt})$ for these surveys are given in Table 5.3. In Figure 5.4(a), the fast vehicle's hotel load, H, is reduced to 1/4 of the standard Odyssey IIb value. Comparing the shape of the survey envelope to that of the fast Odyssey IIb vehicle (Figure 5.2(d)), we see that decreasing the hotel load has increased the survey envelope towards the upper left. The minimum survey error is the same as for the unmodified survey envelope for the fast vehicle: $\varepsilon_{min} = 0.29$. In Figure 5.4(b), the fast vehicle's inefficiency is reduced to 1/4 of its standard value. This pushes the energy boundary (upper left) of the survey envelope toward the left side, with the consequence that the maximum velocity constraint now controls the minimum survey error, which decreases slightly: $\varepsilon_{min} = 0.25$. The vehicle's battery is made four times larger in Figure 5.4(c). The energy boundary of the survey envelope continues to increase

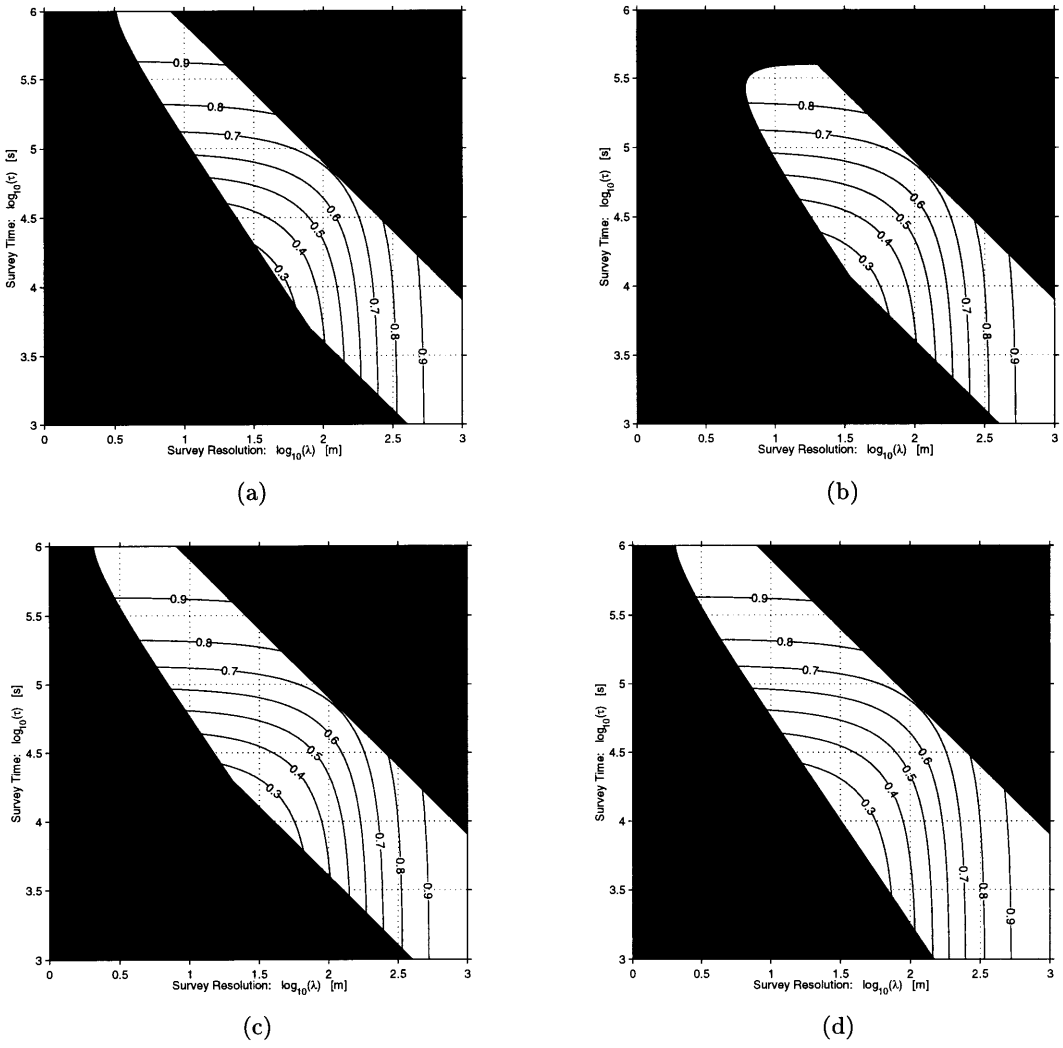

Figure 5.4: Survey analysis plots for modified parameters for a fast vehicle. The analyses of Figure 5.3 is redone with a vehicle which is twice as fast as the standard Odyssey IIb vehicle (i.e., $V_{max} = 5.0$ meters per second. (a) The fast vehicle's hotel load, H, is reduced to 1/4 of the standard Odyssey IIb value. Comparing the shape of the survey envelope to that of the standard Odyssey IIb vehicle (Figure 5.2(d)), we see that decreasing the hotel load has increased the survey envelope towards the upper left. The minimum survey error is the same as for the unmodified survey envelope for the fast vehicle: $\varepsilon_{min} = 0.29$. (b) The fast vehicle's inefficiency, $(1-\eta)$, is reduced to 1/4 of its previous value. This pushes the energy boundary (upper left) of the survey envelope toward the left side, with the consequence that the maximum velocity constraint now controls the minimum survey error. This error decreases slightly: $\varepsilon_{min} = 0.25$. (c) The vehicle's battery is made 4 times larger. The energy boundary of the survey envelope continues to increase towards the upper left corner. Since the minimum error is determined by the maximum velocity constraint, the minimum error is still $\varepsilon_{min} = 0.25$. (d) Four fast vehicles are employed in this survey. The maximum velocity constraint is no longer relevant. The energy boundary again controls the minimum survey error. This minimum error is reduced to $\varepsilon_{min} = 0.22$. Note that the reduction is not nearly as significant as that seen for the standard Odyssey IIb surveys, Figure 5.3.

towards the upper left corner. Since the minimum error is determined by the maximum velocity constraint, the minimum error is still $\varepsilon_{min} = 0.25$. Next, four fast vehicles are employed in Figure 5.4(d). We see that the maximum velocity constraint is no longer relevant. The energy boundary again controls the minimum survey error. This minimum error is reduced to $\varepsilon_{min} = 0.22$. Note that the reduction is not nearly as significant as that seen for the standard Odyssey IIb surveys, Figure 5.3.

Using analyses such as these, the researcher is able to objectively compare the various AUV platforms to determine which platform is best suited to a specific scientific program or field experiment. The analysis plots can also be employed by the vehicle designers to guide them in making crucial trade-offs during the initial phases of a new vehicle design. For existing vehicles, the above analysis suggests design modifications which would be beneficial to the overall vehicle performance. For instance, our analysis for the Odyssey IIb AUV indicates, at least in the context of this example, that little effort should be spent on reducing the hotel load of a vehicle since such a reduction is not likely to result in reduced minimum survey errors or in lower energy consumption. We want to emphasize here that the error results are valid only within the context of the example random field process of Section 5.2.

In this section we have demonstrated the use of the survey analysis tool in guiding the survey and vehicle design processes. In the following section we will apply the survey analysis tool to the design of an AUV survey of a real oceanographic process.

5.4 Application to Open-Ocean Deep Convection

Open-ocean deep convection plays a key role in ocean circulation. It mixes surface water with deeper water and thus renews the intermediate and deep waters of the ocean. It is most likely to occur during prolonged winter storms when the surface heat flux (cooling by low air temperature and gales) is largest. Labrador Sea is one of only a few deep convection locations in the world, along with the Greenland Sea and several locations around Antarctica. Owing to its importance, the Labrador Sea will be intensely studied in the coming years. Several Odyssey IIb AUVs will be utilized in sampling the convective field.

5.4.1 Open-Ocean Deep Convection: The Model

The process of interest can be modeled using a non-hydrostatic model [22, 65]. In one idealized analogue we consider an initially homogeneous and motionless water volume filling a cubic box of dimensions 9.6 km $\times$ 9.6 km in the horizontal and 2 km in depth. The water is cooled at the top surface, inducing convective overturning in the water column. Heat fluxes out of the bottom and sides of the model domain are not allowed. The top surface is subjected to a cooling with a mean temperature decrement of $\Delta T = 4.4 \times 10^{-5}$ °C/s. This is equivalent to a mean buoyancy flux of $B = 5 \times 10^{-7}\,\mathrm{m^2/s^3}$, associated with a surface heat flux of about 1000 $\mathrm{W/m^2}$, which is typical of the loss at the height of a winter-time storm. To initiate convective instability, the decrement of temperature is modulated by a random number between 0.5 and 1.5 over the whole top surface.

The model's temporal autocorrelation function for vertical velocity is shown in Figure 5.5(a). The autocorrelation function has a maximum time lag of 12 hours with granularity of 30 seconds and was calculated as an average of time-series observations at 192 fixed locations throughout the model domain. We see from this figure that the autocorrelation function decays to zero after approximately 12 hours. To calculate the horizontal spatial energy density spectrum of vertical velocity, the model was allowed to evolve for 12 hours at which time the convection has become well established. We then sampled a horizontal plane at a depth of 600 m and these observations were used to calculate the horizontal spatial spectrum shown in Figure 5.5(b). The spectrum exhibits a peak at a corresponding wavelength of 1000 m, this being the characteristic distance between convective plumes. We see from Figure 5.5(b) that the spatial structure of the convection process is dominated by long-wavelength motions which are well resolved by the 50 m numerical grid spacing of the model. These space and time scales are not atypical of the real process.

Let us now assume, for the sake of an example, that we wish to grid survey over a fixed square area, $A = 1\,\mathrm{km^2}$, using an Odyssey IIb AUV. By numerical integration using Equations 3.17, 3.20, and 3.21, we combine the spatial and temporal survey errors and form the total survey error, which is shown in Figure 5.6(a). When combined with the survey envelope and its underlying energy surface, the resulting survey analysis plots allow us to analyze several aspects of the survey design process.

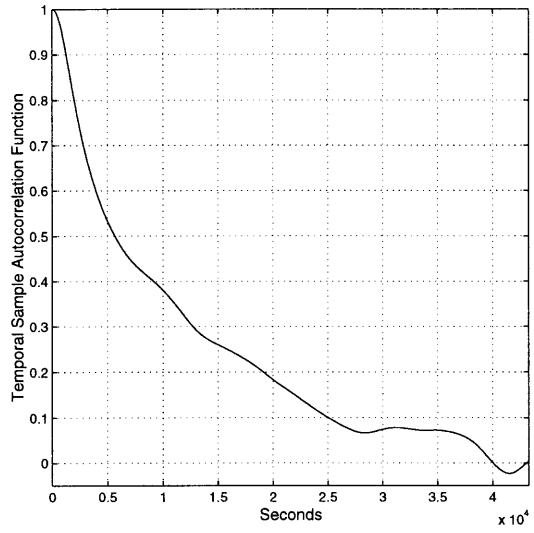

(a)

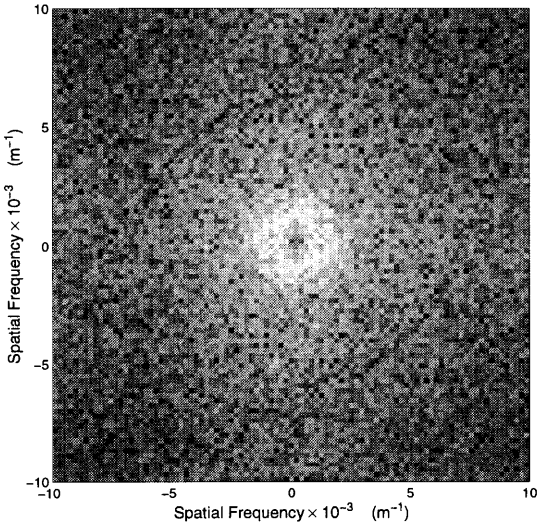

(b)

Figure 5.5: Open-ocean deep convection statistics. (a) The temporal sample autocorrelation function is calculated from observations of an open-ocean deep convection model [22, 65]. We see that the $\frac{1}{e}$-correlation time is approximately 10^4 seconds. The temporal sample autocorrelation goes to zero after approximately 12 hours. The function has the general shape of a decaying exponential. (b) Spatial frequency energy density spectrum is also calculated from observations of the convection model. We see a spectral peak at approximately $10^{-3}\,\mathrm{m}^{-1}$, corresponding to the characteristic separation distance of the convection plumes of approximately 1000 meters. We also see that the spectrum is isotropic in the horizontal spatial dimensions.

5.4.2 Surveys of the Convection Model

The error as a function of survey time and grid spacing is shown in Figure 5.6(a). As expected, Figure 5.6(a) indicates that minimum error surveys are accomplished rapidly, and with fine spatial resolution. Given the relatively short mission times required by the temporal autocorrelation (less than about three hours) and a maximum speed constraint on the vehicle of 2.5 m/s, missions are not constrained by battery capacity. Consequently, the important survey constraint for this example is maximum vehicle speed. The fact that the energy constraint does not influence the survey envelope in this instance indicates that increasing the size of our battery will not effect the shape of the survey envelope and, hence, we will see no reduction in total survey error.

By superimposing the survey envelope on top of the total error surface (Figure 5.6(b)), we are able to locate the combination of spatial resolution and total survey time which gives a minimum total survey error while remaining within the operational capabilities of the AUV. For this example a survey area of one square kilometer is used. The minimum survey error is $\mathcal{E}_{min} = 0.40$ and lies at the point $(\lambda, \tau) = (75$ m,5200 s) in the survey parameter space.

Decreasing the area covered by the survey or increasing the number of AUVs used in the survey allows the total survey error to be reduced significantly. In Figure 5.6(c), we have reduced the total survey region to $A = (1/2\,\mathrm{km})^2$. This has the effect of changing the error surface underlying the survey envelope, resulting in a minimum survey error of $\varepsilon_{min} = 0.20$.. Alternatively, if we use three AUVs to survey the original survey area, $A = (1\,\mathrm{km})^2$, we can again lower the total survey error, Figure 5.6(d). In this case, the total survey error is decreased because the collective survey speed of the vehicle is faster, pushing the limiting edge downward, with a resulting minimum error of $\varepsilon_{min} = 0.25$. In all cases, it is important to note that the optimal survey parameters, $(\lambda_{opt}, \tau_{opt})$, may lie in a region of the survey parameter space to the left of the region shown. We have not been able to explore this region because we are limited on the spatial resolution axis by the grid spacing of the convection model and by our numerical treatment of that model.

From the survey analyses of Figure 5.6 we can better appreciate the trade-offs necessary in surveying open-ocean deep convection using an AUV. For example, since the characteris-

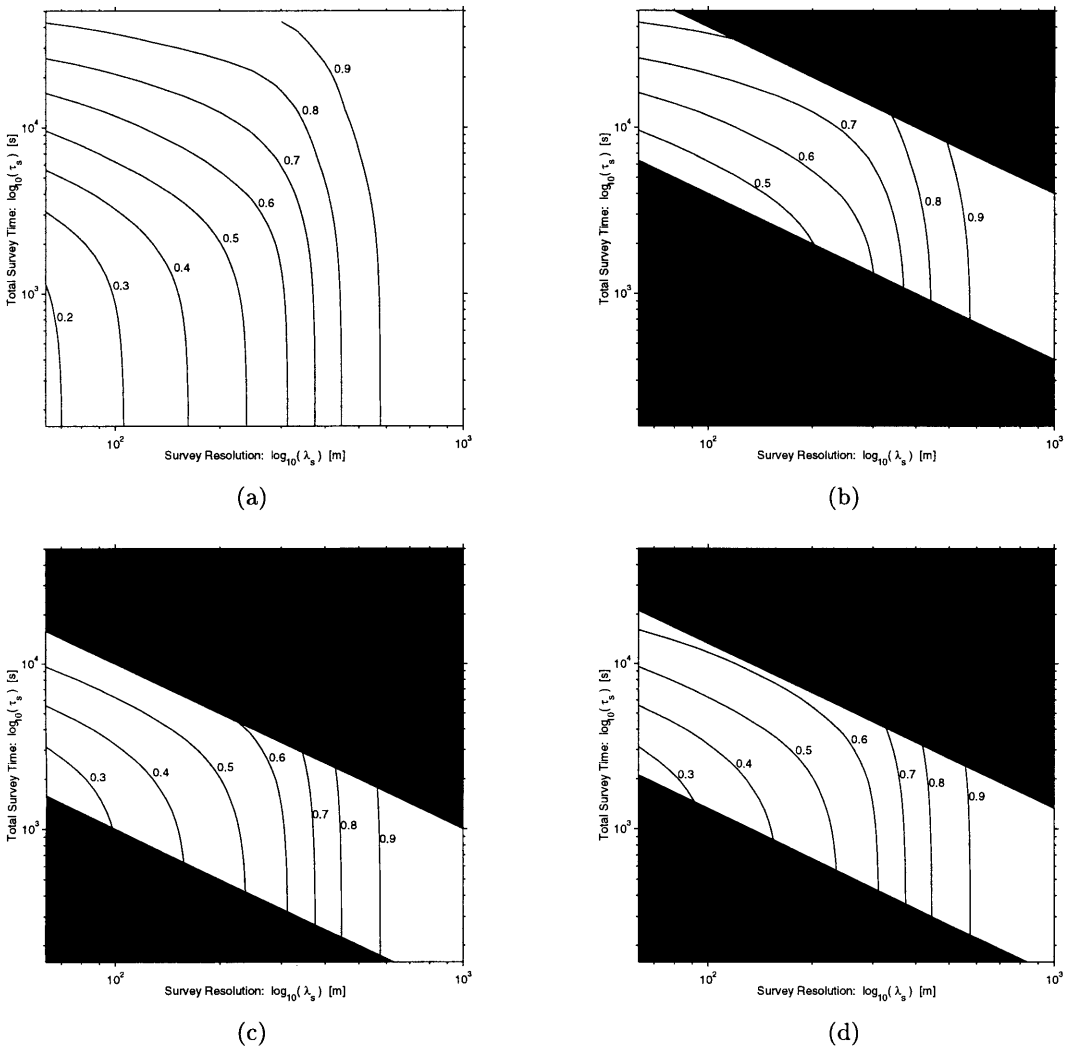

Figure 5.6: Survey analyses for open-ocean deep convection. (a) Total Survey Error as a function of (λ, τ). Note that minimal error is achieved for surveys which are sampled densely and quickly. Conversely, $\mathcal{E}_{tot}$ is maximized for slow and coarsely samples surveys. (b) Survey analysis plot for a survey of an open-ocean deep convection process over a square domain of area $A = (1\,\text{km})^2$. We see that the energy boundary of the survey envelope is not relevant for this survey. The resulting minimum total survey error is $\mathcal{E}_{min} = 0.40$. (c) Survey analysis plot for a grid survey over a square domain of area $A = (0.5\,\text{km})^2$. The survey envelope translates downward, giving access to surveys with lower total error. The vehicle's maximum velocity constraints the minimal error to be $\mathcal{E}_{min} = 0.20$. (d) Survey analysis plot for a grid survey in which three Odyssey IIb AUVs are used to grid survey a square domain of area $A = (1\,\text{km})^2$. This survey achieves performance comparable to that of (c) with a minimum total survey error of $\mathcal{E}_{min} = 0.25$.

tic distance between convective plumes is approximately 1000 m, the minimum error survey of Figure 5.6(c) would give acceptable performance if the scientific objective is, for instance, to make an accurate estimate of the vertical heat within the interior of a single plume. Alternatively, if the mission goal is gather information about the distribution or formation of the convective plumes, then the surveys of Figure 5.6(c) would not be well suited because they are too spatially localized. The minimum error surveys of Figures 5.6(b) and 5.6(d) or ones over even larger survey domains would be more appropriate for this scientific objective.

5.5 Discussion

The above analyses demonstrate how grid surveys of dynamic phenomena can be optimized given statistical knowledge of the process under study. Clearly the difficult part of this exercise is obtaining the statistics. Here we have used a convection model to obtain the required information. Others sources include prior observations from such platforms as moorings, drifters, towed bodies, and satellites. Of course there is no guarantee that either a convection model or the prior observations will be valid for the actual survey run.

For occasions when there is no a priori knowledge of the phenomena, one promising scenario involves multiple AUV runs. Initial runs would be used to obtain the spatial statistics, which would in turn allow design of the final survey. However, while the AUV can readily characterize spatial variability, temporal variability is not so easily obtained. For the AUV to make such measurements implies a longer mission, and requires the vehicle to measure the same volume of water repeatedly. This last requirement imposes navigation demands which may or may not be achievable.

Finally, it is worth noting the difficulty of synoptically mapping a dynamic phenomena. For the open-ocean deep convection survey designs of Section 5.4, the best synoptic map one could hope to achieve only covers one square kilometer, even with three vehicles. For a single towed body behind a ship, however, a synoptic map is probably not achievable on any scale at the specified 600 m depth. Clearly, further work on survey and platform design is necessary to enable the collection of synoptic-scale data from rapidly evolving, spatial phenomena.

Chapter 6

Conclusion

In this work we have explored the problem of reconstructing spatially distributed, time evolving process fields with samples from AUV surveys. We have identified general issues and challenges involved in surveying with AUVs, developed survey performance metrics which quantify vehicle energy consumption and both spatial and temporal survey errors. We have then used these performance metrics to gain insight into the design of AUV surveys of oceanographic processes and to identify useful ways to customize the design of an AUV to a particular class of processes of interest. These contributions are discussed in greater detail in Section 6.1. The contributions of this thesis to the general problem of surveying with AUVs are important because they place the survey design problem firmly within a quantitative framework. However, significant modifications and improvements to the current work are certainly possible and will definitely be needed as the use of AUVs in oceanographic and other settings grows and matures. With this in mind, the discussion of Section 6.2 focuses on continuations of the work of this thesis as well as new directions and problems to be explored.

6.1 Contributions

In Chapter 1 we asked the questions: Given an oceanographic process of interest with its associated spatial and temporal scales, what are the AUV survey trajectories which give the best survey performance in terms of some performance metric? What should

this performance metric be? In this thesis, we have addressed these questions within the context of the field estimation problem. The contributions which we have made towards these problems are described below.

6.1.1 Exploration of Issues

In Chapter 2, we examined several issues and challenges inherent in surveying with AUVs. These issues were necessary context for the development of later chapters. They also point to areas in which further exploration is required. In particular, the lack of computationally efficient inversion algorithms for spatially distributed data is a difficulty which goes to the heart of the whole sampling problem. We will see in Section 6.2 that new and promising spatial data processing techniques are on the horizon. The application of these techniques to the AUV survey sampling problem has the potential to revolutionize the way that oceanography is practiced through the realization of fully functional coupled observational/modeling systems. However, for this to be possible, many of the engineering challenges identified in Chapter 2 must also be addressed. Power management and improved battery technologies will be vital to the implementation of autonomous ocean sampling networks, as will the development of reliable and fast underwater communication and navigational networks. Finally, advances in the area of reactive and adaptive survey design will be necessary as an enabling technology of the AOSN paradigm.

6.1.2 Performance Metrics

In Chapter 3 we reviewed the energy economics of surveying with AUVs and created the survey "envelope" which quantifies AUV energy consumption for a given survey domain in terms of the survey's spatial resolution, λ_s, and the total survey time, τ_s. We also explored the errors inherent in reconstructing a spatial field from temporally blurred survey samples. Two error metrics were developed, one of which measures the error due to spatial undersampling of the phenomenon of interest. The second metric estimates the errors due to the temporal evolution of the process field over the course of the survey. These error metrics were combined into a single total survey error metric. In developing these metrics, we made several simplifying assumptions in order to make the problem tractable. These

assumptions were:

1. The process of interest is temporally stationary and spatially homogeneous. Although spatial isotropy was not a requirement, *per se*, imposed by Equation (3.17), it was nevertheless assumed in the development of following chapters in order to simplify the computations.

2. The frequency and wavenumber spectra (or, equivalently, the spatial and temporal autocorrelation functions) of the process of interest were assumed to be known. It was further assumed that these spectra (autocorrelation functions) were separable functions of frequency and wavenumber (time and space). This was a consequence of the assumption that the temporal and spatial error metrics were uncorrelated (see Section 3.3.3) and placed restrictions upon the class of processes for which the total survey error metric would be valid.

3. Errors due to AUV positional uncertainties were assumed to be negligible. This stipulation is equivalent to claiming that the uncertainties in the position of the AUV are much smaller that the spatial resolution scale of a given survey. This seems reasonable given some external navigational aid such as an acoustical long-baseline system [61], which can give positional uncertainties as low as 1-10 m.

4. The process of interest was assumed to be the only oceanographic phenomenon at play in the survey region. This assumption excludes, for example, ocean currents and tides. As discussed Chapter 2, the presence of currents can severely impact the quality of AUV sampled data.

5. Errors due to the finite length of the AUV surveys (i.e., truncation errors) were also assumed to be negligible. While this may be a reasonable assumption for densely grided surveys, it will be an increasingly poor assumption for low-resolution surveys as the number of tracklines across a survey domain decreases.

6. All survey trajectories were considered to be "mow-the-lawn" (grid) patterns. No irregular trajectories were considered. While this constraint could certainly be ac-

commodated by the researcher, there are also situations in which grid surveys would be less efficient in terms of the amount and quality of data which they generate.

Problems that meet these assumptions can be addressed with the framework of error metrics developed in Chapter 3.

6.1.3 Simulations and Verification

In Chapter 4, we developed a simple space-time random field simulation based on the method of sampling from the spectrum. This technique is powerful in that it does not require unnecessary computation and is flexible in terms of the size and shape of the survey domain as well as its ability to compute field values along arbitrary space-time survey trajectories. Even though it was not necessary for the experimentation undertaken in this work, a slight modification of simulation equation, Equation (4.14), could allow us to incorporate dynamics to couple the spatial and temporal evolution of the resulting random fields.

Having developed the random field simulation, we employed this capability in the generation of simulated AUV surveys of the random fields. We employed these simulated surveys in the verification of the survey error metric of Equation (3.21). We found good agreement between the errors from the simulated surveys and the theoretical errors. This agreement is not surprising since the assumptions made in formulating the total survey error metric are met by the formulation of the simulated random fields. The most profound of these assumptions is that the wavenumber-frequency spectral density function is a separable function of wavenumber and frequency (or, equivalently, that the space-time autocorrelation function is a separable function of space and time lags). These assumptions were included in the formulation of the simulation so that the errors derived from the simulated AUV surveys of the random field could serve to validate the total survey error metric. However, this particular stipulation has the effect of precluding any coupling of the spatial and temporal evolution of the random field. Thus, the dynamics of the simulated fields are not representative of realistic oceanographic phenomena. If we were to simulate a random field which incorporated a dynamical constraint (such as a dispersion relation) on the space-time evolution of the field, we would find that the total survey error metric was no longer accurate, although it would still be useful for providing insight into the design of AUV surveys of real

oceanographic phenomena. This is an area in which further research is required.

6.1.4 Survey Design and Vehicle Customization

The performance metric was employed in the analysis of AUV surveys of random fields in Chapter 5. These analyses gave insight into the process of survey sampling with AUVs. Several trade-offs of spatial resolution vs. total survey time were discovered and their implications for AUV survey design were discussed. We also demonstrated the optimization of a uniform grid survey over a square domain of a simple random process field. The spatial resolution, λ_s, and total survey time, τ_s, parameters indicated by this analysis were shown to be optimal in the sense that they minimized the expected survey error while constraining the survey to lie within the survey envelope.

The analyses of Chapter 5 also demonstrated that grid surveys of real, dynamic oceanographic phenomena can be optimized, given statistical knowledge of the process under study by employing the survey performance metrics developed earlier. Clearly the difficult part of this exercise is obtaining accurate statistics for the oceanographic process. We used a model of the convection process to obtain the required information. Others sources include prior observations from such platforms as moorings, drifters, towed bodies, and satellites. Of course there is no guarantee that either a convection model or the prior observations will be valid for the actual survey run.

Finally, we employed the survey performance metrics in an analysis of several vehicle design parameters, such as propulsion efficiency, hotel load, and battery size (total available energy). We also considered using several AUVs to conduct a single survey. We found, not surprisingly, that methods which allow an AUV to move more quickly through the water give the most dramatic decreases in total survey error. Thus, increasing battery size and using multiple vehicles were found to be the most beneficial and straightforward methods of improving overall survey performance. The insight gained from these simple vehicle redesign experiments indicates that survey analyses such as these can be a powerful tool for tailoring the design of an AUV to a particular class of oceanographic problems or for improving the design of existing AUVs.

6.2 Future Work

In the course of this thesis, we have uncovered several new and potentially fruitful areas in which further research is needed. Not the least of these is the desire to extend the development of the work contained herein. Extentions to the survey error metric of Chapter 3 and to the simulation environment of Chapter 4 are considered in Section 6.2.1, below. In Section 6.2.2 we examine the use of multiscale processing techniques to address certain algorithmic and computational issues in the modeling of ocean processes and in field inversion techniques.We examine adaptive survey strategies in Section 6.2.3 and the idea of adaptive sampling is itself expanded upon in Section 6.2.4, where we discuss coupled model/observational systems. Finally, we discuss the use of AUV surveys for the purpose of spectral estimation of ocean fields in Section 6.2.5.

6.2.1 Extensions

The development of the survey error metric in Chapter 3 relied on the assumption that the spatial and temporal components of the evolution of the process field were uncorrelated. This assumption was made to reduce the difficulty of the problem at hand. However, this is a particularly poor assumption for many dynamic ocean phenomena. Thus, research into extending the survey error metric to account for the coupled spatial-temporal evolution of the process fields is necessary. Within the framework of this thesis, additional work must also be done to update the process simulations to include more realistic process dynamics.

Simulations

A dynmical relationship between wavenumbers and frequencies, such as a dispersion relation, is required to couple the spatial and temporal evolution of a simulated field. If we have a an arbitrary dispersion relation, $\omega = f(\mathbf{k})$, then the simulation framework of Chapter 4 can be modified to exhibit the required spatial and temporal dynamics. In the specific case of a linear (wave equation) dispersion relation, $\omega = c|\mathbf{k}|$, the random field simulation

equation becomes

$$\begin{aligned} y(x_1, x_2, t) &= \sqrt{\tfrac{4}{MN}} \sum_{i=1}^{M} \cos[k_i(x_1 \cos\alpha_i + x_2 \cos\alpha_i) + w_i t + \theta_i] \\ &= \sqrt{\tfrac{4}{MN}} \sum_{i=1}^{M} \cos[k_i(x_1 \cos\alpha_i + x_2 \cos\alpha_i + ct) + \theta_i], \end{aligned} \tag{6.1}$$

where we have the used the dispersion relation to formulate the temporal evolution in terms of the same series of random wavenumbers which governs the spatial evolution.

Error Metrics

The total survey error metric of Chapter 3 assumed that the spatial and temporal components of the evolution of the process field were uncorrelated. From Equation (6.1) we see that this is no longer a valid assumption for our simulated random field. Unfortunately, we cannot undo this assumption of uncorrelatedness in the error metric nearly as easily as it was done for the simulation fields. If we attempt to insert a linear dispersion relation into our development of Chapter 3, we radically alter the nature of the error metric in ways which are not desirable.

Recall the development of the spatial survey error metric in Section 3.3.1. We related the spatial error to the effects of undersampling. If we were to blindly apply the dispersion relation to our spatial survey error to yield a new temporal survey error metric we would, in essence, be measuring the error due to temporal undersample of a *single point* in the survey domain. While this would be valid for some observational systems, such as moorings, this new error metric would fail to capture the fundamental nature of sampling with AUVs, i.e, temporal blurring of spatial samples. Further work is needed to sort out these issues.

6.2.2 Multiscale Stochastic Processing

When surveying with AUVs, we want to find ways of allocating our scarce observational resources to maximize the information content of the collected data. For this reason, we want to be able to adaptively alter the AUV survey trajectory to respond to non-stationary features observed in the survey domain. To facilitate this, an interpolated map of the

process based on the available observations and a measure of uncertainty for the interpolated values is desired. Unfortunately, current algorithms for generating such interpolated maps are extremely computationally intensive [55],[24] and usually do not allow for an efficient calculation of estimate uncertainty. Thus, it is not possible to adaptive survey in real-time using traditional field inversion methods due to the long computation times necessary to run these algorithms.

However, the recently developed theory of multiscale stochastic processes [63],[56] and the estimation framework which accompanies it [64],[66],[67],[68] allow such field inversion problems to be addressed in a scale-recursive manner, leading to dramatic reductions in computational requirements. The key notion which gives this theory such great power is the realization that multidimensional systems can often be represented by models which are Markov in scale [47] (analogous to the Markovianity of time-series problems - note that scale is a scalar variable, independent of the number of dimensions of the problem domain). This fact leads to algorithms which have computational complexities which grow linearly with the number of nodes in the domain of interest, regardless of the dimensionality of the domain. This is in sharp contrast to most multidimensional algorithms which have computational complexities which grow exponentially with the dimension of the problem domain. Furthermore, the multiscale inversion framework is inherently parallelized and automatically generates estimation error variance maps in addition to the interpolation maps.

Background: Wavelets and Multiscale Stochastic Processes

Due to the unique ability of the wavelet transform [69],[70] to easily capture (or model) non-stationary events in signals, this new processing technique has opened the door to a wide array of new processing algorithms for problems which previously had been poorly posed. One such success is the recognition that wavelet bases are well suited for describing $1/f$-like processes [71],[72]. This result is particularly useful since $1/f$-like signals have been shown to be natural descriptors for a broad range of processes, such as sea floor and landscape topologies, various geophysical time series, images of natural objects, noise in electrical systems, and burst errors in communication channels. Signal processing with

$1/f$-like signals was not previously practical due to the "lack of a convenient mathematical characterization" [72] of these processes. Thus, wavelet representations of this class of signals have engendered a large body of new theory and practice in the signal processing and estimation community.

Building upon this new signal processing paradigm, the works of Willsky [63] and Chou [56],[73],[64],[74] have generalized the multiresolution nature of the wavelet transform into a rich theory of multiscale representations of stochastic processes on lattices. The works of Luettgen [47] on multiscale representations of Markov Random Fields (MRFs) and of Irving [48] on multiscale realizations and model identification serve to round out the theoretical framework of multiscale stochastic processes. Several examples of the application of multiscale techniques to large-scale estimation problems are given in the literature: Fieguth demonstrates the application of multiscale techniques to the inversion of satellite altimetry observations of the ocean surface [66],[68] while Menemenlis [67] demonstrates the same for hydrographic and other oceanographic data. Tomographic reconstruction using the multiscale framework is discussed in Bhatia [75] and Miller [76] develops techniques for multi-sensor inversion problems in the wavelet domain.

Numerical Simulations

One promising approach would be to draw upon previous work in the area of Markov Random Fields to generate simulations of processes which are qualitatively equivalent to those which an AUV might be used to study. For instance, we could combine the work Chellappa [77] on MRFs with the work of Legg, et. al., [78] on numerical simulations of convection events to create simulations of open-ocean deep convection at various stages of the process. Specifically, a least-squares algorithm could be employed to estimate the coefficients of a low order MRF using data from numerical simulations of open-ocean deep convection. Since it has been shown that all MRFs can be generated with the multiscale framework [47], the MRF representation of the convection phenomenon would facilitate the application of multiscale processing techniques to the specific problem of surveying open-ocean deep convection events with AUVs. The MRF convection simulations would be carried out on a dense grid in a two-dimensional domain. Since the simulation is based

upon an FFT method, the simulated fields would be inherently stationarity in time but could be non-homogeneous and non-isotropic in space. Also, the computational complexity would be such that numerous simulations could be generated in an efficient manner.

Interpolated Maps

Heuristic survey trajectory algorithms would next be used to simulate an AUV survey of an oceanographic process. Irregular sampling by the AUV would be accommodated by taking the survey samples from the nearest grid point of the dense simulation grid. Using the multiscale processing framework developed by Willsky [63] and Chou [64] and further extended by Fieguth [66] and Menemenlis [67], we would generate interpolated maps of the oceanographic process in "real-time". As the vehicle moves through the survey domain collecting data, an interpolated map based upon all available measurements would be generated during each trajectory decision cycle. The remarkable computational efficiency of the multiscale interpolation scheme would allow the algorithm to be implemented on a real AUV and used to study real oceanographic processes.

Error Analysis

In addition to the interpolated maps created with the multiscale field inversion techniques, estimation error variances at each interpolation point would be generated during each trajectory decision cycle. The point-wise variances would be combined to form an estimation error variance map. Such maps would be vital to both the analysis of the quality of the interpolated map and as a driving force in the adaptive survey trajectory decision process. Note that error cross-covariances are not automatically provided by the multiscale processing framework of Chou [64], but could be calculated via a model for the error dynamics [79]. This calculation would effectively double the computational load of the algorithm. It is not yet clear whether knowledge of the cross-covariance is necessary for interpolation map validation or in the adaptive sampling strategy design process. This issue would need to be explored further.

6.2.3 Adaptive Sampling

Adaptive sampling strategies attempt to increase the efficiency of a survey by concentrating measurements in scientifically interesting regions of the survey domain. These strategies range from fairly unsophisticated techniques (e.g., appropriately sizing grid surveys as in Chapter5) to complex algorithms (e.g., coupled observation-modeling systems). Between these two extremes lie various methods by which measurements are concentrated in the regions of greatest interest (such as areas with high spatial gradients). For example, to map an ocean front, an AUV might first run a very coarse survey to localize the front, then concentrate operations in the vicinity of the front. Substantial savings could be realized in terms of both the expended energy and the time required to characterize the front. To quantify the benefits of adaptive sampling, consider two scenarios. The first scenario is a survey with no prescribed completion time and no constraint of the total survey time. This scenario demonstrates the most conservative estimate of the benefits of adaptive sampling. The second scenario is a survey which must be completed within a fixed amount of time.

Surveys without Time Constraints

Given the total survey distance, L, we can compute the energy, E, required to complete a survey. For an AUV cruising at its most efficient speed, the total energy required is given by Equation (3.6).

As stated previously, adaptive surveys concentrate measurements in regions of interest, thereby reducing the total distance that the survey vehicle must travel. If an adaptive sampling strategy reduces the distance traveled by a factor f, then the energy required to complete the adaptive survey, E_{as}, is simply

$$E_{as} = \frac{E}{f}. \tag{6.2}$$

To phrase the benefit in direct terms, an adaptive survey which cuts the overall length of the survey trajectory by a factor of three provides the same benefit as creating a new battery chemistry which has a factor of three higher energy density. These results apply to surveys which have no maximum duration.

Surveys with Time Constraints

Processes which evolve rapidly in time, such as open-ocean deep convection, require AUV surveys which are completed quickly so that the process field can be approximated as being locally stationary. Also, in a coastal environment, tidal forcing might dictate a survey completion time of six hours or less. Surveys such as these are constrained by a maximum total survey time. If a survey must be completed in time τ_c, then the required survey velocity is given by

$$V = \begin{cases} \frac{L}{f\tau_c} & \text{if } V_{opt} < \frac{L}{f\tau_c} \\ V_{opt} & \text{otherwise} \end{cases}, \tag{6.3}$$

where V_{opt} is the vehicle's optimal cruising speed, given previously. Thus, the energy to complete the survey is

$$E_{as} = \begin{cases} H\tau + \frac{1}{f^3}\left(\frac{\rho C_d S L^3}{2\eta\tau_c^2}\right) & \text{if } V_{opt} < \frac{L}{f\tau_c} \\ \frac{3L}{2f}\left(\frac{\rho C_d S H^2}{\eta}\right)^{1/3} & \text{otherwise} \end{cases}. \tag{6.4}$$

For the case where the required vehicle velocity is significantly greater than V_{opt}, propulsion consumes the largest fraction of the energy. Thus the second term in the expression for E_{as} dominates. Here the energy goes as $\frac{1}{f^3}$, indicating that even small increases in survey efficiency can dramatically improve overall system performance. For example, a two-fold decrease in the distance travelled in a survey would correspond to an eight-fold reduction in energy consumed. This reduction in energy comes from the fact that the vehicle was able to survey the given domain twice as quickly as a non-adaptively surveying vehicle would have been able to do.

Adaptive Survey Strategies

There are a number of possible methods by which the overall length of the trajectory might be reduced. Although very little work on adaptive sampling strategies has been done in the AUV community, several disciplines have addressed problems of a similar nature. We have collected references for these contributions in Table 6.1. The problems domain is

	One AUV	Multiple AUVs	Tomo AUVs	Comm AUVs
Metrics for Survey Comparison	[11, 80, 26, 37, 81]	[80, 26, 37, 82]	[26, 82, 83]	[80, 26, 82, 83]
Model Based Experiment Design	[11, 12, 84, 85, 86, 52, 37, 59, 60, 87]	[88, 84, 85, 86, 52, 37, 59, 89]	[90]	
Reflexive Survey Strategies	[91, 92, 53, 93, 94]	[91, 95]	[90, 82, 83]	[82, 83, 95]
Model Based Adaptive Sampling	[37]			

Table 6.1: Adaptive survey strategy problem domain with related references.

grouped by the type of AUV being employed and the broad category of adaptive sampling being employed. Surveys which employ one or several AUVs, as well as tomographically and communicationally instrumented AUVs, are considered. References for survey error metrics and for survey strategies which are predesigned with the aid of a process model are given in first and second rows of the table, respectively. The third row gives references for surveys which are able to react to observations of the process field in real-time (such as gradient following surveys). Although these surveys can react to incoming observations, they do not have a predictive capacity that would allow them to incorporate the expected state of the future field into their surveying strategy. References for surveys which do have this ability are found in the fourth row of the table. The work of this thesis falls into the first two columns of the first and second rows.

6.2.4 Coupled Model/Observational Systems

The detailed plan for implementing a multiscale processing based adaptive survey design framework described above in Section 6.2.2 is a simple embodiment of a coupled model/observational system. The individual vehicle is the sole observational system and the multiscale Markov Random Field coefficients form the process model. The model and

observations are combined in the generation of interpolated maps (estimates) of the process field. These maps aid in the identification of scientifically interesting features of the field, such as convective plumes and field gradients. This information, in turn, drives the adaptive survey trajectory decision cycle, continuously repositioning the vehicle to improve the scientific relevance of the survey data. In addition, an estimation error variance map is automatically generated as part of the field inversion process. These maps could be used to "close the loop" of the adaptive survey strategy, allowing the vehicle to make quantitative decisions about the relevance of features identified in the interpolation map and to locally adjust the density of survey coverage as appropriate.

The simple coupled model/observational system described above enhances the current state of the art in surveying oceanographic processes with AUVs. However, this scheme is limited by the fact that the vehicle is the only source of field observations and by the implicit assumption that all model computations must be performed on the AUVs main vehicle computer. A system which removes these restrictions, incorporating numerous observational systems and combining several process models, is shown in Figure 6.1. This figure implies that the an autonomous ocean sampling network (see Section 1.1.3 and Figure 1.2) with multiple communicating AUVs is employed to gather observations and to organize those observations so that time-critical information can be relied to the scientist. A system such as that represented in this figure would require the interconnection of several process models (with all computation being performed at a central location, such as a mooring or support vessel). We see that there are three main categories of observational resources: AOSN-like networks for in situ observations of the process; remote sensing platforms, such as satellite- and aircraft-based instruments, for broad spatial scale observations; and historical databases which help identify long time scale trends as well as rapidly evolving features. These databases are also used to assess the predictive skill of the assembly of process models employed in the model/observational system.

The observation of the phenomenon of interest comprises the first phase of the three phase process of adaptive sampling. The second phase involves the processing of these data to constrain the physical and biological process models which are running in real-time, concurrent with the collection of the data. Since the data are collected over varying time

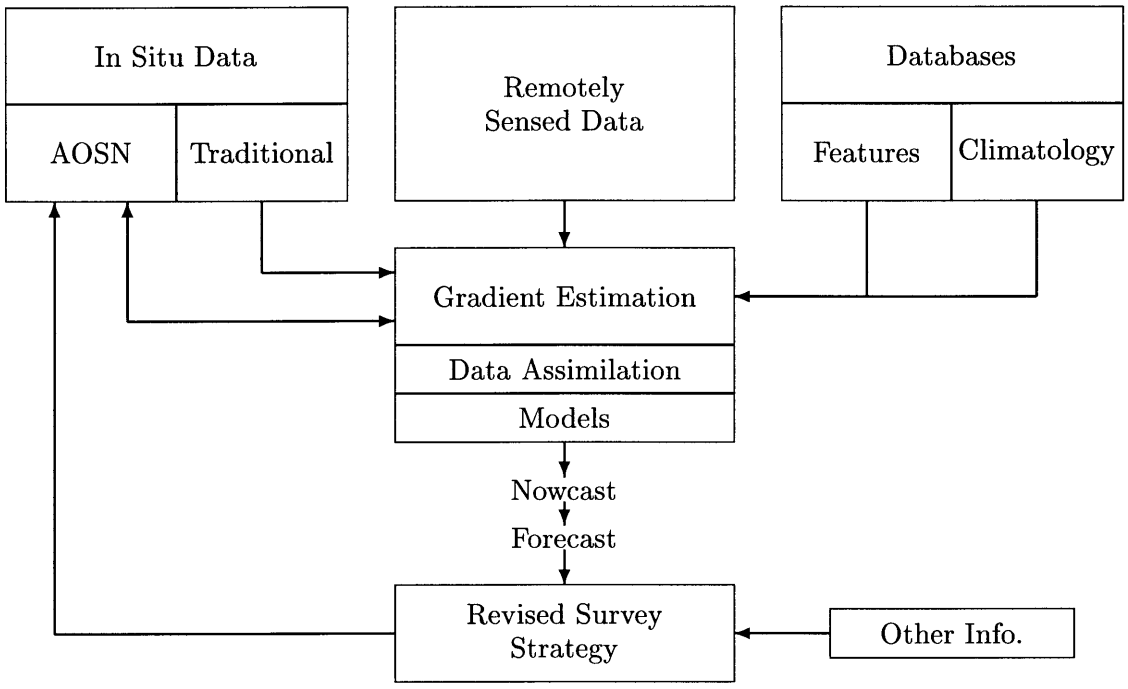

Figure 6.1: A coupled observation/modeling systems for oceanographic research consisting of three phases. In the initial phase, data is collected both remotely and in the water and combined with historical quantitative and qualitative knowledge drawn from databases. In the second phase, this data is fed into a suite of algorithms which assimilate the various data and uses these data to constrain physical and biological models which are running in real time. In the third phase, the output of the models are used to update the survey strategies of the available sensor platforms. At this point the cycle repeats. Figure after Curtin [96].

and space scales, the assimilation of these data into the various process models is a complex task, as is the combination of the models into a coherent whole. In the third phase of the adaptive sampling process, the products of the process models are used to inform the adaptive sampling decision cycle. Nowcasts of the current state of a process are used to identify features of interest in the process field. The system also makes benificial use of the predictive skill of the process models by using model forecasts to maintain the observational assets within interesting features while using a minimum of resources (such as an AUV's energy).

6.2.5 Spectral Analysis

We have assumed throughout this thesis that the scientific objective of an AUV's survey has been to develop a spatial "snap-shot" of the process of interest. There is another broad class of problems which we could also explore with AUV surveys, specifically, the estimation of the wavenumber-frequency spectrum of a process of interest. To do this, we would need to rethink much of the development of this thesis in terms of that problem. It might seem that estimating wavenumber-frequency spetral from AUV observations would be less complex than developing interpolated maps of random fields since phase information is not required in the spectral estimate. Unfortunately, it is even more difficuly to generate spectral estimates with AUVs due to the coupling of multiple spatial dimensions with the time dimension through the survey trajectory.

To better understand this difficulty, we consider the case of sampling in a domain which has one spatial dimension and one temporal dimension. If the speed of the AUV is v and the sampling period is Δt, then the spatial sampling period is $\Delta x = v\Delta t$. The process of sampling is described as the convolution of the continuous time signal $f(x,t)$ with a sequence of two dimensional impulses. The samples are

$$f_s(n) = f(n\Delta x, n\Delta t) = \sum_{n=0}^{N-1} f(x,t)\delta(x - n\Delta x, t - n\Delta t). \tag{6.5}$$

The process of surveying with an AUV on this two dimensional domain is shown in Figure 6.2. Note that the angle made by the survey trajectory with the spatial axis is a nonlinear function of the vehicle speed alone. As the vehicle speed goes to zero, the line of samples in the space-time domain swings toward the time axis. Similarly, when $V \to \infty$ the line of samples coincides with the spatial axis, i.e., $\theta \to 0$. An analogous relationship is present in the transform domain.

To see this analogous form, first consider the Fourier transform of the sequence of two-dimensional impulses which describe the sample locations. The Fourier transform reveals that we are also sampling in the transform domain, with sample locations given by

$$F(n) = F(n/\Delta x, n/\Delta t) = F(n\Delta k, n\Delta\omega), \tag{6.6}$$

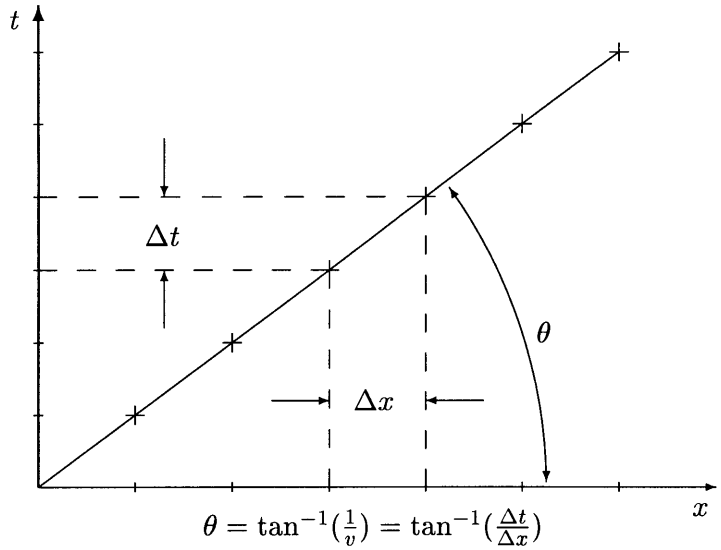

Figure 6.2: Sampling in space and time along the survey trajectory of an AUV. The angle θ between the line of samples and the spatial axis is given by $\theta = \tan^{-1}(v^{-1})$, where v is the speed of the AUV. The figure is shown for a survey through a survey domain which has a single spatial dimension and a single temporal dimension. Hence, the survey trajectory is the straight line shown with survey samples indicated by $+$.

where Δk and Δt are the sampling wavenumber and frequencies corresponding to the spatial(Δx) and temporal (Δt) sampling periods, respectively. The samples in frequency-wavenumber space are parameterized by a single number, n, analogous to the space-time case. This effect is shown in Figure 6.3. As $V \to 0$ the sampling becomes purely temporal and the sampling line aligns with the frequency axis. Similarly, as $V \to \infty$ the sampling line approaches the spatial axis, giving purely spatial samples.

If we now increase the number of spatial dimensions, either to two or three dimensions, it is difficult to understand the effects of sampling with an trajectory through these multidimensional domains. The sampling is still parameterized by a single number, n, which effectively gives the number of the sample (where the first sample corresponds to $n = 0$). Further investigation into using AUVs to generate spectral estimates of oceanographic processes is much needed and would complement the work contained in this thesis.

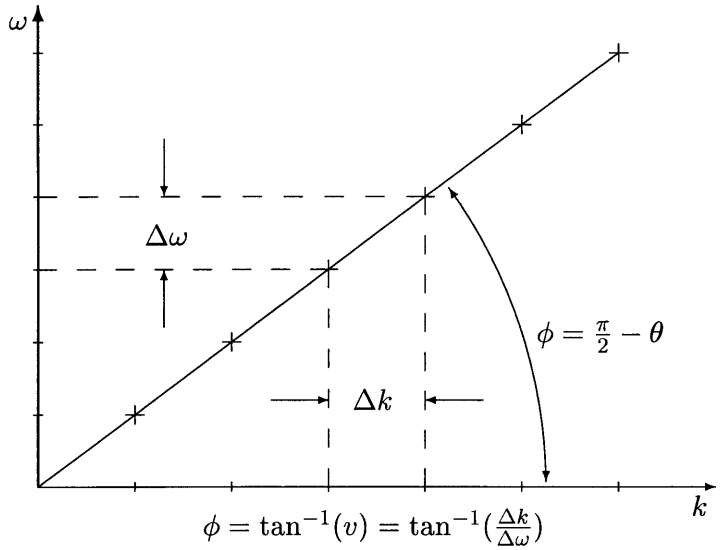

Figure 6.3: Sampling in space-time (see Figure 6.2) leads to sampling in the Fourier transform domain, as well. The angle made by the line of samples with the wavenumber axis is $\frac{\pi}{2} - \theta$, and is thus a non-linear function of the vehicle velocity. The wavenumber-frequency samples are denoted by + along the survey's "trajectory" through the transform plane.

6.3 Conclusion

The work contained in this thesis begins the process of building a quantitative framework for the design of surveys of oceanographic processes with autonomous underwater vehicles. This framework consists of survey error metrics for simple oceanographic phenomena with known spatial and temporal spectra and also includes a survey analysis tool which aids the survey designer in making trade-offs of survey spatial resolution and total survey time. We have also shown that the survey analysis tool can be employed in the vehicle selection/redesign process to tailor an AUV to a particular class of applications or oceanographic processes. With these tools, simple AUV surveys of oceanographic phenomena can be made which also give an estimate of the errors inherent in making these surveys. The author believes that this capability has not been previously demonstrated for oceanographic surveys using AUVs.

The progress that has been achieved in this thesis only begins to address the overall problem of using AUVs in an oceanographic research setting. As mentioned in Chapter 2, many additional facets of this problem exist and the discussion of Section 6.2 details ways in which some of these new resarch areas might be addressed. Additional investigation into

these areas is needed to realize the full potential of the autonomous underwater vehicle as an oceanographic research platform. It is our hope that the field of AUV-based oceanography will grow and flourish.

Bibliography

[1] T. D. Dickey, "The emergence of concurrent high-resolution physical and bio-optical measurements in the upper ocean and their applications", *Reviews of Geophysics*, vol. 29, no. 3, pp. 383–413, August 1991.

[2] D. R. Blidberg and G. Sedor, "An interdisciplinary workshop to assess the scientific needs for a long range autonomous underwater vehicle", Tech. Rep., Marine Systems Eng. Lab., University of New Hampshire, 1991.

[3] J. G. Bellingham, T. R. Consi, C. Goudey, J. W. Bales, and C. Chryssostomidis, "Performance characteristics of the Odyssey AUV", in *Proc. Int. Symp. on Unmanned Untethered Submersible Technology*, 1993, pp. 37–49.

[4] J. G. Bellingham, C. A. Goudey, T. R. Consi, J. W. Bales, D. K. Atwood, J. J. Leonard, and C. Chryssostomidis, "A second generation survey AUV", in *IEEE Conference on Autonomous Underwater Vehicles*, Cambridge, MA, 1994.

[5] S. M. Smith and S. E. Dunn, "The Ocean Voyager II: An AUV designed for coastal oceanography", in *IEEE Conference on Autonomous Underwater Vehicles*, Cambridge, MA, 1994.

[6] C. von Alt, B. Allen, T. Austin, and R. Stokey, "Remote Environmental Measuring Units", in *IEEE Conference on Autonomous Underwater Vehicles*, Cambridge, MA, 1994.

[7] S. M. Smith, K. Heeb, N. Frolund, and T. Pantelakis, "The Ocean Explorer AUV: A modular platform for coastal oceanography", in *Ninth Int. Symposium on Unmanned Untether Submersible Technology*, September 1995.

[8] D. R. Yoerger, A. Bradley, R. Bachmayer, R. Catanach, A. Duester, S. Liberatore, H. Singh, and B. Walden, "Near-bottom magnetic surveys of the coaxial ridge segment using the Autonomous Benthic Explorer survey vehicle", *RIDGE Events*, vol. 7, no. 1, February 1996.

[9] Russell E. Davis, "Observing the general circulation with floats", *Deep-Sea Research*, vol. 38, no. Suppl. 1, pp. S531–S571, 1991.

[10] Dana R. Yoerger, Albert M. Bradley, and Barrie B. Walden, "The Autonomous Benthic Explorer (ABE): An AUV optimized for deep seafloor studies", in *Seventh International*

Symposium on Unmanned Untether Submersible Technology, Durham, NH, Sept. 1991, pp. 60–70.

[11] J. G. Bellingham and J. S. Willcox, "Optimizing AUV Oceanographic Surveys", in *IEEE Symposium on Autonomous Underwater Vehicle Technology*, Monterey, CA, June 1996.

[12] J. Scott Willcox, Yanwu Zhang, James G. Bellingham, and John Marshall, "AUV survey design applied to oceanic deep convection", in *Proceedings of MTS/IEEE Oceans '96*, Fort Lauderdale, FL, Sept. 1996.

[13] K. H. Coale, C. S. Chin, G. J. Massoth, K. S. Johnson, and E. T. Baker, "*In-situ* chemical mapping of dissolved iron and manganese in hydrothermal plumes", *Nature*, vol. 352, pp. 325–328, 1991.

[14] C. Chryssostomidis, J. G. Bellingham, J. W. Bales, and T. R. Consi, "Rapid response to episodic events in the ocean", Tech. Rep., MIT Sea Grant College Program, 1996.

[15] J. G. Bellingham, C. Chryssostomidis, M. Deffenbaugh, J. J. Leonard, and H. Schmidt, "Arctic under-ice survey operations", in *Proc. Int. Symp. on Unmanned Untethered Submersible Technology*, 1993, pp. 50–59.

[16] J. G. Bellingham, J. J. Leonard, J. Vaganay, C. Goudey, D. Atwood, T. Consi, J. Bales, H. Schmidt, and C. Chryssostomidis, "AUV operations in the Arctic", in *Proceedings of the Sea Ice Mechanics and Arctic Modeling Workshop*, Anchorage, Alaska, USA, April 1995.

[17] Henrik Schmidt, James G. Bellingham, Mark Johnson, David Herold, David M. Farmer, and Richard Pawlowicz, "Real-time frontal mapping with AUVs in a Coastal Environment", in *Proceedings of MTS/IEEE Oceans '96*, Fort Lauderdale, Florida, Sept. 1996, vol. 3, pp. 1094–1098.

[18] John Marshall, "Ocean Convection: Theories and Observations", Talk given at the MIT Sea Grant Autonomous Underwater Vehicle Seminar Series, March 12, 1996.

[19] John Marsall and Martin Visbeck, "The Labrador Sea Convection Experiment 1996-1998", April 1995, World Wide Web white paper.

[20] T. B. Curtin, J. G. Bellingham, J. Catipovic, and D. Webb, "Autonomous Oceanographic Sampling Networks", *Oceanography*, vol. 6, no. 3, pp. 86–94, 1993.

[21] Ghassem Asrar and Jeff Dozier, *EOS: Science Strategy for the Earth Observing System*, American Institute of Physics Press, Woodbury, NY, 1994.

[22] Helen Jones and John Marshall, "Convection with rotation in a neutral ocean: A study of open-ocean deep convection", *Journal of Physical Oceanography*, vol. 23, pp. 1009–1039, June 1993.

[23] Rafael L. Bras and Ignacio Rodriguez-Iturbe, *Random Functions and Hydrology*, Dover Publications, Mineola, N.Y., 1993.

[24] Edward H. Isaaks and R. Mohan Srivastava, *An Introduction to Applied Geostatistics*, Oxford University Press, New York, 1989.

[25] Claude E. Shannon, "Communication in the presence of noise", *Proc. IRE*, vol. 37, pp. 10–21, Jan. 1949.

[26] Claude E. Shannon and Warren Weaver, *The Mathematical Theory of Communication*, University of Illinois Press, Urbana and Chicago, 1963.

[27] Norbert Wiener, *Extrapolation, Interpolation, and Smoothing of Stationary Time Series*, MIT Press, Cambridge, MA, 1949.

[28] Athanasios Papoulis, "Generalized sampling theorem", *IEEE Trans. on Circuits and Systems*, vol. CAS-24, no. 11, pp. 652–654, 1977.

[29] A. J. Jerri, "The Shannon sampling theorem — its various extensions and applications: A tutorial review", *Proceedings of the IEEE*, vol. 65, no. 11, pp. 1565–1596, Nov. 1977.

[30] D. P. Petersen and D. Middleton, "Sampling and reconstruction of wave-number-limited functions in n-dimensional euclidean spaces", *Information and Control*, vol. 5, pp. 279–323, 1962.

[31] H. Miyakawa, "Sampling theorem of stationary stochastic variables in multi-dimensional space", *J. Inst. Elec. Commun. Engrs. (Japan)*, vol. 42, pp. 421–427, 1959.

[32] Dan E. Dudgeon and Russell M. Mersereau, *Multidimensional Digital Signal Processing*, Prentice-Hall, Englewood Cliffs, New Jersey, 1984.

[33] Francis P. Bretherton and James C. McWilliams, "Estimations from irregular arrays", *Reviews of Geophysics and Space Physics*, vol. 18, no. 4, pp. 789–812, Nov. 1980.

[34] Farokh Marvasti, "Nonuniform sampling", in *Advanced Topics in Shannon Sampling and Interpolation Theory*, Richard J. Marks, II, Ed. Springer-Verlag, 1993.

[35] Abdul J. Jerri, "Error analysis in application of generalizations of the sampling theorem", in *Advanced Topics in Shannon Sampling and Interpolation Theory*, Richard J. Marks, II, Ed., pp. 219–298. Springer-Verlag, New York, NY, 1993.

[36] Rafael L. Bras and Ignacio Rodriguez-Iturbe, "Evaluation of mean square error involved in approximating the areal average of a rainfall event by a discrete summation", *Water Resources Research*, vol. 12, no. 2, pp. 181–184, 1976.

[37] Allan R. Robinson, "Physical processes, field estimation and an approach to interdisciplinary ocean modeling", Tech. Rep., Division of Applied Sciences, Department of Earth and Planetary Sciences, Harvard University, Oct. 1994.

[38] Francis P. Bretherton, Russ E. Davis, and C. B. Fandry, "A technique for objective analysis and design of oceanographic experiments applied to MODE-73", *Deep-Sea Research*, vol. 23, pp. 559–582, 1976.

[39] Jose M. Mejia and Ignacio Rodriguez-Iturbe, "On the sythesis of random field sampling from the spectrum: An application to the generation of hydrologic spatial processes", *Water Resources Research*, vol. 10, no. 4, pp. 705–11, 1974.

[40] Mark S. Handcock and James R. Wallace, "An approach to statistical spatial-temporal modeling of meteorological fields", *Journal of the American Statistical Association*, vol. 89, no. 426, pp. 368–390, June 1994.

[41] John A. Goff and Thomas H. Jordan, "Stochastic modeling of seafloor morphology: Inversion of sea beam data for second-order statistics", *J. of Geophys. Res.*, vol. 93, no. B11, pp. 13,589–13,608, Nov. 1988.

[42] John A. Goff and Thomas H. Jordan, "Stochastic modeling of seafloor morphology: A parameterized Gaussian model", *Geophys. Res. Let.*, vol. 16, no. 1, pp. 45–48, Jan. 1989.

[43] Aristotelis Mantoglou and John L. Wilson, "Simulation of random fields with the Turning Bands Method", Tech. Rep. Report No. 264, Ralph M. Parsons Laboratory, Dept. of Civil Engineering, Massachusetts Institute of Technology, Cambridge, MA, July 1981.

[44] Aristotelis Mantoglou and John L. Wilson, "The Turning Bands Method for simulation of random fields using line generation by a spectral method", *Water Resources Research*, vol. 18, no. 5, pp. 1379–1394, 1982.

[45] Erik Vanmarcke, *Random Fields: Analysis and Synthesis*, The MIT Press, Cambridge, Massachusetts, 1983.

[46] Haluk Derin and Patrick A. Kelley, "Discrete-index Markov-type random processes", *Proceedings of the IEEE*, vol. 77, no. 10, pp. 1485–1510, Oct. 1989.

[47] Mark R. Luettgen, William C. Karl, Alan S. Willsky, and Robert R. Tenney, "Multiscale representations of markov random fields", *IEEE Trans. Signal Processing*, vol. 41, no. 12, pp. 3377–3396, Dec. 1993.

[48] William W. Irving, *Multiscale Stochastic Realization and Model Identification with Applications to Large-Scale Estimation Problems*, PhD thesis, Massachusetts Institute of Technology, Sept. 1995.

[49] Ignacio Rodriguez-Iturbe and Jose M. Mejia, "The design of rainfall networks in time and space", *Water Resources Research*, vol. 10, no. 4, pp. 713–728, 1974.

[50] Sudarshan Kumar and John H. Seinfeld, "Optimal location of measurements for distributed parameter estimation", *IEEE Trans. on Automatic Control*, vol. AC-23, no. 4, pp. 690–698, Aug. 1978.

[51] Nelson G. Hogg, "Oceanographic data for parameter estimation", in *Modern Approaches to Data Assimilation in Ocean Modeling*, P. Malanotte-Rizzoli, Ed., pp. 57–76. Elsevier Science, 1996.

[52] Valerii V. Fedorov, "Design of spatial experiments: Model fitting and prediction", Tech. Rep., Mathematical Sciences Section, Computer Science and Mathematics Division, Oak Ridge National Laboratory, Mar. 1996.

[53] Erik Burian, Dana Yoerger, Albert Bradley, and Hanumant Singh, "Gradient search with autonomous underwater vehicles using scalar measurements", in *IEEE Symposium on Autonomous Underwater Vehicle Technology*, Monterey, CA, June 1996, pp. 86–98.

[54] James W. Bales, "Endurance of a lithium-battery Odyssey II", Tech. Rep., MIT Sea Grant AUV Laboratory, Cambridge, MA, 1997, AUV Lab. Tech. Note 97-126.

[55] Carl Wunsch, *The Ocean Circulation Inverse Problem*, Cambridge University Press, Cambridge, England, 1996.

[56] Kenneth C. Chou, *A Stochastic Modeling Approach to Multiscale Signal Processing*, PhD thesis, Massachusetts Institute of Technology, May 1991.

[57] Paul W. Fieguth, *Apllication of Multiscale Estimation ro Large Scale Multidimensional Imaging and Remote Sensing Problems*, PhD thesis, Massachusetts Institute of Technology, June 1995.

[58] Albert M. Bradley, "Low power navigation and control for long range autonomous underwater vehicles", in *Proc. of the Second Intl Offshore and Polar Eng. Conf.*, San Francisco, CA, June 1992.

[59] N. Barth and C. Wunsch, "Oceanographic experiment design by simulated annealing", *Journal of Physical Oceanography*, vol. 20, pp. 1249–1263, September 1990.

[60] N. Barth, "Oceanographic experiment design II: Genetic algorithms", *J. of Atmo. and Oceanic Tech.*, vol. 9, pp. 434–443, August 1992.

[61] J. Vaganay, J. G. Belligham, and J. J. Leonard, "Comparison of fix computations and filtering for autonomous acoustic navigation", in *International Advanced Robotics Programme*, Toulon, France, 1996.

[62] George Christakos, *Random Field Models in Earth Sciences*, Academic Press, London, 1992.

[63] Alan S. Willsky, "Modeling and estimation for multiresolution stochastic processes", Tech. Rep. LIDS-P-1914, M.I.T. Laboratory for Information and Decision Systems, Oct. 1989.

[64] Kenneth C. Chou, Alan S. Willsky, and Albert Benveniste, "Multiscale recursive estimation, data fusion, and regularization", *IEEE Trans. Automatic Control*, vol. 39, no. 3, pp. 464–478, Mar. 1994.

[65] B. A. Klinger and J. Marshall, "Regimes and scaling laws for rotating deep convection in the ocean", *Dynamics of Atmosphere and Oceans*, vol. 21, pp. 227–256, 1995.

[66] Paul W. Fieguth, William C. Karl, Alan S. Willsky, and Carl Wunsch, "Multiresolution optimal interpolation and statistical analysis of TOPEX/POSEIDON satellite altimetry", *IEEE Trans. Geoscience and Remote Sensing*, vol. 33, no. 2, pp. 280–292, Mar. 1995.

[67] Dimitris Menemenlis, Paul Fieguth, Carl Wunsch, and Alan Willsky, "Adaptation of a fast optimal interpolation algorithm to the mapping of oceanographic data", *J. Geophys. Res.*, vol. 102, no. C5, pp. 10,573–10,584, May 15 1997.

[68] P. Fieguth, D. Menemenlis, T. Ho, and A. Willsky, "Mapping mediterranean altimeter data with a multiresolution optimal interpolation algorithm", Aug. 1996, to appear.

[69] Ingrid Daubechies, "Orthonormal bases of compactly supported wavelets", *Comm. on Pure and Applied Math*, vol. 91, pp. 909–996, 1988.

[70] Ingrid Daubechies, "The wavelet transform, time-frequency localization and signal analysis", *IEEE Trans. Information Theory*, vol. 36, pp. 961–1005, 1990.

[71] Gregory W. Wornell, "A Karhunen-Loève-like expansion for $1/f$ processes via wavelets", *IEEE Trans. Information Theory*, vol. 36, no. 4, pp. 859–861, July 1990.

[72] Gregory W. Wornell, *Synthesis, Analysis, and Processing of Fractal Signals*, PhD thesis, Massachusetts Institute of Technolgy, Sept. 1991.

[73] Kenneth C. Chou, Stuart A. Golden, and Alan S. Willsky, "Multiresolution stochastic models, data fusion, and wavelet transforms", Tech. Rep. LIDS-P-2110, M.I.T Laboratory for Information and Decision Systems, May 1992.

[74] Kenneth C. Chou, Alan S. Willsky, and Ramine Nikoukhah, "Multiscale systems, kalman filters, and Riccati equations", *IEEE Trans. Automatic Control*, vol. 39, no. 3, pp. 479–492, Mar. 1994.

[75] M. Bhatia, W. C. Karl, and A. S. Willsky, "Using natural wavelet bases and multiscale stochastic models for tomographic reconstrucion", Tech. Rep. LIDS-P-2196, M.I.T. Laboratory for Information and Decision Systems, Oct. 1993.

[76] Eric L. Miller and Alan S. Willsky, "Wavelet transforms and multiscale estimation techniques for the solution of multisensor inverse problems", Tech. Rep. LIDS-P-2224, M.I.T. Laboratory for Information and Decision Systems, Jan. 1994.

[77] R. Chellappa, B. S. Manjunath, and T. Simchony, "Texture segmentation with neural networks", in *Neural Networks for Signal Processing*, Bart Kosko, Ed., chapter 2, pp. 37–60. Prentice Hall, Englewood Cliffs, NJ, 1992.

[78] Keith Julien, Sonya Legg, Jim McWilliams, and Joseph Werne, "Penetrative convection in rapidly rotating flows: Preliminary results from numerical simulation", *Dynamics of Atmospheres and Oceans*, vol. 24, pp. 237–249, 1996.

[79] Mark R. Luettgen and Alan S. Willsky, "Multiscale smoothing error models", Tech. Rep. LIDS-P-2234, M.I.T. Laborartory for Information and Decision Systems, Mar. 1994.

[80] Arie Yavnai, "Entropy-based autonomability criteria for intelligent autonomous systems", in *Seventh International Symposium on Unmanned Untethered Submersible Technology*, Durham, NH, Sept. 1991.

[81] Hanumant Singh, *An Entropic Framework for AUV Sensor Modeling*, PhD thesis, Woods Hole Oceanographic Institution and the Massachusetts Institute of Technology, May 1995.

[82] Arie Yavnai, "Distributed decentralized architecture for autonomous cooperative operation of multiple agent systems", in *IEEE Symposium on Autonomous Underwater Vehicle Technology*, Cambridge, MA, July 1994, pp. 61–67.

[83] Steven G. Chappell, James C. Jalbert, Paul Pietryka, and John Duchesney, "Acoustic communication between two autonomous underwater vehicles", in *IEEE Symposium on Autonomous Underwater Vehicle Technology*, Cambridge, MA, July 1994, pp. 462–469.

[84] Richard L. Smith, "Estimating nonstationary spatial correlations", Preliminary Version, June 1996.

[85] Valerii V. Fedorov, *Theory of Optimal Experiments*, Academic Press, 1972.

[86] Valerii V. Fedorov and Peter Hackl, "Optimal experiment design: Spatial sampling", *Calcutta Statistical Association Bulletin*, 1994.

[87] Edward R. Levine, Andrew Shein, and John Kloske, "Simulation of uuv environmental sampling in modeled ocean frontal zones", in *IEEE Symposium on Autonomous Underwater Vehicle Technology*, Cambridge, MA, July 1994, pp. 439–442.

[88] M. Triantafyllou and K. Streitlien, "Distributed control of multiple auvs forming effective chains", in *Proc. Int. Symp. on Unmanned Untethered Submersible Technology*, 1991, pp. 499–518.

[89] N. Barth, "Choosing altimeter orbits as a problem in experiment design", *Oceanologica Acta*, vol. 15, no. 5, pp. 459–470, 1992.

[90] Max Deffenbaugh, *Optimal Ocean Acoustic Tomography with Moving Sources*, PhD thesis, Massachusetts Institute of Technology, Cambridge, Massachusetts, April 1997, MIT/WHOI Joint Program in Applied Ocean Science and Engineering.

[91] R. A. Brooks, "A robust layered control system for a mobile robot", *IEEE Journal of Robotics and Automation*, vol. RA-2, no. 1, pp. 14–23, March 1986.

[92] James G. Bellingham, E. Eric Adams, Nicholas M. Patrikalakis, James W. Bales, and Thomas R. Consi, "Adaptive sampling for polution monitoring in the coastal environment", An Unpublished Proposal to the National Sea Grant College Program, Nov. 1994.

[93] Andrew Bennett, "Combining planning with reactive architectures in an autonomous underwater vehicle", in *Proc. Int. Symp. on Unmanned Untethered Submersible Technology*, Sept. 1993, pp. 437–444.

[94] R. P. Bonasso and J. Barratt, "A reactive robot system for find and visit tasks in a dynamic ocaen environment", in *Proc. Int. Symp. on Unmanned Untethered Submersible Technology*, 1993, pp. 69–80.

[95] Christiane N. Duarte and Dominick J. Carlino, "Using a fleet if autonomous bottom crawling vehicles for surf zone operations", in *IEEE Symposium on Autonomous Underwater Vehicle Technology*, Cambridge, MA, July 1994, pp. 317–322.

[96] Tom Curtin, "Coupled modeling-sampling systems for ocean nowcasting and forecasting", Talk given at the MIT Sea Grant Marine Industry Collegium Symposium on Coupled Ocean Observation/Modeling Systems, Nov. 1997.